N71-31382

LR 24529
JULY 14, 1971

NASA CR-111923

CASE FILE COPY

ORBITAL FATIGUE TESTER FOR USE IN SKYLAB EXPERIMENT T032 - PHASE I, DESIGN AND TESTING OF SPECIMENS HAVING VARIOUS SIZES

(FINAL REPORT ON PHASE I)

Prepared By: LOCKHEED - CALIFORNIA COMPANY
BURBANK, CALIFORNIA

For: NATIONAL AERONAUTICS AND
SPACE ADMINISTRATION
LANGLEY RESEARCH CENTER

LOCKHEED-CALIFORNIA COMPANY • BURBANK, CALIFORNIA
A DIVISION OF LOCKHEED AIRCRAFT CORPORATION

LR 24529
JULY 14, 1971

NASA CR-111923

ORBITAL FATIGUE TESTER FOR USE IN SKYLAB EXPERIMENT T032 - PHASE I, DESIGN AND TESTING OF SPECIMENS HAVING VARIOUS SIZES

(FINAL REPORT ON PHASE I)

Prepared By: LOCKHEED - CALIFORNIA COMPANY
BURBANK, CALIFORNIA

For: NATIONAL AERONAUTICS AND
SPACE ADMINISTRATION
LANGLEY RESEARCH CENTER

LOCKHEED-CALIFORNIA COMPANY • BURBANK, CALIFORNIA
A DIVISION OF LOCKHEED AIRCRAFT CORPORATION

LOCKHEED • CALIFORNIA COMPANY
A DIVISION OF LOCKHEED AIRCRAFT CORPORATION

REPORT NO. LR 24529
DATE July 14, 1971
MODEL
COPY NO.

TITLE

ORBITAL FATIGUE TESTER FOR USE IN SKYLAB EXPERIMENT T032 - PHASE I, DESIGN AND TESTING OF SPECIMENS HAVING VARIOUS SIZES (FINAL REPORT ON PHASE I)

REFERENCE 31-2250-6458
CONTRACT NUMBER(S) NAS1-9942

PREPARED BY P. E. Sandorff J. P. Sandifer
P. E. Sandorff J. P. Sandifer

APPROVED BY J. B. Ryan
J. B. Ryan, Group Engineer
Dynamics-Structures Laboratory

APPROVED BY
R. N. Ketola, Department Engineer
Structures Laboratory

APPROVED BY
R. H. Wells, Division Engineer
Structures-Science and Engineering

The information disclosed herein was originated by and is the property of the Lockheed Aircraft Corporation, and except for uses expressly granted to the United States Government, Lockheed reserves all patent, proprietary, design, use, sale, manufacturing and reproduction rights thereto. Information contained in this report must not be used for sales promotion or advertising purposes.

REVISIONS

REV. NO.	DATE	REV. BY	PAGES AFFECTED	REMARKS

FORM 402-2

FOREWORD

This report was prepared under Contract NAS1-9942 for NASA Langley Research Center, Materials Division, under the technical direction of Mr. Edward C. Phillips and Mr. C. Michael Hudson. The work was conducted in the Rye Canyon Research Laboratories, Lockheed-California Company, Burbank, California, and was supported by the technical contributions of many specialists in diverse fields, including:

N. D. Brule	D. W. Hoeppner	J. B. Ryan
W. F. Bush	S. Krystkowiak	D. L. Taylor
V. P. Danford	K. Last (LMSC)	E. K. Walker
J. B. Harlin	C. T. Rollins	F. T. Wimmer

ABSTRACT

Constant amplitude axial load fatigue tests at a stress range ratio of R = 0.02 were conducted on various sizes of unnotched sheet specimens of Ti-6Al-4V titanium alloy and 2024-T3 aluminum alloy, to evaluate size effects and to determine a minimum size suitable for orbital fatigue test work in the Skylab spacecraft. Tests were also conducted to investigate the effects of extremes of humidity and to determine the S-N curve for Ti-6Al-4V material in a vacuum of 10^{-6} torr.

Strong size effects were found at stress levels below the proportional limit, which were in accordance with the statistical theory of strength. Two modes of failure under constant amplitude load were identified in Ti-6Al-4V materials; the mode that was in the very high stress/low cycle range was ductile in nature and not characteristic of fatigue. The effect of vacuum conditions was to reduce the stress level at which the ductile mode occurred by about 5% and to increase the fatigue life under the true fatigue mode by about 60 times. For investigating the effects of space environment, it is recommended that comparison be based on tests of identically sized specimens under normal conditions and in orbit.

Key Words:

Metals: fatigue: test results: size effect: vacuum: constant amplitude: titanium: aluminum: scatter: statistics.

TABLE OF CONTENTS

	Page Number
FOREWORD	ii
ABSTRACT	iii
TABLE OF CONTENTS	iv
LIST OF TABLES	v
LIST OF FIGURES	vii
SYMBOLS	ix
INTRODUCTION	1
SCOPE	2
SPECIMENS	2
TEST APPARATUS	5
GENERAL PROCEDURE	9
EXPERIMENTAL RESULTS	10
ANALYSIS OF TEST RESULTS	15
DISCUSSION	19
CONCLUSIONS	24
APPENDIX: Handling Cleaning and Machining of Titanium Alloy Sheet Material.	26
REFERENCES	29
TABLES	31
FIGURES	55

LOCKHEED
CALIFORNIA COMPANY

LIST OF TABLES

Table 1.	Certificated Properties of Test Materials.	Page 31
Table 2.	Static Tensile Properties of Ti-6Al-4V Sheet Material.	32
Table 3.	Fatigue Specimen Fabrication.	33
Table 4.	Testing Speeds.	34
Table 5.	Estimated Probable (0.67 σ) Errors in Specimen Load.	34
Table 6.	Fatigue Test Data on 0.750-in. Wide Ti-6Al-4V Specimens Tested in Standard 10,000-lb S-N Machine.	35
Table 7.	Fatigue Test Data on 0.750-in. Wide Ti-6Al-4V Specimens Tested in New Low Capacity Fatigue Machine.	36
Table 8.	Fatigue Test Data Obtained at Extremes of Humidity.	37
Table 9.	Fatigue Test Data Obtained on 0.572-in. Wide Ti-6Al-4V Specimens.	38
Table 10.	Fatigue Test Data Obtained on 0.438-in. Wide Ti-6Al-4V Specimens.	39
Table 11.	Fatigue Test Data Obtained on 0.250-in. Wide Ti-6Al-4V Specimens.	40
Table 12.	Fatigue Test Data Obtained on 0.750-in. Wide 2024-T3 Specimens.	41
Table 13.	Fatigue Test Data Obtained on 0.438-in. Wide 2024-T3 Specimens.	42
Table 14.	Fatigue Test Data Obtained on 0.250-in. Wide 2024-T3 Specimens.	43
Table 15.	Fatigue Test Data Obtained on 0.572-in. Wide Ti-6Al-4V Specimens in Vacuum.	44
Table 16.	Fatigue Test Data Furnished by NASA Langley Research Center.	45
Table 17.	Fatigue Test Data on 0.750-in. Wide Ti-6Al-4V Specimens Exchanged Between Laboratories.	46

LIST OF TABLES (Cont'd)

Table 18.	Photographic Crack Propagation Data Obtained in Tests of Ti-6Al-4V Specimens.	Page 47
Table 19.	Observations on Crack Propagation Time in Tests of 0.750-in. Wide 2024-T3 Specimens.	48
Table 20.	Summary of Statistical Properties of Replicate Tests Bearing on Test Conditions.	49
Table 21.	Statistical Tests for Significance of Incidental Variations in Test Conditions.	50
Table 22.	Statistical Tests for Effects of Humidity.	51
Table 23.	Summary of Statistical Properties of Replicate Tests Bearing on Differences Between NASA and Lockheed S-N Determinations.	52
Table 24.	Statistical Tests for Differences in Test Results as Obtained at NASA Langley Research Center and at Lockheed-California Company.	53
Table 25.	Summary of Statistical Properties of Replicate Tests Bearing on Size Effects.	54

LIST OF FIGURES

Figure 1.	Fatigue Test Specimen Details.	Page 55
Figure 2.	Specimen Locations in Sheet Stock.	56
Figure 3.	Typical Sectional Micrographs of Ti-6Al-4V Sheet Material.	57
Figure 4.	Photoelastic Models of 0.750-in and 0.250-in Wide Specimen Geometries Under Static Load in New Low Capacity Fatigue Machine.	58
Figure 5.	Standard 10,000-lb S-N Machine.	59
Figure 6.	Fatigue Test Machines, Schematic.	60
Figure 7.	New Lockheed Low Capacity Fatigue Machine.	61
Figure 8.	Installation of Low Capacity Fatigue Machine in Vacuum Chamber.	62
Figure 9.	Specimen Humidity Control Enclosure.	63
Figure 10.	Typical Ti-6Al-4V Specimens After Fatigue Test.	64
Figure 11.	Typical 0.572 Ti-6Al-4V Specimens After Test.	65
Figure 12.	Typical 2024-T3 Specimens After Fatigue Test.	66
Figure 13.	Crack Propagation in Ti-6Al-4V Specimen 2B8.	67
Figure 14.	Photomicrographs at 100X of Crack in Ti-6Al-4V Specimen 1D24.	68
Figure 15.	Photomicrographs at 500X of Crack in Ti-6Al-4V Specimen 1D24.	69
Figure 16.	Electron Microfractographs of Short-Lived Ti-6Al-4V Specimen.	70
Figure 17.	Electron Microfractographs of Long-Lived Ti-6Al-4V Specimen.	71
Figure 18.	Electron Microfractographs of Ti-6Al-4V Tested in Fatigue under Vacuum.	72

LIST OF FIGURES (Cont'd)

Figure 19.	Inelastic Deformations in Ti-6Al-4V Fatigue Tests.	Page 73
Figure 20.	Failure Locations, 0.750-inch Wide Ti-6Al-4V Specimens.	74
Figure 21.	Failure Locations, 0.572-inch Wide Ti-6Al-4V Specimens.	75
Figure 22.	Failure Locations, 0.438-inch Wide Ti-6Al-4V Specimens.	76
Figure 23.	Failure Locations, 0.250-inch Wide Ti-6Al-4V Specimens.	77
Figure 24.	Failure Locations, 0.750-inch Wide 2024-T3 Specimens.	78
Figure 25.	Failure Locations, 0.438-inch Wide 2024-T3 Specimens.	79
Figure 26.	Failure Locations, 0.250-inch Wide 2024-T3 Specimens.	80
Figure 27.	Location of Fatigue Crack with Respect to Specimen Edge vs. Fatigue Life.	81
Figure 28.	Deviation from Mean Life vs. Distance from Minimum Section (Normalized).	82
Figure 29.	Baseline S-N Data: 0.750-inch Wide Ti-6Al-4V Specimens.	83
Figure 30.	NASA Langley Research Center S-N Data.	84
Figure 31.	S-N Data Obtained at Extremes of Humidity.	85
Figure 32.	S-N Data Obtained on 0.572-inch Wide Ti-6Al-4V Specimens.	86
Figure 33.	S-N Data Obtained on 0.438-inch Wide Ti-6Al-4V Specimens.	87
Figure 34.	S-N Data Obtained on 0.250-inch Wide Ti-6Al-4V Specimens.	88
Figure 35.	S-N Data Obtained on 0.750-inch Wide 2024-T3 Specimens.	89
Figure 36.	S-N Data Obtained on 0.438-inch Wide 2024-T3 Specimens.	90
Figure 37.	S-N Data Obtained on 0.250-inch Wide 2024-T3 Specimens.	91
Figure 38.	S-N Data Obtained on Ti-6Al-4V Specimens Tested in Vacuum Compared with Tests in Air.	92
Figure 39.	Size Effect in S-N Tests.	93
Figure 40.	Distributions of Fatigue Life Data.	94

SYMBOLS

K_t	Geometric stress concentration factor
L	Characteristic length in geometrically similar specimens
N	Test life in cycles of load to failure
R	Cyclic stress range ratio = f_{min}/f_{max}
S	Cyclic stress intensity
SS	Sum of squares of deviations = $\Sigma (X - \overline{X})^2$
X	Test life expressed as logarithm to base 10 of cycles to failure.
$\overline{X}$	Mean of $\log_{10}$ cycles to failure = $\Sigma X/n$
X_M	Median value of $\log_{10}$ cycles to failure
exp	The exponential function
f_{max}	Maximum-peak stress in cyclic loading
f_{min}	Minimum-peak stress in cyclic loading
k	Parameter controlling skewness in Weibull distribution expression
n	Number of replicate tests
p(z)	Probability density, function of z
s	Estimated standard deviation = $\sqrt{\Sigma(X - \overline{X})^2/(n - 1)}$
z	Fatigue life variate expressed in standard deviations; also variate in Weibull distribution function.
Γ	The gamma function
α	Level of significance in hypothesis test
σ	Standard deviation
μ	Population mean

LOCKHEED
CALIFORNIA COMPANY

ORBITAL FATIGUE TESTER FOR USE IN SKYLAB EXPERIMENT T032-PHASE I, DESIGN AND TESTING OF SPECIMENS HAVING VARIOUS SIZES (FINAL REPORT ON PHASE I)

By P. E. Sandorff and J. P. Sandifer
Lockheed-California Company

INTRODUCTION

The overall objective of the Orbital Fatigue Tester program is the design, fabrication and testing of a prototype axial load fatigue testing machine which may operate in the space environment while mounted on the exterior of a Skylab spacecraft. A critical initial problem was the development of a small but meaningful specimen configuration, in order that power, size and weight of the test machine could be minimized. Phase I of the program was concerned with the constant amplitude axial load fatigue testing of variously sized unnotched sheet metal specimens at a stress range ratio R = 0.02 in order to determine an optimum size for orbital test work.

Specific objectives of the Phase I investigation included the following:

1. Calibration of Testing Procedures: Determination of a baseline S-N curve for 0.016 inch thick Ti-6Al-4V titanium alloy sheet material in the range of 10^4 to 5×10^6 cycle life, using full-size (0.750-inch wide) specimens and controlling temperature and humidity to simulate test conditions at NASA Langley Research Center. Comparison of test results with those produced at NASA Langley to determine any systematic differences.

2. Effects of Extremes of Humidity: Determination of any major effects of testing at approximately 100 percent relative humidity (saturated air) and at approximately 0 percent relative humidity (dry argon gas) on the fatigue life of full-size Ti-6Al-4V specimens. Selection of most practical environmental condition for size effects tests.

3. Size Effects Evaluation: Determination of the effect of reduction in specimen size on the S-N properties of 0.016-inch Ti-6Al-4V titanium alloy sheet and 0.032-inch 2024-T3 aluminum alloy sheet material. Selection of the size considered optimum for the Orbital Fatigue Tester.

4. Confirmation of Selected Specimen Configuration Under Vacuum Environment: Establishment of the S-N curve for 0.016-inch Ti-6Al-4V titanium alloy sheet in a vacuum environment of 10^{-6} torr or lower, using the selected size specimen.

LOCKHEED
CALIFORNIA COMPANY

SCOPE

The test program was directed primarily at the determination of S-N properties for the various sizes of test specimens and test conditions. Fatigue loading in all cases was constant amplitude axial load at a stress range ratio R = 0.02; that is, the applied stress varied cyclically from slightly above zero to the specified maximum tensile stress, and test life determinations at various stress levels established the S-N curve. Testing speed ranged within a few percent of 1700 cpm. All test specimens were subject to rigorous cleaning and handling provisions during preparation and prior to testing, and environmental conditions were controlled during tests. Except for the exploratory study of the effects of humidity extremes on results obtained with Ti-6Al-4V specimens, and the tests of Ti-6Al-4V specimens under vacuum conditions, all tests were conducted with relative humidity of the environment controlled to between 65 and 70 percent. Temperature was monitored and remained between 70° and 80°F.

The size effects investigations involved four sizes of 0.016-inch thick Ti-6Al-4V titanium alloy sheet specimens and three sizes of 0.032-inch thick 2024-T3 aluminum alloy sheet specimens. The "full-size" specimen in each case measured 0.750-inch in width at the minimum section; smaller sizes were geometrically similar and ranged down to 0.250-inch. In each series, tests were conducted at 4 or 5 different stress levels, to a total of 24 or more. Assessment of the effects of different specimen sizes and test conditions was provided by statistical analysis.

In addition to the S-N data, variations in the nature of the failures were studied, measurements were obtained of the location and size of the fatigue cracks, and their geometrical distributions were investigated. A number of supporting studies were conducted during the course of the program, including, for example, determination of static tensile properties of the titanium alloy sheet, metallurgical and electron microscope fractographic studies, and crack growth investigations using time lapse photography.

SPECIMENS

Specimen Details

In order to minimize variations due to fabrication and testing, fatigue test specimens were designed to permit the same milling machine set-up to be used in fabrication, and the same test machine and grip arrangement to be used in the testing of a complete series of geometrically similar unnotched flat sheet specimens. Details of the test specimens are presented in Figure 1. The test section of the largest (0.750-inch width at the minimum section) is identical to that of NASA Langley Research Center Drawing Number LB 903380.

Titanium Alloy Material

The Ti-6Al-4V titanium alloy specimens were all cut from two 0.016 x 36 x 128-inch mill annealed sheets, both from Titanium Metals Corporation of America Heat Number K-2263. In the manufacture of this material, a number of sheets in a steel-enclosed sandwich pack are cross-rolled until an individual thickness of about 0.025-inch is reached. Annealing follows, and then about 0.002-inch is removed from each surface of each sheet by a smooth-grinding operation made parallel to the long dimension of the sheet. A brief acid etch is used to remove the outer 0.0005-inch of heavily worked metal. The grind and etch operations are repeated, to obtain a final nominal thickness of 0.016-inch. Properties of the material as certificated by the manufacturer are reported in Table 1.

A pattern was laid out on each sheet comprised of 9 zones subdivided into specimen blanks, as shown in Figure 2. Blanks for static tensile test coupons were included from various zones selected so as to reveal any systematic variation in properties. All specimen blanks were oriented with the long axis parallel to the 128-inch dimension of the sheet. The blanks were identified at both ends with an electric pencil according to the code of Figure 2 and the sheet was then sheared. The blanks were cleaned in hot alkaline solution, rinsed and dried, inspected for scratches, and packaged in clean dry paper. Special handling provisions as outlined in the Appendix were applied from this point, to avoid possible surface damage and contaminant action.

Standard static tensile test coupons having a 0.50-inch constant width section 2.50 inches long were fabricated and tested according to ASTM Standard Method E8-69. The results of these tests are summarized in Table 2. Yield and ultimate strengths were slightly lower than indicated by the manufacturer's tests but not atypical; variation amounted to a maximum of 3.5 percent and showed no consistent relationship to the location of the coupon in the original sheets.

Two sections, one longitudinal and one transverse, were cut from each of eight samples of material selected from various locations in the two sheets, and examined metallographically. The observed microstructure consisted of equiaxed alpha phase (hcp) grains with retained beta phase grain boundaries and triple points, which is typical for annealed Ti-6Al-4V alloy. Representative views are shown in Figure 3. All sections were examined for uniformity of the microstructure with respect to alpha grain size, amount and distribution of beta particles and the absence of inclusions or surface contamination, i.e., alpha case. No defects or abnormal variations of any type were found; the microstructure was typical very fine grain, uniform, and virtually identical throughout the two sheets.

Fabrication of Ti-6Al-4V Specimens

Using a random selection process, the fatigue test blanks were assembled into stacks of 30 to 36 each. The stacks were identified and machined into fatigue test specimens according to Table 3. Machining was performed by a climb milling process intended to remove a substantial and specific amount of material with each chip and thus minimuze local work-hardening and heating. Machining specifications are given in the Appendix.

In machining the first two stacks a 6-tooth cutter was used. Because of minor eccentricities of the cutter as mounted in the milling machine, it was found impossible to hold the desired chip size and still achieve the specified surface smoothness; one tooth of the cutter invariably cut slightly deeper than the others and established the final finish. Surface roughness of the machined edges from these stacks was approximately 170 RHR. For all other stacks, a single-tooth cutter was used with one-sixth the feed rate, resulting in surface finish consistently better than 32 RHR.

After machining, the fatigue test specimens were again alkaline cleaned and inspected. Edges were deburred using several light strokes of 400 grit silicon carbide paper. Dimensions at the minimum width section were determined using a standard micrometer for thickness and a vernier caliper for width, with paper or mylar interposed to prevent any damage to the surfaces of the specimen. (For a limited number of specimens the protective facing was omitted to improve measurement accuracy; however, this resulted in some rejection because of edge nicks.)

Aluminum Alloy Material and Specimen Fabrication

Fabrication of aluminum alloy specimens followed methods in most respects the same as those for the titanium alloy specimens. In this case all specimens were cut from a single 0.032 x 48 x 144-inch sheet of bare 2024-T3 material according to the pattern shown in Figure 2. Specimen axes were "with grain", i.e., parallel to the 144-inch dimension of the sheet, which is the direction of rolling and of a subsequent stretcher-levelling operation which introduces approximately one percent permanent tensile deformation. No static tensile test coupons were made of this material. Manufacturer's certificated properties are reported in Table 1.

The special handling and cleaning procedures outlined in the Appendix were followed as for the titanium alloy except that cleaning was accomplished by a wash and a rinse in methyl ethyl ketone. Specimen blanks were grouped by a random process in stacks of 18 each. Machining was performed on the same equipment and using the same templates and tools as had been used for the titanium specimens; however, no cutting fluid was used when machining the aluminum alloy. Machining was accomplished as reported in Table 3.

Photoelastic Studies of Specimen Loading

In order to confirm the detail design of the test specimens, photoelastic models of the 0.750 and the 0.250-inch wide specimens were fabricated full-size from 0.130-inch thick Photolastic, Inc., PS-1 plastic sheet. These specimens were mounted and loaded in the new low capacity fatigue machine (described in the next section) in exactly the same manner as for the fatigue specimens, except that reduced grip-clamping pressure was used, and static loads were applied using the mean load system in manual override mode. Figure 4 presents photographs of the fringe patterns developed in models under the maximum applied loads of 67.0 and 22.3 lb., respectively.

The highly uniform stress distribution in the test section, free of in-plane shear and essentially identical for both specimens, is evident in the photographs and attests to the accuracy of loading conditions in the fatigue machine.

The geometric stress concentration factor, evaluated approximately from the photoelastic specimens as the ratio of fringe values observed at the edge and at the centerline of the minimum width section, was 1.05 for the 0.250-inch specimen and varied in different trials from 1.06 to 1.09 for the 0.750-inch specimen. These values may be compared with a Neuber notch factor of 1.038, calculated by the method of Ref. 1. The difference between the two specimens is ascribed to different end conditions for the constant-radius test section. In the 0.250-inch specimen, a shear redistribution is permitted by the long length of material between the test section and the friction grips; in the 0.750-inch specimen, this redistribution is prevented by the proximity of the rigid grip plates. The difference in the end conditions, as indicated by the fringe patterns, is evident in Figure 4. Because fatigue failures originated at points scattered over the entire central region of the test section, the difference in stress concentration factor is believed not to influence the size effects comparison.

TEST APPARATUS

Fatigue Machines

Approximately one-half of the fatigue tests of 0.750-inch Ti-6Al-4V specimens were conducted on the "standard 10,000-lb S-N machine" shown in Figure 5. This is a resonant beam type of axial load machine of Lockheed design and construction. Mean load is applied by a screw jack through a coil spring, and excitation is obtained by an eccentric mass driven at a constant speed slightly below resonance, so that fine control of amplitude can be obtained by speed adjustment. Loads are measured and monitored

during the test by means of a calibrated load cell utilizing a compensated electrical resistance strain gage bridge which is placed in series with the specimen, and electronic circuitry which provides rectified and filtered signals proportional to bridge output. A schematic drawing showing the mechanical arrangement of this machine is given in Figure 6. This equipment was used for the first 34 tests of 0.750-inch Ti-6Al-4V specimens under 65-70 percent relative humidity conditions, and for all but one of those tested at extremes of humidity.

The "new low capacity fatigue machine," which was used for all the remaining tests, is an electro-mechanical oscillator which is driven at resonance and is servo-controlled to obtain continuous adjustment of both mean and varying load components. The mechanical system is comprised of two flexible beams flexure-mounted in a tuning fork arrangement; the test specimen constitutes a relatively rigid link between the beam-ends. Mean load is applied to the beams by cantilever springs actuated by a motor-driven ball-screw jack. The beams are excited in the fundamental mode by means of two symmetrically arranged electromagnetic shakers of commercial manufacture. Use of flexure pivots and short-length friction joints minimizes dissipative losses: a "Q" (ratio of power realized to input power) of about 1200 is obtained for the mechanical system. A schematic of this machine is presented in Figure 6; photographs are shown in Figures 7 and 8.

The control and drive system for the machine is packaged in the console shown in Figure 7. A load cell placed in series with the specimen furnishes an electrical signal which is proportional to the instantaneous load in the specimen. The signal is differentiated, amplified, and used to drive the electromagnetic shakers; the amount of amplification is controlled by a servo-loop system which compares the rectified and filtered signal from the load cell with the command value for the varying load. A second servo-circuit compares the strongly filtered and smoothed load cell signal to the command value for the mean load and actuates a relay to operate the mean load motor. Automatic shut-down is provided by a comparator circuit which opens a master relay if the varying load component falls outside a preselected range. Test time is measured by a clock timer operated by the automatic shut-down circuit; speed of cyclic loading was measured for each different specimen size using an electronic pulse counter. Testing speeds are summarized in Table 4.

Several load cells of different ranges are available and were used interchangeably during the tests; these were of Lockheed design and construction, and were calibrated statically using a Baldwin Southwark testing machine, the calibration of which is traceable to the National Bureau of Standards. Each load cell is equipped with two complete strain gage bridges, permitting one to be used in an independent load monitoring system such as an oscilloscope display.

Friction grips of a new short-length design were used in both machines; these featured removeable alignment pins, to position the specimen on the

loading axis, and soft copper grip plates to provide a defined region of load transfer with minimum fretting tendencies. Clamping bolts were first brought up uniformly, to minimize installation stresses, then torqued to a value at least 50 percent above that at which any indications of slip occurred, as determined in preliminary investigations.

The 6.5-inch length of the specimen between grips was lightly supported at two equally spaced intermediate points by soft polymer foam pads, bearing with a few ounces pressure through five mil thick teflon sheeting. The central 2 inches of the specimen remained untouched. The pads were cemented to the environmental control enclosure to be described below, and can be seen in Figure 9. Their purpose was to prevent a "violin-string" mode of resonance observed to occur in the 0.250-inch specimens at about 1900 cps when the varying load was increased to R somewhat less than 0.10, and in the full-size specimens at R = 0.

Estimates of the accuracy of loading obtained with this equipment are presented in Table 5. Except in the case of entries under Uniformity of Stress, these estimates are based on calibration data or on observations of performance made during the course of the program. Estimates of stress due to non-axiality of loading are based on an assumed eccentricity of the load axis of 0.001-inch and a division of the resultant in-plane bending moment between the specimen and the test machine in inverse proportion to their rigidites. Estimates of in-plane bending stress due to installation are based on a typical axial load of 0.15 percent of maximum, observed to be introduced on tightening the grips and assumed to be applied at a 0.50-inch moment arm.

Environmental Control Apparatus

For purposes of humidity control, air from the factory compressed air system was bubbled through a bath of distilled water and fed into a plenum chamber of about 2 cu ft volume. The distilled water bath and plenum chamber can be seen in Figure 5. A commercial hygrometer which used a cord of synthetic fiber as the sensing element was fitted with a light weight leaf-shutter to interrupt a low pressure pneumatic circuit when humidity dropped below the desired level. Standard fluidic control elements (turbulence generator and pneumatic switch) were arranged to utilize this signal and admit saturated air to the plenum chamber. The hygrometer was calibrated against wet bulb-dry bulb readings in actively moving air. The consistently low humidity of ambient conditions at the laboratory made this one-sided servo system adequate for controlling relative humidity to within the range between 65 and 70 percent.

Temperature of the air in the plenum chamber was not controlled but was monitored by thermometer readings every hour or two, except for long running tests which usually ran unattended overnight. In no case during the program was a temperature recorded outside of the range of 70 - 80° F.

The atmosphere of the plenum chamber was circulated to the lightweight specimen enclosure, shown in Figure 9, by means of a small positive displacement air pump. The system arrangement, including the plenum chamber, was such as to establish positive pressure at all possible leakage points. Check tests were conducted which confirmed that relative humidity and temperature in the specimen enclosure were essentially identical to those in the chamber.

For tests under 95-100 percent relative humidity, the same apparatus was used, except that a continuous flow of saturated air was fed to the plenum chamber. Limited heat was supplied to the water bath to make up for evaporative cooling. In the argon atmosphere tests, commercial dry bottled argon was fed directly to the specimen enclosure at a low positive pressure and allowed to escape by leakage.

Crack Propagation Photography

Photographic records of crack propagation were obtained by means of a 16mm Siemens pulse camera using a 50mm f/5.6 lens, arranged so that the critical test section of the specimen filled the field of view. For these tests the upper half of the specimen humidity control enclosure shown in Figure 9 was replaced with one in which was mounted on optical window of low-reflectance coated glass. Illumination was provided by stroboscopic flash equipment triggered simultaneously with the camera shutter. The output of the monitor bridge on the fatigue machine load cell was processed by a pulse shaper and a counting network to obtain a trigger signal for the camera at every 32nd loading cycle. Proper phase relationship so that the picture was taken when the instantaneous specimen load was at its peak was obtained by means of a slip-sinc electronic phasing control and a dual trace oscilloscope. To ensure obtaining records when the crack first appeared, photography was started prior to the lower limit of the established scatter band.

Vacuum Test Apparatus

For the tests of the 0.572-inch Ti-6Al-4V specimens at vacuum the new low capacity fatigue machine was placed inside a small (24-in. dia. x 30-in. long) vacuum chamber. For operation under vacuum the mean load motor and drive train were covered with a hermetically tight enclosure. To minimize air entrapment and outgassing possibilities, only one electromagnetic shaker was used; this produced no change in the operating characteristics, and was adequate for the load involved. A supporting fixture within the chamber and a removeable table outside were arranged so that the machine could be readily withdrawn from the chamber in order to remove and install specimens. Photographs showing this installation are presented in Figure 8.

Vacuum in the 10^{-7} torr range was obtained by a combination of mechanical and diffusion pumps and a "cold wall" lining in the vacuum chamber through which was circulated liquid nitrogen. Chamber pressure was measured with an ionization gage. Radiative cooling of the specimen was prevented by a "warm wall" shroud of 0.050-inch thick aluminum alloy on which electrical resistance heating elements were mounted, and a stainless steel radiation shield, both of which were mounted on the fatigue machine structure. These shrouds can be seen in end view in the lower photograph of Figure 8. Several additional heating elements were mounted on the fatigue machine structure to maintain reasonable operating temperatures, to a total of about 100 watts. Power to the heaters was regulated automatically by a thermostat control, using as a sensor a thermocouple which was held in mechanical contact with one end of the specimen, outside the test section, with a spring clip.

GENERAL PROCEDURE

Prior to the start of the testing program it was recognized that fatigue life could be based either on first observable fatigue cracking or on total specimen failure. Investigations were therefore planned to determine the proportion of the fatigue life which was spent in macro-crack propagation. Even in the largest size specimens, however, it was found that the number of load cycles required for the crack to grow from less than 0.010-inch length to completely across the specimen width was less than 2 percent of the total life. Consequently complete specimen failure was used throughout as the criterion for determining fatigue life.

The first task of the program was concerned with the establishment of a "baseline" S-N curve for full-size Ti-6Al-4V specimens, and with validation of laboratory practices and equipment as being essentially equivalent to those at NASA Langley Research Center. Sixty-four tests were conducted at five different stress levels, which provide statistical bases for judging the consistency and validity of various procedures and equipment. For these tests, specimen environmental conditions were held at 70-80°F and 65-70 percent relative humidity. A comparison was made with the results of similar tests made at NASA Langley Research Center, and a small number of specimens were exchanged between the two laboratories and additional tests conducted in an attempt to separate effects of preparation and testing procedures.

In the second task, 15 tests were conducted at 95-100 percent relative humidity, and 12 under an atmosphere of dry argon gas, to evaluate the effects of humidity extremes. In other respects the tests were identical to those of Task 1, the test points being distributed among 4 different stress levels. Test results were examined to ascertain if humidity extremes

produced any marked changes in properties, particularly in the reduction of test scatter. No effects were found of such significance as to warrant using any different environmental conditions for the balance of the program than those used in the baseline tests. The third task, the study of size effects, was therefore conducted under controlled relative humidity of 65-70 percent.

The size effects investigation was originally planned as a sequential test program in Ti-6Al-4V material, covering a matrix of fifteen reduced-size specimen designs ranging from 0.655-inch down to 0.097-inch width. By starting with 0.250-inch specimens, then selecting larger or smaller sizes consecutively, several series of tests were to be conducted to determine the smallest size specimen which would produce data equivalent, to within a 1σ accuracy and 95 percent confidence level, to that obtained with the full-size specimens. However, after only a few tests of the 0.250-inch specimens, it was evident that a strong size effect existed, and subsequent results indicated that the size effect could be evaluated as a continuous function. Accordingly, a full complement of 24 or more tests were conducted on each of three sets of reduced size titanium alloy specimens. These tests were distributed in larger number to the intermediate stress levels in order to maximize the usefulness of the data: at the highest stress level the size effect was small, while at low stress levels the test life frequently extended beyond the region of specified interest and the tests were discontinued without failure.

Following completion of the size effects tests of titanium alloy, a similar experimental study was made of 2024-T3 aluminum alloy. In this case three different sizes of specimens (0.750, 0.438, and 0.250-inch width) were selected a priori. Test procedures and equipment, as well as almost all aspects of fabrication, were identical to those used in the previous tests of titanium alloy, including the control of specimen environment. During the course of the aluminum alloy tests, a limited number of titanium alloy specimens were tested at random times in order to provide a comparison with previous test results, and to confirm that test conditions had remained essentially unchanged.

On the basis of the results obtained in the size effects studies, the 0.572-inch width was selected as the size of the titanium alloy specimens to be used in the S-N tests under vacuum.

EXPERIMENTAL RESULTS

Fatigue Test Data

Fatigue test data obtained in the course of this program are summarized in Tables 6 through 17. Included are "baseline" S-N data obtained with the two different test machines on 0.750-inch wide specimens of Ti-6Al-4V

LOCKHEED
CALIFORNIA COMPANY

material; tests to determine the effect of extremes of humidity; tests of three reduced sizes of Ti-6Al-4V specimens; tests of full size and two reduced sizes of 2024-T3 specimens; and tests of 0.572-inch wide Ti-6Al-4V specimens under vacuum conditions. Also included are experimental data furnished by NASA Langley Research Center reporting the results of a set of similar tests made on 0.750-inch wide Ti-6Al-4V specimens from another mill heat of material, and test data obtained on specimens exchanged between the two laboratories. In addition to the S-N data, Tables 6 through 15 include measurements of the location of the origin and the size of the fatigue crack, as well as notation of any unusual features.

Nature of Fatigue Failures

Photographs illustrating the general features of the failures obtained in typical specimens are shown in Figures 10, 11, and 12. Except for the instances of an unusual ductile mode of failure described in the next section, failure characteristics were in general similar for the two materials and typical of fatigue failure in high strength, ductile alloys. The region of "slow" fatigue crack growth was readily identifiable by the characteristic flat, bright zone oriented normal to the axis of loading; outside of the beach mark area failure took place in shear fracture, leaving a surface of rough texture. In Ti-6Al-4V specimens, shear fracture planes were oriented approximately 30 degrees to a plane normal to the loading axis; in 2024-T3 specimens, this angle was about 35 degrees. Fatigue failure origins occurred both at the mill-finished sheet surfaces and at the machined edges of the specimens, but in every case, as nearly as could be determined, at an external surface. In Ti-6Al-4V material the origin of the fatigue crack was usually marked by a dark spot, which, however, did not appear dark under high magnification, indicating that the difference in appearance was due to surface texture.

In a number of the specimens of both alloys which were tested at the higher stress levels, multiple fatigue cracks were noted, usually after failure; often several were joined by shear fracture in the final specimen failure. Notations of the number of multiple fatigue origins found in the 0.750-inch width specimens are included in Tables 6, 7, and 13 (notation was not made for the smaller size specimens, although multiple origins did occur). In the majority of cases, however, only one fatigue crack could be found: an indication that the time required for a crack of visible size to propagate to failure was small compared to the variation in fatigue life of the material from point to point.

Crack propagation time was investigated by lapse time photography in tests of six of the 0.750-inch wide Ti-6Al-4V specimens. One of the specimens failed outside the field of view. Figure 13 is representative of the data obtained on the other five. Crack location and size as a function of cycles before failure, measured from the film record, are summarized in Table 18.

No photographic records were obtained in tests of 2024-T3 specimens, but a number of visual observations bearing on crack propagation rate are summarized in Table 19. These tabulated data confirm the general observation, that the time required for a crack to progress from smallest visible size to complete failure was very brief, comprising typically from 0.1 to 2 percent of the total life of the specimen.

Microphotographs of a representative fatigue failure in Ti-6Al-4V material are shown in Figures 14 and 15. The test of this specimen was stopped before the crack progressed to the rapid fracture stage; in Figure 14 it is seen at 100 times magnification, first in the as-tested condition, and second with 0.0002-inch of the surface of the sheet polished away. No etchant was used; the markings on the polished surface are depressions or pits which remain from sheet manufacture. Figure 15 shows the region of the origin at 500 times magnification, in views from above and looking at the fractured surface. The crack did not originate at a pit, and no inclusion or irregularity is evident. This observation is typical; many of the Ti-6Al-4V specimens contained half a dozen or more blemishes (folds or pits) in the central area which were visible under low power magnification, yet no failure was ever observed to originate at a blemish.

Electron microscope fractographs of two Ti-6Al-4V specimens representing the extremes in fatigue life at the 115 ksi stress level are presented in Figures 16 and 17. In each case, all views are from the immediate region of the fatigue origin, as close as permitted by the replication technique. Both cases furnish examples of regular fatigue striations, disrupted by steps and beta particles, interspersed with flat indistinctive areas identified as quasi-cleavage in nature. Both are typical of Ti-6Al-4V; no unusual features are noted, and no significant differences were found in these regions to explain the factor of over 100 times difference in fatigue life.

Ductile Mode of Failure Occurring Under High Stress and Under Vacuum

In the tests of 0.572-inch wide Ti-6Al-4V specimens under vacuum, at stress levels of f_{max} = 125 ksi and above, a ductile type of failure was observed which had none of the usual characteristics of fatigue except that it occurred under cyclic loading. This mode of failure was later duplicated under normal atmospheric pressure conditions with the same type specimen but at a stress level of 137.5 ksi and at a much shorter cycle life.* Gross features of this failure mode are apparent in several of the specimens shown in Figure 11. It is characterized by: (1) an overall specimen elongation of about 0.10-inch, 3 to 10 times that noted ordinarily; (2) substantial necking of the width dimension, to perhaps 90% of the original width, occurring in the central half-inch of the specimen; (3) no identifiable fatigue origin or fatigue crack region; (4) a shear fracture, apparently following a Luders' line, passing almost exactly through the geometrical center of the specimen; (5) a fracture surface rough and

* Under a steady tensile stress of 137.5 ksi, in air at room temperature, similar specimens exhibit creep and fail in stress rupture in several hours.

jagged over most of the central region, changing to a rather smooth, bright surface about 0.04-inch from each edge. In many cases a second Luders' line was visible, crossing the fracture at the center of the specimen. Most of the specimens were warped after failure. Except for localization of the failure zone to the center of the specimen, these characteristics are identical to those observed in the static tensile tests of Ti-6Al-4V material.

Electron microscope fractographs of one of the specimens which failed in the ductile mode under vacuum conditions are shown in the upper two plates of Figure 18. Several replicas were made and scanned but the search revealed no surface pattern except the large tear dimples, which are considered characteristic of highly ductile tensile fracture. These features may be compared with those occurring in a specimen also tested under vacuum but at a slightly lower stress, shown in the two lower plates of Figure 18. The fracture surfaces here are seen to be typical of fatigue, although the striations, interspersed with featureless areas, are unusually light and short.

Plastic Deformation in Ti-6Al-4V Specimens

The overall plastic deformations which occurred during the course of several of the tests of Ti-6Al-4V specimens at high stress levels were determined by noting, as a function of test time, the corrective pulses of the mean load servo-system of the fatigue machine. This system was adjusted to provide automatic compensation for error variations in the mean load exceeding 0.4 percent, by applying displacement increments each amounting to approximately 0.0006-inch motion of the specimen grips. The observations are reduced to a plot of overall inelastic elongation versus number of cycles of applied fatigue loading in Figure 19. Shown as representative are the deformations of specimens failing in the ductile mode, both under normal atmospheric pressure and at vacuum, and a specimen which failed in the "true fatigue" mode. Deformations prior to failure as extensive as those shown in Figure 19 were observed to occur only at the highest stress levels and in Ti-6Al-4V material. In other tests, no large or monotonic corrective action of the mean load was noted until after the appearance of a fatigue crack of visual size in the specimen.

Overall elongation determinations made on the 0.572-inch wide Ti-6Al-4V specimens after failure are included for reference in Tables 9 and 15. These data were obtained by placing the fractured surfaces in contact without overlapping and measuring the distance between alignment pin holes.

Failure Location

The location of the fatigue crack with respect to specimen orientation in the test machine was studied as a check on test irregularities. No consistent pattern was found, either top to bottom, side to side, or favoring

one side of the original sheet stock. All data on crack origins are therefore presented with respect to the coordinates of a quadrant of the specimen. These data are plotted in Figures 20 through 26, together with histograms indicating the distribution of failures widthwise and longitudinally.

Additional studies were made of maximum fatigue crack width as a function of location and fatigue life; however, no distinct pattern was found. A typical representation, as obtained for the 0.750-inch wide Ti-6Al-4V specimens at 110 ksi reported in Tables 6, 7, and 8, is presented in Figure 27.

Other studies were made of the deviation in test life from the mean as a function of the distance of the fracture origin from the specimen minimum section. Again, no strong interrelationship was apparent. Figure 28, which presents data obtained for 0.750-inch wide Ti-6Al-4V specimens from Tables 6 and 8, shows typical results.

S-N Diagrams

The fatigue life data reported in Tables 6 through 16 are plotted against conventional S-N coordinates in Figures 29 through 38. In Figure 29, which presents the results of tests of full-size (.750-inch width) Ti-6Al-4V specimens under 65-70 percent relative humidity, smooth curves representing 10, 50, and 90 percent probability of failure are drawn through the median and fractile points established at each stress level from faired plots of the test data on probability paper. These "baseline" P-S-N curves are included in Figures 30 through 34, to facilitate comparison with other size specimens and other test conditions. Similar baseline curves are derived from the test results obtained with 0.750-inch wide 2024-T3 specimens, Figure 35, and are included in Figures 36 and 37.

On both of these sets of S-N curves, a stress level identified "P.L." marks the approximate stress at which the specimen proportional limit was exceeded, as determined by the behavior of the mean load servo-system during initial test load application in correcting for inelastic specimen extension. For both Ti-6Al-4V and 2024-T3 specimens, stresses in excess of the P.L. value caused plastic deformation only during the first few cycles of load application.

The test results obtained on 0.572-inch wide Ti-6Al-4V specimens under vacuum, Table 15, are plotted in Figure 38 along with the data from Table 9, obtained on similar specimens under normal atmospheric pressure. The vacuum data include results from four tests during which, as noted in Table 15, brief excursions of the chamber pressure to values as high as 11.0×10^{-7} occurred; no correlation with fatigue life is apparent, and all points are therefore included in Figure 38. To aid in making comparisons, S-N curves are faired by eye to fit the median values of the test data at each stress level. The ductile mode of failure is represented for either test condition by a straight line which, if extended,

would pass through the material tensile ultimate stress at 1/4 cycle. Tests under vacuum at stress levels below f_{max} = 125 ksi are too few to establish the S-N relationship for the true fatigue mode; it appears, however, that the slope of the curve may change with the mode of failure as it does in the case of tests under normal atmospheric pressure, and this suggestion is indicated in the diagram.

ANALYSIS OF TEST RESULTS

Statistical Properties

Statistical analysis is helpful in evaluating test data when, as in the present program, test scatter tends to obscure the results. Such analyses do not furnish absolute indications, but provide statements regarding the probabilities involved. Usually these are in a form such as, "The difference between the two groups is significant at an α level of 0.05," which means that if the two groups were assumed to be different, the chance of error would be only 5 percent (Ref. 2, p. 91, for example).

Fundamental to such analyses is the assumption that all variables bearing on the experiment contribute in a random way to the experimental error, i.e., to the scatter. In the present case these variables include basic material variations, the many controlled test conditions within the limits of control, and possibly some unknowns. In accordance with generally accepted practice the logarithm to base 10 of cycles to failure is used as the variate (Ref. 3, 4). The effect of a particular set of test conditions is characterized by the mean of all possible test results (μ), and the scatter by the standard deviation (σ). The limited number of tests conducted in each case comprises a sample, which provides estimates of the mean and standard deviation ($\bar{X}$ and s). The accuracy of these estimates depends on the number of tests in the sample and the extent of the scatter.

For hypothesis testing, replicate data on log of test life is assumed to be normally distributed. Actually, if material variability is the cause of scatter, each specimen is a "weakest link" determination, and according to Gumbel (Ref. 5), the resultant distribution of test results is given by an extreme (smallest) value distribution function. As will be seen in a following section, distributions obtained in this program may be approximately fitted by such functions. However, Stagg (Ref. 6), after a thorough review of the literature on fatigue test scatter in aluminum alloys, found inadequate justification for using other than the normal distribution. For practical purposes this practice is followed here, but it is recognized that non-normality of the distribution reduces the confidence level of the statis-

LOCKHEED
CALIFORNIA COMPANY

tical tests, particularly for cases involving unequal sample numbers and for inferences regarding the variance (Ref. 7).

Treatment of Run-Out (No Failure) Points

At the lowest stress level in each group, one or more tests frequently exceeded the practical range of interest and testing was discontinued without failure. In these cases a special analysis, shown in Ref. 8 as the method of maximum likelihood for Type I censoring, which in effect employs the other test data at that stress level to help predict the test life of the run-out points, is applied to obtain an improved estimate of the mean. The strength of this determination, of course, is less than if based on actual failure points, and the process itself may suffer degradation because it involves the assumption of normality of distribution. Data at the lowest stress levels, therefore, has not been used in making direct comparisons of different treatments.

Effect of Incidental Variations in Test Conditions

The program was not designed to study the effect of different machining methods, different test machines, or extended periods between tests; but these variations were nevertheless introduced by practical considerations. A number of directly comparable test data are available for evaluating their effect; these data are summarized in Table 20.

In Table 21 statistical tests are applied to determine whether any change in the mean value or the extent of scatter resulted from the differences in test conditions. No strong indications of any changes are found; i.e., significant at $\alpha = 0.05$. Most of the comparisons indicate that differences, if they do exist, are not large compared to the basic experimental error.

Similar conclusions are reached by making S-N plots for each condition, which provide comparisons of a broader array of data although qualitative in nature. As a consequence, these variations in testing method are ignored in further evaluations, and all test points obtained under otherwise similar conditions are grouped together as replicates.

Effects of Extremes of Humidity

The experiments directed at determining the effects of wide humidity variations on the S-N properties of Ti-6Al-4V are summarized in Table 20 and evaluated in Table 22. For this purpose all test data at the stress levels 130, 110, and 105 ksi are pooled together; the means and variances derived under the 65-70 percent relative humidity condition being used as reference

values to normalize those obtained under humidity extremes. While this method conceals possible effects of stress level, and the normalized means and variances so derived provide only an approximation for measuring the effect of the test variations, the comparisons are statistically stronger for revealing overall, unidirectional effects.

The significance tests in Table 22, Part B indicate insufficient evidence for assuming that use of either saturated air or dry argon atmosphere resulted in a general change in the amount of test scatter, as compared with the 65-70 percent relative humidity test environment. The analysis of variance in Part C provides strong indication that no sizeable shift in the S-N relationship was produced by either of the humidity extremes.

Because of the limited number of tests conducted in this study, environmental effects below a certain size but possibly important for other purposes could remain undetected. For example, a check for β- error by the method of Ref. 2, Page 107 indicates a 50-50 chance that the scatter was actually increased or decreased by 70 or 80 percent by the extreme humidity conditions, even though the analysis furnishes no strong indication that a change occurred.

Comparisons With Tests at NASA Langley Research Center

The statistical parameters for the tests conducted at NASA Langley Research Center, and for the data obtained with the test specimens exchanged between NASA and Lockheed-California Company, are summarized in Table 23. Statistical tests which compare the S-N data obtained at the two laboratories are summarized in Table 24.

Comparisons of the S-N data indicate that, at stress levels of 115 and 110 ksi, the Lockheed baseline data showed less scatter than the NASA investigation, and at all stress levels, the Lockheed data showed lower mean life determinations. These differences are believed to have been caused chiefly by differences in the basic material properties of the two heats of Ti-6Al-4V material used in the two investigations.

Statistical tests which compare the S-N data obtained by NASA at the 110 ksi stress level with data from the group of three specimens prepared by NASA and tested at Lockheed, indicate that Lockheed test methods result in less scatter; no difference in mean life is discernible at the 95 percent confidence level. Statistical tests which compare the baseline S-N data obtained by Lockheed with data from the group of five specimens prepared by Lockheed and tested by NASA, indicate Lockheed test methods produce less scatter and a lower mean life. These inferences indicate that test procedure may have contributed to the differences observed in the overall S-N determinations. However, as previously noted, the confidence level of these tests is reduced by non-normality of the distribution and unequal sample numbers.

Size Effects

Statistical properties of the test results bearing on size effects are summarized in Table 25. Increases in the mean of log life and in the standard deviation of the test groups, normalized with respect to the standard deviations determined for the full size specimens, are tabulated for each stress level. These data are plotted in Figure 39 against the geometric reductions in specimen size as the abscissae.

Also shown in Figure 39 are curves which indicate theoretically predicted size effects due to material variability according to a solution presented by McClintock in Ref. 9. This treatment assumes that there are multitudinous flaws or weak spots of varying strength distributed randomly throughout the specimen, and that the probability of failure consequently varies with life according to a Gumbel asymptotic extreme (smallest) value distribution of the third kind (also known as the Weibull distribution, Refs. 3, 4, 5). An additional assumption of McClintock's development is that the stress on any cross section of the specimen is uniform and given by load divided by area; the solution for size effects appears valid for two dimensional stress distributions such as noted in the test specimens of this program as long as geometric similarity is preserved. The predicted size effects for geometrically similar specimens are:

$$\frac{\sigma_2}{\sigma_1} = \left[\frac{L_1}{L_2}\right]^{\frac{4}{2k+1}}$$

$$\frac{\mu_2 - \mu_1}{\sigma_1} = \frac{\Gamma\left(1 + \frac{2}{2k+1}\right)}{\left[\Gamma\left(1 + \frac{4}{2k+1}\right) - \Gamma^2\left(1 + \frac{2}{2k+1}\right)\right]^{1/2}} \frac{\sigma_2 - \sigma_1}{\sigma_1}$$

where the subscripts 1 and 2 relate to differently sized specimens, L_2/L_1 is the scale factor, Γ is the gamma function and k is an exponent in the distribution function which is indicative of the skewness in the distribution of material variability.

Histograms of Fatigue Life Data

Figure 39 indicates that size effects are related to material variability as characterized by the parameter k in the Weibull distribution function. The substantially different size effects occurring at different stress levels consequently must reflect changes in the statistical distribution of the fatigue life data.

To investigate these distributions, the data on fatigue life obtained at the different stress levels and for the two materials are plotted in histogram form in Figure 40. The variate used to combine data from differently sized specimens at the same stress level is the deviation from the median measured in standard deviations:

$$z_{ij} = (X_{ij} - X_{Mj}) / s_j$$

where X_{Mj} and s_j are the median and the estimated standard deviation which apply to the group of log test life data obtained at a specific specimen size j. This procedure is not rigorous and is justified only as a step in improving the data display.

Also plotted in Figure 40 are the theoretical distributions which would be produced by material variability effects according to the third asymptotic distribution of smallest values or Weibull distribution (Refs. 3, 10):

$$\text{frequency } (z) = p(z)(z_a - z_o) = k \left(\frac{z-z_o}{z_a-z_o}\right)^{k-1} \exp\left[-\left(\frac{z-z_o}{z_a-z_o}\right)^k\right]$$

where z_o is a lower cut-off corresponding to a postulated limiting flaw size, z_a is a parameter indicative of the spread of the distribution identified as the life at which (1-1/e) (i.e., 63.2 percent) of the population have failed, and p(z) is the probability of failure occurring at the value of z. These curves were constructed with median values equal to those of the histograms, using the values of k indicated by the size effects comparisons of Figure 39, and the values of (z_a-z_o) were established to provide total areas under the curves equal to those under the histograms.

DISCUSSION

Size Effects

Size effects in fatigue testing are recognized as arising from numerous sources: variability of material strength (i.e., macro-) characteristics from point to point, heterogeneity of crystalline (micro-) structure, lack of similitude of stress concentration effects, lack of similitude of the surface layer affecting both microscopic stress concentrations and material strength characteristics, and interaction of grain structure with plastic deformation effects such as slip lines (Refs. 4, 8, 11, 12). To these may be added a variety of interactions with environment, thermal effects, specimen manufacture and control of test load and test conditions.

Figure 39 indicates that in the present program material variability is a source of size effects at low and intermediate stress levels. For Ti-6Al-4V specimens at f_{max} = 105, 110, and 115 ksi, and for 2024-T3 at 45 ksi, both the amount of test scatter and the mean of the test data show large increases when specimen size is reduced.

In analyses to predict these effects, the material is usually modeled as a strong matrix containing many flaws or weak points, ranging in strength down to a lower limit. In large-sized specimens, the probability of including at least one flaw of minimum strength is high, consequently scatter is small and the mean value approaches a lower bound. The smaller the specimen, however, the less satisfactorily does it represent the total range of material properties; therefore, small specimens lead to an increase in test scatter and an increase in the mean of the test data. These effects are noted frequently in the literature; for example, Ref. 6 (limited evidence of increased scatter in smaller specimens); Ref. 11 (scatter and location of S-N curve for steel specimens reduced with increase in size); and Ref. 13 (decrease in cycles for crack initiation with increase in size).

The size effects noted in Figure 39 for Ti-6Al-4V at a stress level of 105 ksi are not as strong as those occurring at 110 and 115 ksi, and a larger value of the distribution parameter k is noted. These results indicate either that different crack nucleation sites are involved, or that the same sites respond differently, possibly because of the proximity of the endurance limit. At the other extreme of the S-N diagram; that is, at stresses which exceed the proportional limit, the test data indicate no consistent pattern of size effects. Included are the results of tests of Ti-6Al-4V at f_{max} = 130 ksi, and 2024-T3 at 50 and 55 ksi. There is negligible size effect on test scatter; the mean life is actually reduced for intermediate sizes but not for the smallest size specimens. This change may be associated with plastic deformation effects which occur at the higher stresses, possibly increasing the number of crack nucleation sites as suggested in Ref. 6, or introducing damage into existing sites so that all are essentially equal at the start. A further possibility is that other size effects occurred, such as might be caused by differences in the degree of restraint to slip line formation, to produce the total result seen in Figure 39.

Fatigue Test Scatter: Extent and Distribution

In Ref. 6, a comprehensive statistical study was made of test scatter in constant amplitude fatigue test data reported for aluminum alloys in the literature. General agreement exists between the observations of that source and the results obtained in the present study. The amount of scatter obtained in the fatigue life data for the 0.750-inch wide specimens appears to be not a great deal larger than the variation in material static tensile properties. (A rough comparison may be made on the basis of the

standard deviation of the tensile strength data from Table 2, and the vertical distance between the 10 and 90 percentile curves of Figure 29, which would be 1.28 σ for a normal distribution.)

While the increased scatter observed for the smaller size specimens is attributed to material variability, the limited studies made here revealed no physical explanation for such variability. Particularly for Ti-6Al-4V material, some metallographic studies were made, and all fractures were studied at low magnification, yet it was not possible to identify defects in metallurgy or structure as the cause. The limited data on propagation of cracks of visible size (Tables 18 and 19) indicate considerable irregularity; if the same variability applies for the micro-crack stage it may account for a substantial part of the scatter. However, this program furnishes no data on the relative portions of the fatigue life spent in crack nucleation (dimensions less than about 10^{-5} inch) and micro-crack propagation.

The fatigue life data, displayed in histograms in Figure 40, are insufficient in number to define statistical distributions. However, some of the characteristic properties of the histograms are seen to be represented quite well by the theoretical curves which are based on the Weibull distribution function, using values of k indicated by Figure 39. For distributions which are fitted by mathematical curves corresponding to small values of k , the implication of the Weibull distribution is that flaws vary in strength above a certain minimum value (Ref. 3, 4). In the original sheet material, the fatigue life would in this case vary randomly from point to point but never be less than a lower limiting value corresponding to z_o. This condition appears to apply, approximately, to Ti-6Al-4V at the 115, 110, and 105 ksi levels, and to 2024-T3 at 45 ksi.

For those cases which are fitted by large values of k; viz., fatigue tests of both materials at the highest stress levels, the parameter z_o becomes a negative quantity. The resulting distribution might then be interpreted as approximating the first asymptotic distribution of smallest values, as shown in Ref. 10. This distribution would be applicable when material variations in the original sheet stock followed a normal or an exponential distribution. Other interpretations, however, may be suggested; for example, the effects of material variation are too small to measure, or are obscured by larger, unknown factors.

Crack Origin Location

The considerable data on location of the fatigue origin and fatigue crack size and life displayed in Figures 20 through 28 furnish few indications of strong interrelationships such as might be expected from Ref. 4 and 9. A general trend is seen of increasing numbers of failures in the region of the specimen minimum section, but from Figure 28, this trend does not correlate with fatigue life. Figure 27 indicates no relationship between edge distance, size of fatigue-cracked region, and fatigue life.

The predominance of edge failures for tests of 2024-T3 specimens is apparent in Figures 24 through 26; it contrasts with the relatively few edge failures obtained in Ti-6Al-4V specimens, shown in Figures 20 through 23. As noted previously, the stresses in the specimen are maximum at the edges, and edge failures should be expected. However, a marked amount of work-hardening occurs in Ti-6Al-4V material under the machining process (Ref. 14). It appears this may have improved the edges of the Ti-6Al-4V specimens so that they were no longer critically stressed. The next critical region, as may be seen from the photoelastic studies of Figure 4, is a broad area extending far to either side of the minimum section. This type of stress distribution would not produce well-defined trends in failure location.

Vacuum Effects on Fatigue Properties of Ti-6Al-4V

The effect of vacuum on the S-N properties of Ti-6Al-4V, as seen from Figure 38, is to reduce the stress level for the occurrence of the ductile mode of failure under cyclic loading, and at the same time to increase the fatigue life for failure in "true fatigue"; i.e., by crack formation and propagation. The considerable increase in fatigue life is similar to that observed for other metals and alloys (see Ref. 15, for example) and in accordance with limited published data on Ti-6Al-4V material tested under different loading conditions (Ref. 16).

Marked increase in ductility is also generally found to result under vacuum of about 10^{-5} torr or less (Ref. 16, 17). While substantial differences in plastic behavior were noted between tests in vacuum and air in the present program, there was no marked difference in the overall elongation after failure for specimens failing in the same mode (from comparison of elongation data in Tables 9 and 15). Also, the number of cycles which produced the first measurable plastic deformation in fatigue tests at high stress levels under vacuum was greater than for comparable tests under air. Figure 19 presents a typical comparison at a stress level of f_{max} = 130 ksi. In this case, however, the modes differed, and plastic deformation in the vacuum test, once started, progressed much more rapidly and soon exceeded by many times that which occurred in air at the same stress level.

These effects, and the incidence of the ductile mode of failure, are probably peculiar to the constant load-amplitude test. Under constant strain-amplitude, which is often used for tests in vacuum, as well as for low-cycle fatigue tests, initial plastic deformation relieves the peak stress and subsequent cycling is elastic in nature. Under constant load-amplitude, however, the reduction in section area which results from plastic deformation causes an increase in the true stress. Thus the minute amount of slip occurring under each load application becomes larger with each cycle of loading until finally plastic instability results.

In the static tensile test, the stress for plastic instability is a direct function of the slope of the true stress-true strain curve, i.e., of the strain-hardening rate (Ref. 18). The effect of vacuum, therefore, in

depressing the stress level at which the ductile mode occurs, may be to reduce the strain-hardening capability of the material. Such an effect has been noted in tests of magnesium monocrystals in Ref. 17. Reduction in the plastic instability stress may also have resulted from a reduction in the proportional limit, although, from Figure 19, this does not seem to have occurred.

Various mechanisms have been suggested to explain the improved fatigue performance of metallic materials in vacuum, such as cold welding of surfaces at the tip of a fatigue crack, or a decrease in deleterious interaction between the material and the environment (e.g., atmospheric corrosion) (Ref. 15). A mechanism proposed in Ref. 16 and 17 which also appears to fit the effects observed here, is that in a contaminating environment a surface film, formed on any new surface created by deformation processes, acts to pin dislocations and cause dislocation pile-up, thus promoting work-hardening and providing sources for crack nucleation. In vacuum, the absence of the surface film is said to facilitate dislocation egress and provide conditions more conducive to slip than to crack formation; in crack propagation, it may lead to blunting of the crack tip.

The electron microscope fractographs presented in Figure 18 may be compared with the results obtained by Pelloux (Ref. 19), who found no striation formation during the process of fatigue crack propagation in vacuum. As can be seen in the surfaces of Specimen 2D16, striations were formed in Ti-6Al-4V under fatigue at 10^{-6} torr. The growth rate seen here is about 0.3 microns per cycle. However, the striations are shorter and much less distinct than those formed under normal atmosphere, Figures 16 and 17, and thus do not contradict Pelloux's contention that striation formation is the result of environmental action at the crack tip.

Specimen Size for Tests on Orbit

The weight, size, and power requirements of fatigue test equipment to be used on orbit in Skylab experiments will vary in direct relation to the size of the test specimen. On this basis the smallest size specimen compatible with the problems of handling, fabrication tolerances, and precision of measurement would be the most advantageous.

However, the increase in test scatter which is found to occur in smaller size specimens makes necessary a corresponding increase in the number of tests which must be conducted (in proportion to the square of the standard deviation) in order to obtain the same precision and confidence level in determination of S-N data, as is obtained with full-size specimens. For example, in the case of a reduction in the size of Ti-6Al-4V specimens from 0.750-inch to 0.438-inch width, the increase in estimated standard deviation at intermediate stress levels noted in Table 25 would impose either a ten times increase in number of tests required, or a degradation in precision of the data. The trade-off factors in utilization of Skylab are not studied here; however, the penalties associated with reduction in

specimen size to less than 0.572-inch width appear to be severe even for ordinary laboratory practice.

In addition, the possibility that the mean of the log of test life may change when specimen size is changed introduces questions of interpretation and validity of test data. While the results of this program provide a measure of the effects occurring in the materials tested, there is the possibility that material variability, surface effects, and other size effects may be different for tests conducted in vacuum. To evaluate the effect of space environment, it therefore appears necessary that comparisons be based on tests utilizing specimens of identical size and shape in the ground-based laboratory and in orbit.

CONCLUSIONS

Size Effects

A substantial size effect occurs in unnotched 0.016-inch thick Ti-6Al-4V and 0.032-inch thick 2024-T3 sheet specimens tested under constant amplitude fatigue. The effect involves both an increase in the mean value of the logarithm of cycles to failure, and an increase in the amount of test scatter, for smaller size specimens, when tested at stresses which do not exceed the proportional limit of the material.

Specimen Size for Orbital Tests

Chiefly because of the increased scatter which occurs in test results obtained with smaller size specimens, and which either increases the number of tests required or reduces the precision of the results, use of specimens smaller than 0.572-inch in width appears inadvisable. Even with this reduction to 3/4 of the "full-size" specimen, some size effects are evident, and under vacuum others may be introduced which were not evaluated here. Comparisons between orbital test data and ground test data should, therefore, be based on identically sized specimens.

Theoretical Explanation for Size Effects

The size effects observed at fatigue stress levels below the material proportional limit fit the predictions of a statistical theory of strength, which assumes material variability resulting in a probability of failure vs. log of test life according to an asymptotic extreme value (Weibull) distribution. The actual test data distribute in histograms which also agree in their general features with the mathematical distribution functions. The magnitude of the size effects, and the shape of the distributions, change

with fatigue stress level. At stress levels exceeding the proportional limit, size effects due to material variability were either small and irregular, or other sources were equally large and compensating.

Effects of Variations in Relative Humidity

No major change in either the test scatter or the mean of the test life could be attributed to variation in the relative humidity of the test environment, as obtained by using dry argon gas, factory air humidified to 65-70 percent relative humidity, or factory air saturated (95-100 percent relative humidity). These tests were limited in number, however, and differences below a certain magnitude could go undetected.

Effects of Vacuum on the S-N Properties of Ti-6Al-4V Material

The observed effects of vacuum of 10^{-6} torr on the fatigue performance of Ti-6Al-4V specimens in the constant amplitude-load fatigue tests conducted here included an increase in fatigue life as well as a reduction in the stress level at which a plastic instability type of failure occurred. Two distinctly different modes of cyclic load failure, "true fatigue" and "ductile" both of which occurred in air, occurred also in vacuum but were displaced in S-N coordinates. The true fatigue mode (i.e., crack formation and propagation), which established the entire S-N curve above about 10^4 cycles in air, was displaced out to beyond 10^6 cycles in vacuum tests. The ductile mode (shear fracture with large elongation and no crack propagation) was found only in the very high stress-low cycles range in air, but in vacuum it occurred at stresses of between 125 and 130 ksi and provided S-N data ranging from 10^4 to 10^6 cycles.

Comparison of S-N Data With That Produced at NASA Langley Research Center

Appreciable differences were found, both in the amount of test scatter and in the mean of the test life, between S-N tests conducted at NASA Langley Research Center and those conducted at Lockheed-California Company. The differences are not surprising in view of the fact that the sheet materials being tested came from two different mill heats. Some indications were found that unidentified differences in test procedure may also have contributed to the differences in results.

APPENDIX

HANDLING, CLEANING AND MACHINING OF TITANIUM ALLOY SHEET MATERIAL FOR FATIGUE TEST COUPONS

Handling

Special care is to be taken at all times in handling of coupon materials to prevent scratches, abrasion, marring of the specimen surfaces, or exposure to possible contaminants such as halogens, acids, and normal secretions of the human skin. Sheet materials are to be separated by clean dry paper, not adhesive backed, during all handling operations and during storage. Subsequent to initial cleaning, clean white cotton gloves are to be used when handling specimen materials. Specimens or materials which by any chance have become marred or scratched in the test section, or are suspect of contamination, are to be discarded.

Cleaning

Titanium sheet material shall be cleaned only with solvents and an alkaline cleaner specified herein. In no case shall chlorinated or chloride- containing solvent or cleaner be used under any condition. Abrasive cleaning methods shall not be used at any time. Acid pickling is not to be employed at any time.*

Solvent cleaning shall be used to remove contaminants such as oil, grease, ink, dust, and fingerprints from sheet surfaces if necessary just prior to alkaline cleaning. Hand solvent wiping shall be accomplished with clean cloths or soft paper.

After shearing of blanks and after machining of specimens, hot alkaline cleaning shall be employed. The cleaning agent shall be a water-soluble, non-electrolytic type such as Wyandotte ALTREX 1077 silicated cleaner.

Following initial cleaning, special handling provisions as previously described are to be used to protect the material from damage and contamination and to maintain it in a clean condition.

* It is recognized that a controlled acid pickling treatment is customarily used in the manufacture of titanium sheet material, prior to receipt at the laboratory.

Machining

Normal shop practices for the machining of titanium alloys shall be employed, with the following specific notes:

1. Cleaning and "white-glove" handling procedures noted above are to be followed.

2. No inks, cutting fluids, or other materials which are either chlorinated or acidic in nature are to be used at any time.

3. Cutting fluids are to be clean and fresh, and are to consist of a diluted sulfonated petroleum oil made water miscible with an emulsifying agent.

4. Scratches and scribe marks in the central region of reduced width identified as "critical" are not permitted.

5. All longitudinal sheared edges are to be machined off a minimum of 0.060 inch.

6. Machined surfaces in the critical test section are to have a surface finish of RHR32 or better.

7. Shop will not deburr reduced sections or holes. Specimens are to be deburred in these areas by Laboratory personnel using 400 grit or finer silicon carbide paper.

8. Specimens are to be machined (milled) in one inch maximum stack-up using 0.25-inch thick 160-180 ksi heat treated back-up plates which have been ground flat to a maximum surface roughness of RHR 32.

9. Specimens are to be milled in a vertical milling machine, Gorton 230 Automatic Tracemaster, with specimen shape established by master template.

10. End mill used is to be BRUBAKER-GEMINI A6 series end cutter of 3/4 inch diameter.

11. Work to be machined must be held rigidly. Setup must be sufficiently rigid so that there is no measurable deflection of end cutter during the machining operation.

12. Cutter must be kept sharp and smooth.

13. Climb cut, not conventional, is to be used.

14. Tooth load (initial bite) is to be a minimum of 0.005-inch per tooth per revolution.

15. Surface speed is to be approximately 40 feet per minute.

16. Depth of last cut is to be 0.005 - 0.008-inch to produce a surface finish of RHR 32 or better.

17. Absolutely no dwell is allowed when making cuts in critical reduced section.

18. No touch-up or smooth-up of machined surface is permitted. No grinding is allowed anywhere on fatigue specimen.

REFERENCES

1. H. Neuber, Theory of Notch Stresses, Springer Verlag, 1958, translation, AEC-tr-4547, 1961.

2. W. J. Dixon and F. J. Massey, Jr., Introduction to Statistical Analysis, McGraw Hill, 1957.

3. Anon., A Guide for Fatigue Testing and the Statistical Analysis of Fatigue Data, ASTM STP 91A, Amer. Soc. Testing Mat'ls., 1963.

4. W. Weibull, Fatigue Testing and the Analysis of Results, Pergamon Press, 1961.

5. E. J. Gumbel, Statistical Theory of Extreme Values and Some Practical Applications, Nat'l Bur. St'ds App. Math. Series No. 33, 1954.

6. A. M. Stagg, An Investigation of the Scatter in Constant Amplitude Fatigue Test Results of Aluminum Alloys 2024 and 7075, C.P. No. 1093, Gt. Brit. Royal Aircraft Establishment, April 1969.

7. H. Scheffe, The Analysis of Variance, Wiley and Sons, 1959.

8. H. A. David, Order Statistics, John Wiley and Sons, 1970, p. 112.

9. F. A. McClintock, The Statistical Theory of Size and Shape Effects in Fatigue, Jr. App. Mech., Trans. ASME, Vol. 77, 1955, p. 421-426.

10. A. M. Freudenthal and E. J. Gumbel, Distribution Functions for the Prediction of Fatigue Life and Fatigue Strength, Proc. International Conference on Fatigue of Metals, Institution of Mechanical Engineers/ ASME, London/New York, 1956, p. 267-271.

11. R. D. Vagapov, The General Theory and Methods of Evaluation of the Scale Effect in Cyclic Loading, translated from Zavodskaya Laboratoriya (Industrial Laboratory), Vol. 26, No. 9, Sep 1960, p. 1108-1116.

12. W. L. Phillips and R. W. Armstrong, The Influence of Specimen Size, Polycrystal Grain Size, and Yield Point Behavior on the Fatigue Strength of Low Carbon Steel, J. Mech. Phys. Solids, Vol. 17, 1969, p. 265-270.

13. W. Weibull, Size Effects on Fatigue Crack Initiation and Propagation in Aluminum Sheet Specimens Subjected to Stresses of Nearly Constant Amplitude, Aeronautical Research Inst. of Sweden, FFA Report 86, 1960.

14. W. P. Koster, Surface Integrity of Machined Structural Components, AFML-TR-70-11, March 1970.

15. C. M. Hudson, Problems of Fatigue of Metals in a Vacuum Environment, NASA TN D-2563, Jan. 1965.

16. H. Shen, Effect of Vacuum Environment on the Mechanical Behavior of Materials, AFOSR 68-0371, Dec. 1967.

17. H. G. Nelson and D. P. Williams, The Effect of Vacuum on Various Mechanical Properties of Magnesium, SAMPE Proceedings, Vol. 11, April 1967, p. 291-297.

18. A. Nadai, Theory of Flow and Fracture of Solids, McGraw Hill, 1950.

19. R. M. N. Pelloux, Mechanisms of Formation of Ductile Fatigue Striations, Trans. A.S.M., Vol. 62, 1969, p. 281-285.

TABLE 1. CERTIFICATED PROPERTIES OF TEST MATERIALS

Ti-6Al-4V Titanium Alloy

Description

.016 x 36 x 128 sheet annealed to MIL-T-9046F Type 3 Comp C
Heat No. K-2263, Titanium Metals Corp of America

Chemical Analysis

.022 C	6.0 Al
.12 Fe	4.2 V
.010 N	.006-.007 H

Mechanical Properties

	Yield Str	Tens Str	Elong	Bend Test
Typical	136,800	148,000	10.0	4.0
Low	134,700	144,200	9.0	4.0
High	145,000	154,500	11.0	4.0

2024-T3 Aluminum Alloy

Description

.032 x 48 x 144 bare aluminum alloy sheet, QQ-A-250/4
manufactured by Aluminum Company of America.

Chemical Composition

1.20 - 1.80 Mg	3.80 - 4.90 Cu
0.50 Max Si	0.30 - 0.90 Mn
0.10 Max Cr	0.25 Max Zn
0.50 Max Fe	0.15 Max Others

Mechanical Properties

64000 min. tensile strength
42000 min. tensile yield
15 percent min. elongation

LOCKHEED
CALIFORNIA COMPANY

TABLE 2. STATIC TENSILE PROPERTIES OF Ti-6Al-4V SHEET MATERIAL

(All Coupons parallel to 128 inch sheet dimension)

Specimen Identification	Tensile Yield Stress (ksi)	Tensile Ultimate Stress (ksi)	(% in 2 in)
1AT3	136.7	143.3	10
1AT4	134.0	141.7	10
1CT3	131.3	136.3	11
1CT4	133.3	141.3	11
1DT2	134.4	139.4	11
1DT3	134.0	138.9	11
1ET1	138.1	145.0	12
1ET3	135.0	141.9	11
1FT1	136.3	141.9	12
1FT4	136.3	142.5	11
1FT5	134.4	140.0	10
1GT1	140.7	146.4	11
1GT2	131.3	138.3	9
1IT1	136.7	142.7	13
1IT2	136.0	143.3	12
2CT3	131.3	138.1	13
2CT4	136.7	142.7	11
2DT2	133.1	138.1	11
2DT4	138.1	143.8	10
2ET1	140.0	145.0	13
2ET3	138.8	144.4	12
2FT1	-	136.0	12
2FT2	132.3	138.8	12
2FT5	131.2	136.5	10
2GT1	134.0	139.3	10
2GT2	136.0	142.0	11
2IT1	138.0	145.3	12
2IT2	137.3	144.0	9
Mean	135.38	141.32	
Std dev'n	2.64	2.95	

TABLE 3. FATIGUE SPECIMEN FABRICATION

Material	Stack No.	Week Machined	Dimensions of Minimum Section*		
			Nominal Width	Actual Width Range	Actual Thickness Range
Ti-6Al-4V	1	7/24/70	.750	.745 - .751	.0140 - .0160
	2	7/24/70	.750	.745 - .753	.0150 - .0165
	3	7/24/70	.250	.245 - .247	.0148 - .0163
	4	7/31/70	.750	.736 - .744	.0144 - .0165
	5	10/30/70	.438	.402 - .407	.0140 - .0164
	6	11/6/70	.438	.434 - .438	.0145 - .0166
	7	11/20/70	.572	.570 - .575	.0148 - .0167
	8	2/5/71	.572	.562 -.567	.0146 - .0165
2024-T3	1	1/22/71	.750	.753 - .756	.0329 - .0336
	2	1/27/71	.750	.750 - .753	.0327 - .0335
	3	1/27/71	.750	.750 - .753	.0330 - .0336
	4	2/5/71	.438	.442 - .445	.0333 - .0336
	5	2/5/71	.438	.434 - .436	.0330 - .0337
	6	1/27/71	.250	.240 - .241	.0331 - .0337
	7	1/27/71	.250	.255 - .258	.0328 - .0334
	8	2/5/71	.438	.436 - .437	.0330 - .0334
	9	2/5/71	.438	.438 - .444	.0333 - .0336

* Specimen details given in Figure 1.

TABLE 4. TESTING SPEEDS

Material	Specimen Size (Min Width-in)	Test Conditions	Testing Speed (Cycles/min)
0.016 Ti-6Al-4V	0.750	Std 10-kip S-N machine	1570 - 1730**
		New Low cap.fat.machine	1710*
	0.572	New low cap.fat.machine, Normal atmosphere	1690*
		Vacuum	1690 - 1703**
	0.438	New low cap.fat.machine, Normal atmosphere	1677*
	0.250	" "	1645*
0.032 2024-T3	0.750	" "	1735*
	0.438	" "	1711*
	0.250	" "	1677*

* Speed constant for any one test to within 0.2%
** Speed constant for any one test to within 1.0%
Differences in vacuum tests ascribed to variation in beam temperature.

TABLE 5. ESTIMATED PROBABLE (0.67 σ) ERRORS IN SPECIMEN LOAD

	Standard Machine	New Low Capacity Fatigue Machine			
Specimen Width (in.)	0.750	0.750	0.572	0.438	0.250
Load Cell Identification	074	201	201	201	401
Specimen Area					
Width	0.10%	0.10%	0.13%	0.17%	0.30%
Thickness	0.5	0.5	0.5	0.5	0.5
Measurement of Load					
Load cell precision	0.3	.10	.13	.17	.13
Drift of zero reference	0.9	.30	.40	.51	.45
Control of Load					
Mean load	0.7	.3	.3	.3	.3
Varying load	0.7	.03	.03	.03	.03
Uniformity of Stress					
Installation Stress	0.20	.20	.26	.35	.60
Non-axiality of loading	0.24	.24	.20	.14	.07
RMS Sum, % of peak stress	1.5%	0.7%	0.8%	0.9%	1.0%

TABLE 6. FATIGUE TEST DATA ON 0.750-IN WIDE Ti-6Al-4V SPECIMENS TESTED IN STD 10,000-LB S-N MACHINE
(All tests at 65-70% RH, 70-80°F, and R = 0.02)

Test Stress f_{max} (ksi)	Coupon Ident.	Machining Stack No.	Approx. Test Date (1970)	Test Life 10^3 Cycles	Failure Origin Location: Dist. from Edge (in.)	Failure Origin Location: Dist. from Midp't (in.)	Max Fat Crack Growth-Origin to Front (in.)	Remarks
130	1I7	1	8/11	22.5	.09	.11	.04	
	1C15	4	8/11	24.9	.18	.11	.02	3 failure origins
	1A15	1	8/12	25.0	.20	.19	.04	
	2E10	4	8/11	26.4	.03	.21	.03	2 failure origins
	2G7	4	8/11	34.6	.06	.21	.04	3 failure origins
119	2B10	1	7/27	31.6	.00	.08	.04	Adj. to 115 ksi = 37.6*
116	1G13	1	7/26	26.7	.04	.05	.035	Adj. to 115 ksi = 28.3*
	1H7	1	7/27	37.4	.10	.15	.04	Adj. to 115 ksi = 39.7*
	1I6	2	7/29	48.0	.10	.17	.07	Adj. to 115 ksi = 51.0*
115	1H12	1	8/12	27.0	.02	.63	.02	2 failure origins
114	1A7	1	7/29	83.8	.21	.27	.095	Adj. to 115 ksi = 77.5*
111	1B13	2	8/16	75.0	.09	.21	.06	Adj. to 110 ksi = 88.1*
110	1F23	1	7/28	28.0	.00	.21	.04	2 failure origins
	1F6	1	8/6	42.9	.02	.05	.04	
	2C3	4	8/4	62.1	.037	.27	.04	
	1F7	4	8/4	71.8	.23	.07	.10	
	2F21	4	8/4	86.0	.18	.05	.07	
	1B11	4	8/5	93.0	.05	.43	.04	
	1E4	4	8/5	102.0	.017	.05	.015	
	2D22	4	8/5	119.0	.085	.31	.065	
109	2D17	1	8/6	70.8	.10	.01	.06	Adj. to 110 ksi = 59.9*
	1F11	2	7/29	89.0	.16	.03	.055	Adj. to 110 ksi = 75.1*
106	1E9	1	8/3	60.1	.21	.41	.105	Adj. to 105 ksi = 108.2*
	2E1	1	7/31	1900.0	.015	.37	.04	Adj. to 105 ksi = 3420*
105	2G10	1	8/10	193.0	.10	.01	.06	
	2C13	1	8/7	364.0	.025	.25	.025	
	2C20	4	8/10	630.0	.07	.53	.05	
	2B18	2	7/30	1380.0	.06	.23	.04	
	1B20	1	8/10	1498.0	.03	.41	.03	
104	2C8	1	8/3	615.0	.35	.37	.15	Adj. to 105 ksi = 342*
103	1D7	1	8/4	1374.0	.06	.43	.06	Adj. to 105 ksi = 425*
100	1G5	1	9/6	4900.0	.02	.11	.03	
	2E9	4	8/29	5033.0	.15	.45	.08	
	1E3	1	9/4	5097	-	-	-	Did not fail

* Test life adjusted to correspond to specified test stress according to local slope of mean S-N curve.

TABLE 7. FATIGUE TEST DATA ON 0.750-IN WIDE Ti-6Al-4V SPECIMENS TESTED IN NEW LOW CAPACITY MACHINE
(All tests at 65-70% RH, 70-80°F, and R = 0.02)

Test Stress f_{max} (ksi)	Coupon Ident.	Machining Stack No.	Test Compl. Date (1970)	Test Life 10^3 Cycles	Failure Origin Location: Dist. from Edge (in.)	Failure Origin Location: Dist. from Midp't (in.)	Max. Fat. Crack Growth-Origin to Front (in.)	Remarks
130	2D24 *	2	10/30/70	30.4	.36	.09	.03	5 failure origins
115	2H16	4	9/17/70	21.0	.00	.17	.04	Edge failure
	1D12 *	1	11/ 2/70	37.1	.01	.03	.03	
	1I18	4	9/17/70	38.3	.07	.27	.04	
	1D24	4	9/17/70	42.9	-	-	-	
	2D18	4	9/18/70	45.5	.05	.15	.04	
	2F17 *	2	10/30/70	49.7	.02	.41	.02	
	1I20	1	10/ 1/70	49.9	.03	.10	.02	
	2E17	4	9/17/70	53.0	-	-	-	
	1G16	4	9/18/70	54.2	.02	.25	.015	
	2I20	4	9/17/70	56.4	.05	.13	.03	
	1A3 *	4	11/ 4/70	59.1	.04	.17	.03	
	1H17	4	2/ 1/71	39.3	.15	.16	.05	Tested as controls during course of 2024-T3 test program.
	1E23	4	3/14/71	52.0	.02	.24	.02	
	1G3	1	1/28/71	59.0	.07	.32	.045	
	1D21	4	2/ 4/71	62.4	.03	.28	.02	
	1C16	4	2/24/71	75.2	.20	.18	.05	
110	2B4	4	10/23/70	72.2	.14	.03	.05	
	2F5	1	10/ 1/70	94.5	.22	.69	.10	
	2B8 *	1	11/ 2/70	132.0	.30	.19	.06	
105	1A19	2	9/18/70	61.7	.02	.19	.02	
	1H19	1	9/18/70	82.4	.10	.11	.08	
	2G20	1	10/ 1/70	116.3	.12	.03	.08	
	2F2	4	9/21/70	127.9	.04	.19	.02	
	2E19	1	9/22/70	150.3	.02	.25	.02	
	1D23	2	9/18/70	569	.02	.30	.02	
	1B4	4	9/20/70	1026	.21	.15	.05	
	1D3	4	9/21/70	1582	.01	.10	.04	
100	2H7	4	10/ 8/70	5290	.05	.69	.04	
	1D13	2	10/13/70	11110	-	-	-	Did not fail

* Photographic recording of crack propagation.

TABLE 8. FATIGUE TEST DATA OBTAINED AT EXTREMES OF HUMIDITY
(All tests on 0.750-in wide Ti-6Al-4V specimens at 70-80°F, and R = 0.02.
Tests conducted on Std 10,000-lb S-N Machine, except as marked*)

Environm't Condition	Test Stress f_{max} (ksi)	Coupon Ident.	Machining Stack No.	Test Compl. Date (1970)	Test Life 10^3 Cycles	Failure Origin Location: Dist. from Edge (in.)	Failure Origin Location: Dist. from Midp't (in.)	Max.Fat.Crack Growth-Origin to Front (in.)	Remarks
95-100% RH	130	1I19	2	8/17	18.3	.11	.23	.04	
		1A17	4	8/14	22.8	.18	.05	.06	
		2G13	2	8/17	24.8	-	.35	-	
	110	1F1	2	8/17	57.3	.34	.25	.06	
		1A1	2	8/14	154.1	.08	.47	.06	
		2B12	2	9/22	235.8	.36	.05	.06	
		1B15	4	8/12	328.0	.16	.07	.05	
		2H13	4	8/13	534.6	.16	.35	.04	
		1E20*	2	11/4	545.0	.06	.15	.04	
	105	1E7	2	8/24	58.4	.01	.13	.06	
		2H20	2	9/24	194.0	.34	.17	.08	
		2C11	2	8/24	226.6	.00	.21	-	
	100	1D14	4	9/30	440.7	.35	.18	.06	
		2E14	2	8/31	4013	.06	.30	.05	
		1B6	2	8/27	5055	-	-	-	Did not fail
Argon Atmos	130	2E12	4	8/18	24.1	.20	.03	.02	
		1A12	2	8/19	24.8	.04	.11	.03	
		2G3	2	8/24	28.1	.01	.31	.01	
	110	1F18	4	8/18	70.5	.10	.29	.05	
		1C10	2	8/18	96.0	.012	.27	.01	
		1H11	2	8/18	128.0	.09	.27	.06	
	105	1E24	2	8/22	127.6	.31	.01	.10	
		2I14	2	8/19	290	.15	.29	.07	
		2D2	2	8/21	2920	.36	.44	.08	
	100	2E23	4	9/29	261	.20	.06	.09	
		2D7	1	9/28	6390	.09	.20	.05	
		2H12	1	10/8	6500	-	-	-	Did not fail

* Photographic recording of crack propagation.

TABLE 9. FATIGUE TEST DATA ON 0.572-IN WIDE Ti-6Al-4V SPECIMENS
(All tests at 65-70% RH, 70-80°F, and R = 0.02)

Test Stress ksi	Coupon Ident.	Stack No.	Test Completion Date	Test Life 10^3 Cycles	Failure Origin Location: Dist. from Edge (in.)	Failure Origin Location: Dist. from Midp't(in.)	Max.Fat.Crack Growth-Origin to Front(in.)	Overall Elong. (in.)	Remarks
137.5	2E7	8	5/21/71	3.49			No fatigue zone	.10	Ductile failure at 30°
	2C18	8	5/21/71	3.50			No fatigue zone	.10	Ductile failure at 30°
132.5	1I8	8	5/20/71	14.8	.26	.16	.02	.06	2 origins
	2C10	8	5/20/71	17.5	.10	.06	.01	.04	4 origins
	2H2	8	5/20/71	24.3	.11	.02	.02	.03	2 origins
	1D8	8	5/20/71	25.3	.21	.12	.04	.04	
130.0	1I9	8	5/20/71	18.6	.13	.06	.03	.03	
	1F5	7	12/10/70	18.9	.18	.06	.02	.03	2 origins
	1D16	7	11/28/70	23.5	.19	.06	.02	.02	2 origins
	2E4	8	5/20/71	27.3	.18	.10	.04	.03	
127.5	2I2	7	11/25/70	26.4	.04	.09	.025	.02	
	2D19	8	5/19/71	27.2	.08	.11	.04	.02	
	1F2	8	5/19/71	28.4	.12	.03	.025	.03	2 origins
	1A16	8	5/19/71	36.6	.13	.04	.03	.03	
115	2E13	7	11/28/70	34.3	.03	.09	.025	.01	Edge failure
	2C2	7	11/24/70	57.6	.23	.16	.07	.03	
	1G1	7	11/24/70	64.4	.08	.22	.05	.02	
	2F15	7	11/28/70	68.3	.08	.07	.03	.02	
	1D11	7	11/25/70	70.1	.21	.10	.06	.03	
	1D2	7	11/28/70	77.4	.06	.18	.05	.02	
	1D1	7	11/28/70	82.6	.02	.34	.02	.01	
113	1E12	7	11/28/70	60.7	.22	.18	.06	.02	Adj. to 115 ksi = 50.7*
110	2F22	7	11/25/70	53.6	.03	.22	.03		
	2E18	7	2/ 2/71	71.1	.07	.09	.04		
	1E10	7	2/ 8/71	76.4	.01	.12	.03		
	2E8	7	2/10/71	79.6	.065	.44	.045		
	2H5	7	11/28/70	80.6	.15	.08	.04		
	2E20	7	11/24/70	102.9	.02	.19	.02		
	2I6	7	2/ 5/71	120.7	.045	.04	.04		
	1A14	7	11/25/71	344.9	.003	.18	.03		
105	2I7	7	12/ 4/70	131.7	.06	.16	.03		
	1C11	7	11/24/70	154.0	.22	.12	.08		
	1I13	7	11/30/70	306.5	.003	.16	.04		
	2D13	7	12/ 8/70	9100.	.22	.13	.05		Life msmt accurate to only ±8%
100	1B17	7	12/ 8/70	4555	.25	.39	.08		
	2D14	7	12/12/70	12590	-	.10	-		Includes 2 x 10^6 cycles at RH < 65%

* Test life adjusted to correspond to specified test stress according to local slope of mean S-N curve.

TABLE 10. FATIGUE TEST DATA ON 0.438-IN WIDE Ti-6Al-4V SPECIMENS
(All tests at 65-70% RH, 70-80°F, and R = 0.02)

Test Stress ksi	Coupon Ident.	Machining Stack No.*	Test Completion Date	Test Life 10^3 Cycles	Failure Origin Location: Dist. from Edge (in.)	Failure Origin Location: Dist. from Midp't (in.)	Max. Fat. Crack Growth-Origin to Front (in.)	Remarks
132.5	2I12	5 *	11/15	10.7	.01	.02	.01	
131.5	1E17	5 *	11/14	16.3	.045	.04	.02	
	2D5	6	11/11	19.5	.00	.14	.02	Edge failure
	2F19	5 *	11/14	19.8	.02	.01	.02	
131.0	1A18	5 *	11/14	19.8	.15	.08	.03	
130.5	2I19	6	11/13	22.5	.15	.11	.025	
130	1H14	6	11/7	21.8	.00	.08	-	Edge Failure
	1C18	5 *	11/15	21.8	.055	.04	.02	
	2D8	5 *	11/15	31.0	.16	.08	.03	
115	2H3	6	11/13	35.7	.12	.00	.035	
	1C19	6	11/11	61.5	.035	.01	.03	
	1D6	6	11/6	63.1	.00	.50	.06	Edge failure
	1E13	6	11/11	69.3	.06	.11	.04	
	2C1	6	11/6	71.3	.02	.07	.02	
	2B5	6	11/17	159.8	.17	.15	.06	
	2D6	6	11/11	227.4	.13	.06	.05	
	2G5	6	11/6	712.6	.015	.18	.02	
110	1E8	5 *	12/11	78.8	.02	.14	.02	
	2I5	6	12/16	80.8	.22	.26	.06	
	1E21	6	11/7	87.2	.15	.16	.01	
	1H6	6	12/16	133.8	.03	.12	.02	
	1E2	6	11/16	202.6	.02	.05	.02	
	1H3	6	11/7	282.7	.12	.28	.06	
	2D12	5 *	12/15	3127	.15	.22	.06	
	2F13	6	11/10	3909	.16	.02	.06	
105	1D15	6	11/17	92.7	.027	.26	.02	
	1C2	6	11/13	356.0	.08	.25	.055	
	2I15	6	11/9	3517	.08	.10	.04	
	1D4	6	11/13	3902	.01	.06	.05	
	1G20	5 *	2/8	8595	.005	.54	.06	
	2D23	6	12/18	10080	-	-	-	Did not fail

* Stack No. 5 below dimensional tolerance in width.

TABLE 11. FATIGUE TEST DATA ON 0.250-IN WIDE Ti-6Al-4V SPECIMENS
(All tests at 65-70% RH, 70-80°F, and R = 0.02. All specimens from Stack 3)

Test Stress ksi	Coupon Ident.	Test Completion Date (1970)	Test Life 10^3 Cycles	Failure Origin Location: Dist. from Edge (in.)	Failure Origin Location: Dist. from Midp't(in.)	Max.Fat.Crack Growth-Origin to Front(in.)	Remarks
130	1F16	10/21/70	23.5	.04	.13	.02	
	1D18	10/21/70	29.4	.00	.06	.025	Edge failure
	2H9	10/21/70	29.8	.006	.01	.03	
115	1I15	10/27/70	64.5	.004	.08	.04	
	1G18	9/28/70	128.1	.02	.07	.02	
	1E15	9/28/70	141.1	.095	.04	.03	
	1E19	11/5/70	167.0	.04	.16	.03	
	1C1	10/13/70	230.0	.04	.13	.035	
	1F19	11/6/70	926.0	.04	.14	.03	
	2H15	10/23/70	979.0	.065	.04	.04	
	2H6	10/28/70	2920.0	.03	.10	.025	
110	2G15	10/19/70	87.0	.055	.10	.035	
	2B19	1/9/71	112.2	.03	.10	.02	
	1F24	10/19/70	190.3	.008	.06	.055	
	2G8	10/20/70	925	.05	.10	.035	
	1D20	1/9/70	1015	.03	.08	.02	
	1B7	10/22/70	3280	.018	.14	.025	
	2I18	1/8/71	6883	.09	.16	.04	
	2C7	12/30/70	9583	.10	.10	.04	
105	1G9	9/29/70	2920	.08	.16	.04	
	1C8	1/13/71	4738	.04	.06	.03	
	2I11	10/27/70	8030	.00	.02	.04	Edge Failure
	2B20	1/17/71	9985	-	-	-	Did not fail
	1B1	10/19/70	13440	-	-	-	Did not fail

TABLE 12. FATIGUE TEST DATA ON 0.750-IN WIDE 2024-T3 SPECIMENS
(All tests at 65-70% RH, 70-80°F, and R = 0.02)

Test Stress ksi	Coupon Ident.	Machining Stack No.	Test Completion Date (1971)	Test Life 10^3 Cycles	Failure Origin Location: Dist. from Edge (in.)	Failure Origin Location: Dist. from Midp't(in.)	Max.Fat.Crack Growth-Origin to Front(in.)	Remarks
55	B39	1	1/26	22.4	.00	.12	.04	Edge; 7 failure origins
	B6	3	2/1	29.3	.13	.06	.04	13 failure origins
	A9	2	1/29	31.1	.35	.19	.04	3 failure origins
	H17	1	2/2	31.1	.00	.06	.02	Edge; 7 failure origins
50	F34	1	1/26	48.6	.15	.00	.04	
	C37	1	1/26	56.6	.00	.11	.04	Edge.
	C35	3	2/2	56.7	.00	.18	.02	Edge.
	B41	3	2/24	57.1	.02	.48	.03	
	E23	3	1/29	73.8	.08	.14	.04	
	H4	2	1/29	82.1	.00	.20	.03	Edge; 3 failure origins
	D13	1	1/22	88.2	.00	.46	.03	Edge; 6 failure origins
	B10	2	2/1	114.7	.00	.74	.02	Edge.
45	D7	1	1/26	85.6	.03	.12	.03	
	A10	1	1/26	90.9	.07	.40	.05	
	B25	1	1/26	93.5	.22	.34	.05	
	B20	2	2/2	162.8	.00	.20	.04	
	B32	2	1/29	169.4	.025	.09	.025	2 failure origins
	F40	2	2/24	180.0	.09	.44	.06	2 failure origins
	E11	3	2/1	214.3	.08	.12	.04	
	A3	3	1/31	246.2	.00	.55	.02	Edge.
40.0	B30	1	1/22	314.1	.00	.22	.05	Edge.
	F35	2	1/26	709.9	.15	.96	.07	
	C32	3	2/1	1369.3	.06	.26	.04	
	C38	2	1/29	5006	-	-	-	Did not fail
	E25	3	1/31	5005	-	-	-	Did not fail
	H9	1	2/2	5001	-	-	-	Did not fail
	D15	2	2/11	5001	-	-	-	Did not fail
37.5	B14	1	2/12	5119	-	-	-	Did not fail
35.0	F26	1	1/24	5015	-	-	-	Did not fail

TABLE 13. FATIGUE TEST DATA ON 0.438-IN WIDE 2024-T3 SPECIMENS
(All tests at 65-70% RH, 70-80°F, and R = 0.02)

Test Stress ksi	Coupon Ident.	Machining Stack No.	Test Completion Date (1971)	Test Life 10^3 Cycles	Failure Origin Location		Max.Fat.Crack Growth-Origin to front(in.)	Remarks
					Dist. From Edge (in.)	Dist. from Midp't(in.)		
55	E40	9	2/8	27.9	.00	.08	.03	Edge failure
	B13	8	2/4	22.2	.035	.01	.03	
	A2	4	2/11	25.3	.00	.04	.02	Edge failure
	H37	8	2/4	26.9	.00	.20	.015	Edge failure
50	B40	9	2/22	63.3	.015	.04	.02	
	F36	4	2/23	74.6	.00	.14	.02	Edge failure
	C25	5	2/16	77.8	.00	.10	.02	Edge failure
	F31	8	2/4	78.5	.00	.16	.03	Edge failure
	F39	9	2/8	79.7	.00	.10	.02	Edge failure
	E13	5	2/24	87.1	.00	.28	.03	Edge failure
	E31	8	2/4	89.3	.00	.01	.03	Edge failure
	E37	4	2/11	90.7	.00	.02	.03	Edge failure
45	E3	8	2/5	161.5	.00	.15	.025	Edge failure
	A5	4	2/22	170.9	.00	.22	.04	Edge failure
	E5	9	2/24	189.6	.14	.28	.06	
	A15	8	2/4	232.8	.00	.12	.02	Edge failure
	E27	9	2/8	419.8	.00	.18	.02	Edge failure
	I34	5	2/23	848.7	.06	.12	.04	
	A1	5	2/18	2570	.05	.22	.035	
	I30	4	2/16	3674	.00	.04	.05	Edge failure
40	A7	8	2/13	628.9	.24	.16	.05	
	I39	8	2/7	4995	-	-	-	Did not fail
	A6	9	2/21	5001	-	-	-	Did not fail
	D10	4	2/23	5122	-	-	-	Did not fail
	B21	5	2/30	5890	-	-	-	Did not fail

TABLE 14. FATIGUE TEST DATA ON 0.250-IN WIDE 2024-T3 SPECIMENS
(All tests at 65-70% RH, 70-80°F, and R = 0.02)

Test Stress ksi	Coupon Ident.	Machining Stack No.	Test Completion Data (1971)	Test Life 10^3 Cycles	Failure Origin Location		Max.Fat.Crack Growth-Origin to Front(in.)	Remarks
					Dist. from Edge (in.)	Dist. from Midp't(in.)		
55	E32	6	3/5	27.8	.00	.05	.02	Edge failure
	E7	7	3/11	29.7	.00	.00	.02	" "
	H13	6	3/11	33.5	.00	.05	.02	" "
	C34	7	3/11	35.6	.00	.11	.02	" "
50	H12	6	3/8	66.2	.00	.08	.02	Edge failure
	C28	7	3/11	69.9	.00	.04	.02	" "
	E4	6	3/1	96.1	.02	.14	.03	
	E35	6	3/10	103.3	.00	.22	.025	Edge failure
	H27	7	3/5	110.5	.00	.06	.03	" "
	E41	6	3/12	112.0	.00	.28	.015	" "
	B7	7	3/11	130.6	.00	.13	.02	" "
	H1	7	3/11	136.3	.00	.00	.035	" "
45	E34	7	3/5	245.8	.00	.08	.03	Edge failure
	H28	6	3/1	379.5	.00	.34	.03	" "
	H29	6	3/5	411.9	.00	.06	.035	" "
	B17	6	3/16	1059.7	.06	.18	.04	
	B26	7	3/15	4720	.00	.18	.03	Edge failure
	I38	6	3/18	5001	-	-	-	Did not fail
	H30	7	4/9	5001	-	-	-	Did not fail
	F30	7	3/15	5009	-	-	-	Did not fail
40	F27	6	3/27	5001	-	-	-	Did not fail
	G11	7	3/29	5009	-	-	-	Did not fail
	A11	6	2/28	5240	-	-	-	Did not fail
	H18	7	4/12	6298	-	-	-	Did not fail

TABLE 15. FATIGUE TEST DATA OBTAINED ON 0.572 IN WIDE Ti-6Al-4V SPECIMENS IN VACUUM
(All tests conducted at 70-80°F specimen temperature and R = 0.02. All specimens from Stack 3)

Test Stress ksi	Coupon Ident.	Test Comp.Date (1971)	Test Life 10^3 Cycles	Vacuum Range 10^{-7} Torr.	Failure Origin Location: Dist.From Edge (in.)	Failure Origin Location: Dist. From Midp't (in.)	Max.Fat.Growth Growth-Origin To Front(in.)	Remarks
130	1G17	4/23	10.8	5.4- 6.3				Ductile failure at 30°, .09-in. elong.
	1H10	4/30	11.0	3.7- 3.9				" " " 29°, .09-in. "
	2C12	4/8	11.5	7.8- 8.5				" " " 29°, .10-in. "
	2G14	3/29	19.8	5.4- 7.6				" " " 29°, .10-in. "
	1G19	5/7	29.8	4.0- 4.2				" " " 28½°, .10-in. "
127.5	2B13	4/7	39.6	10.0-10.3				Ductile failure at 29°, .10-in. "
	1B16	5/14	48.8	4.3- 5.4				" " " 28°, .10-in. "
	2C17	4/12	49.3	9.9-11.5				" " " 29°, .10-in. "
	2C16	5/6	80.8	4.2- 4.6				" " " 28°, .11-in. "
	2D9	5/3	82.2	4.8-10.2				" " " 28°, .11-in. "
125	2F11	4/22	50.3	4.0- 6.2				Ductile failure at 30°, .11-in. "
	2E5	4/21	301	4.4- 9.4	.00	.10	.03	Characteristic fatigue, 0°, .03-in. "
	1C20	4/20	367	3.7- 9.2	.16	.10	.05	" " 0°, .02-in. "
	2E2	5/10	810	3.5- 6.0				Ductile failure, 0° and 25°, .10-in. "
	2D16	4/5	2020	8.8-11.0	.07	.14	.04	Characteristic fatigue, 0°, .02-in. "
122.5	1B9	5/5	1878	2.7- 5.4	.00	.10	.04	Characteristic fatigue, 0°, .02-in. "
	1F9	5/18	2030	6.6-10.4	.00	.06	.04	" " .01-in. "
	2D15	4/27	2604	2.5- 7.5	.12	.26	.05	" " .01-in. "
	2G9	4/29	3063	2.3- 6.9	.00	.21	.04	" "
120	2I10	5/13	3720	2.5- 5.5	.00	.16	.04	Characteristic fatigue, 0°, .01-in. "
115	2I3	4/3	5004NF	7.2- 9.9				Did not fail

TABLE 16. FATIGUE TEST DATA FURNISHED BY NASA LANGLEY RESEARCH CENTER ON 0.750-IN WIDE Ti-6Al-4V SPECIMENS

(Tests conducted at NASA Langley Research Center on specimens, test machine, and test conditions similar to those for Table 6. Material from Titanium Metals Corp. of America Heat No. K-4590)

Test Stress f_{max} (ksi)	Test Life (10^3 cycles)	Test Stress f_{max} (ksi)	Test Life (10^3 cycles)	Test Stress f_{max} (ksi)	Test Life (10^3 cycles)
130	28	115	40	105	820
	34		51		1604
	35		225		2397
	37		290		3739
	39		450		3755
120	44		559		6348
	50		671	100	1594
	57	110	139		1943
	70		191		2897
	123		1003		7522
			1397		5000 NF
			1400		5000 NF
			1427		6000 NF
			1600	90	6000 NF
			2626		12000 NF

NF = Did not fail

LOCKHEED
CALIFORNIA COMPANY

TABLE 17. FATIGUE TEST DATA ON 0.750-IN WIDE Ti-6Al-4V SPECIMENS EXCHANGED BETWEEN LABORATORIES

A. Prepared by NASA Langley Research Center and tested by Lockheed-California Company

(All tests conducted at 65-70% RH, 70-80°F, and stress range ratio R = 0.02, at stress level f_{max} = 110 ksi)

Specimen Ident.	Test Machine	Test Date	Test Life 10^3 Cycles
W35-B-19	Std 10 kip S-N Machine	9/8	1554
-22	"	9/8	1870
-23	New Low Cap. Machine	9/21	1397
-24	"	9/22	Lost Load Control
-26	"	9/22	Lost Load Control

B. Prepared by Lockheed-California Company and tested by NASA Langley Research Center

(All tests conducted at 60-75% RH, 70-80°F, and stress range ratio R = 0.00, at stress level f_{max} = 110 ksi)

Specimen Ident.	Test Life 10^3 Cycles
1G7	56
2I4	83
1D10	120
2H8	433
1I11	712

LOCKHEED
CALIFORNIA COMPANY

TABLE 18. PHOTOGRAPHIC CRACK PROPAGATION DATA OBTAINED IN TESTS OF Ti-6Al-4V SPECIMENS

Test Ident.	Total Cycles (±100)	Cycles Prior to Failure (±16)	Crack Front Locations Measured from Edge (in)	Crack Length (in)
2D24	30,000	432	Indistinguishable	
130 ksi		400	Indistinct	-
65-70%RH		368	"	-
(Table 7)		336	.375 - .395	.020
		304	.375 - .395	.020
		272	.375 - .395	.020
		240	.375 - .395	.020
		208	.373 - .398	.025
		176	.366 - .406	.040
		144	.366 - .406	.040
		112	.366 - .406	.040
		80	.360 - .404	.044
		48	.352 - .413	.061
		16	.345 - .420	.075
	30,400	0		Complete
1D12	37,000*	80*	Indistinguishable	
115 ksi		48	Indistinct	
65-70%RH		16	0 - 0.035	.035
(Table 7)	37,100	0		Complete
1A3	58,800	240	Indistinguishable	
115 ksi		208	.040 - .050	.010
65-70%RH		176	.034 - .054	.020
(Table 7)		144	.030 - .054	.024
		112	.020 - .054	.034
		80	.016 - .057	.041
		48	.014 - .060	.046
		16	.009 - .065	.054
	59,100	0		Complete
1E20	544,500*	528*	Indistinguishable	
110 ksi		496	.055 - .061	.006
95-100%RH		464	.055 - .066	.011
(Table 8)		432	.048 - .072	.024
		400	(.050)-(.068)	(.018)
		368	.045 - .072	.027
		336	.044 - .075	.031
		304	.044 - .080	.036
		272	.042 - .080	.038
		240	.042 - .082	.040
		208	.040 - .083	.043
		176	.040 - .088	.048
		144	.040 - .092	.052
		112	.035 - .093	.058
		80	.032 - .094	.062
		48	.025 - .096	.071
		16	.022 - .102	.080
	545,000	0		Complete

Test Ident.	Total Cycles (±100)	Cycles Prior to Failure (±16)	Crack Front Locations Measured from Edge (in)	Crack Length (in)
2B8	129,700*	1328*	Indistinguishable	
110 ksi		1296	.285 - .298	.013
65-70%RH		1264	.286 - .302	.016
(Table 7)		1232	.285 - .305	.020
		1200	.285 - .308	.023
		1168	.280 - .310	.030
		1136	.278 - .312	.034
		1104	.278 - .316	.038
		1072	.278 - .316	.038
		1040	(.278)-(.315)	(.037)
		1008	(.277)-(.312)	(.035)
		976	.276 - .316	.040
		944	.276 - .316	.040
		912	.272 - .316	.044
		880	.270 - .318	.048
		848	.268 - .318	.050
		816	(.264)- .324	(.060)
		784	(.264)-(.323)	(.059)
		752	(.268)-(.320)	(.052)
		720	(.266)- .326	.060
		688	.264 -(.324)	.060
		656	.264 - .328	.064
		624	.264 - .332	.068
		592	.264 - .335	.071
		560	.256 - .334	.078
		528	.256 - .338	.082
		496	.254 - .340	.086
		464	.252 - .340	.088
		432	.250 - .342	.092
		400	.250 - .342	.092
		368	.246 - .343	.097
		336	.246 - .344	.098
		304	.242 - .345	.103
		272	.240 - .346	.106
		240	.238 - .348	.110
		208	.234 - .354	.120
		176	(.236)- .356	.120
		144	.230 -(.354)	.124
		112	.226 - .364	.138
		80	.220 - .367	.147
		48	.216 - .374	.158
		16	.211 -0.380	.169
	131,000	0		Complete
2F17	49,700		Failure outside field of view	
115 ksi				
65-70%RH				
(Table 7)				

* Crack origin on side opposite to that being photographed.

TABLE 19. OBSERVATIONS ON CRACK PROPAGATION TIME IN TESTS OF 0.750-IN WIDE 2024-T3 SPECIMENS

Stress Level f_{max} (ksi)	Specimen Ident.	Test Life (+100 Cycles)	Notation Made No. of Cycles Prior to Failure	Observation
55	B39	22400	700	No cracks visible at 4 x mag.
	A9	31100	1000	" " " " "
	H17	31100	700	" " " " "
50	F34	48600	1700	No cracks visible at 4 x mag.
	C37	56600	500	Crack 0.05 long at edge.
	E23	73800	900	Crack 0.06 long in center.
	D13	88200	230	Crack 0.01 long at edge.
45	D7	85600	900	No cracks visible at 4 x mag.
	B25	93500	700	" " " " "
	B32	169400	500	" " " " "

LOCKHEED
CALIFORNIA COMPANY

TABLE 20. SUMMARY OF STATISTICAL PROPERTIES OF REPLICATE TESTS BEARING ON TEST CONDITIONS

Treatment	Ref. Table	Specimen Size	Stress Level	No. of Tests	Mean of Log Cycles	Sum of Sq's of Dev'ns	Estim Std Dev'n
Method of Machining							
Six-tooth cutter,	7	0.750	115	4	4.6837	0.0211	0.08
stacks 1 and 2	6		110	5	4.7355	0.1779	0.21
Single tooth cutter,	7		115	12	4.6799	0.2194	0.14
stack 4	6		110	6	4.9304	0.0708	0.12
Fatigue Test Machine							
Std 10-kip S-N	6	0.750	115	6	4.6091	0.1468	0.17
machine	6		105	9	5.7446	1.716	0.46
New low cap machine	7		115	16	4.6809	0.2367	0.13
	7		105	8	5.3776	1.986	0.53
Long Period Var'n, New Machine							
Aug - Nov 1970	7	0.750	115	11	4.6492	0.1609	0.13
	9	0.572	110	4	5.0464	0.3628	0.35
Feb - Mar 1971	7	0.750	115	5	4.7507	0.0433	0.10
	9	0.572	110	4	4.9269	0.0292	0.10
Extremes of Humidity							
90-100 Percent RH	8	0.750	130	3	4.3382	0.0102	0.07
			110	6	5.3831	0.6912	0.37
			105	3	5.1361	0.2072	0.32
			100	3	(6.466)*		(0.65)*
Dry argon atmos	8	0.750	130	3	4.4083	0.0039	0.04
			110	3	4.9792	0.0340	0.13
			105	3	5.6770	0.7181	0.60
			100	3	(6.553)*		(0.89)*

* Includes run-out points treated by method of maximum likelihood.

TABLE 21. STATISTICAL TESTS FOR SIGNIFICANCE OF INCIDENTAL VARIATIONS IN TEST CONDITIONS

A. F-test for Equality of Standard Deviations (Ref. 2, p 107)

Comparison	df_1	df_2	$F_{\frac{\alpha}{2}=.025}$	s_1^2/s_2^2	$F_{1-\frac{\alpha}{2}=.975}$	Result
Method of Machining						
115 ksi	3	11	0.069	0.327	4.63	Not significant
110 ksi	4	5	0.107	3.06	7.39	Not significant
Fatigue Test Machine						
115 ksi	5	15	0.156	1.71	3.58	Not significant
105 ksi	8	7	0.221	.753	4.90	Not significant
Long Period Variation						
0.750 at 115 ksi	10	4	0.224	1.69	8.84	Not significant
0.572 at 100 ksi	3	3	0.065	12.2	15.4	Not significant

B. t-test for Equality of Means, $\sigma_1 = \sigma_2$ Unknown (Ref. 2, p 121)

	(n_1+n_2-2)	$\dfrac{\bar{X}_1 - \bar{X}_2}{\left[\dfrac{SS_1+SS_2}{n_1+n_2-2}\left(\dfrac{1}{n} + \dfrac{1}{n_2}\right)\right]^{1/2}}$	$t_{\frac{\alpha}{2}=.025}$	Result
Method of Machining				
115 ksi	14	0.050	2.14	Not significant
110 ksi	9	-1.95	2.29	Not significant
Fatigue Test Machine				
115 ksi	20	-1.08	2.09	Not significant
105 ksi	15	1.52	2.13	Not significant
Long Period Variation				
0.750 at 115 ksi	14	-1.56	2.14	Not significant
0.572 at 100 ksi	6	0.66	2.45	Not significant

(Data from Table 20)

LOCKHEED
CALIFORNIA COMPANY

TABLE 22. STATISTICAL TESTS FOR EFFECTS OF HUMIDITY

A. Properties of Replicate Tests Normalized wrt Values at 65-70% RH

Condition	Stress	n	Mean	SS	df	$s^2 = SS/(df)$
95-100% RH	130	3	0.979	2.74	2	1.100
	110	6	1.101	17.94	5	3.85
	105	3	0.921	0.776	2	0.388
	Pooled	12	1.000	20.972	9	2.330
65-70% RH	130	6	1.000	5.000	5	1.000
	110	14	1.000	13.000	13	1.000
	105	17	1.000	16.000	16	1.000
	Pooled	37	1.000	34.051	34	1.002
Dry Argon	130	3	0.995	0.885	2	0.428
	110	3	1.019	0.882	2	0.442
	105	3	1.020	2.690	2	1.340
	Pooled	9	1.011	4.475	6	0.746

B. F-test for Equality of Standard Dev'ns, Pooled (Ref. 2, p 107)

95%-100% RH versus 65-70% RH: $s_1^2/s_2^2 = 2.33$

$F_{1-\frac{\alpha}{2}} = .975,\ 9,\ 34 = 2.52$

$F_{\frac{\alpha}{2}} = .025,\ 9,\ 34 = 0.28$

H: $\sigma_1 = \sigma_2$ accepted (no effect on scatter)

Dry Argon versus 65-70% RH: $s_1^2/s_2^2 = 0.746$

$F_{1-\frac{\alpha}{2}} = .975,\ 6,\ 34 = 2.90$

$F_{\frac{\alpha}{2}} = .025,\ 6,\ 34 = 0.20$

H: $\sigma_1 = \sigma_2$ accepted at high confidence level (no effect on scatter)

C. Analysis of Variance for Equality of Means, Pooled (Ref. 2, p 151)

	df	SS	MS
Between treatments	2	0.115	.058
Within treatments	55	59.383	1.079
Total	57	59.498	

$s_1^2/s_2^2 = 0.058/1.079 = 0.053$

$F_{.95,\ 2,\ 55} = 3.17$

H: $\mu_1 = \mu_2 = \mu_3$ accepted at very high confidence level

(Change in humidity caused no change in mean)

(Data from Table 20)

LOCKHEED
CALIFORNIA COMPANY

TABLE 23. SUMMARY OF STATISTICAL PROPERTIES OF REPLICATE TESTS BEARING ON DIFFERENCES BETWEEN NASA AND LOCKHEED S-N DETERMINATIONS

(All tests on 0.750-in wide Ti-6Al-4V specimens. Data from Tables 15 and 16.)

Treatment	Stress Level f_{max} (ksi)	No. of Tests n	Mean of Log Cycles $\bar{X} = \Sigma X_i/n$	Sum of Sqs of Dev'ns $SS = \Sigma(X_i-\bar{X})^2$	Estimated Std.Dev'n $s = \sqrt{SS/(n-1)}$
Specimens prepared and tested by NASA Langley Research Center	130	5	4.5364	0.0125	0.056
	120	5	4.8067	0.1221	0.175
	115	7	5.3359	0.1460	0.493
	110	8	5.9368	1.5031	0.463
	105	6	6.4081	0.4974	0.315
	100	7	(6.669)*		(0.35)
Specimens prepared by NASA and tested by Lockheed	110	3	6.2028	0.0088	0.066
Specimens prepared by Lockheed and Tested by NASA	110	5	5.2471	0.9028	0.475

* Includes run-out points treated by method of maximum likelihood.

LOCKHEED
CALIFORNIA COMPANY

TABLE 24. STATISTICAL TESTS FOR DIFFERENCES IN TEST RESULTS AS OBTAINED AT NASA LANGLEY RESEARCH CENTER AND AT LOCKHEED-CALIFORNIA COMPANY

A. F - test for Equality of Std Dev'ns (Ref. 2, p 107)

	df_1	df_2	$F_{\frac{\alpha}{2}}=.025$	s_1^2/s_2^2	$F_{1-\frac{\alpha}{2}}=.975$	Result
NASA S-N Data versus Lockheed S-N Data						
130 ksi	4	5	.11	.67	7.39	No significant diff.
115	6	21	.19	12.38	3.10	Highly significant increase (at $\alpha<.001$)
110	7	13	.22	5.46	3.72	Very significant increase (at $\alpha<.01$)
105	5	16	.16	.37	3.52	No significant diff.
NASA Specimens Tested at Lockheed versus Tests at NASA						
110	2	7	.03	0.020	6.54	Significant decrease
Lockheed Specimens Tested at NASA versus Tests at Lockheed						
110	4	13	.11	5.87	4.02	Significant increase

B. t-test for Equality of Means (Ref. 2, p 121)

f_{max}	(n_1+n_2-2)	$\frac{\bar{Y}_1-\bar{X}_2}{\left[\frac{SS_1+SS_2}{n_1+n_2-2}\left(\frac{1}{n_1}+\frac{1}{n_2}\right)\right]^{\frac{1}{2}}}$	$t_{\frac{\alpha}{2}=.025}$	Result
NASA S-N versus Lockheed S-N Data				
130	9	2.76	2.262	Significant increase
115	27	10.8	2.052	Highly significant increase (at $\alpha<.001$)
110	20	13.3	2.086	Highly significant increase (at $\alpha<.001$)
105	21	3.67	2.080	Significant increase
NASA Specimens Tested at Lockheed versus Tests at NASA				
110	9	0.96	2.262	No significant diff
Lockheed Specimens Tested at NASA versus Tests at Lockheed				
110	17	2.47	2.110	Significant increase

(Data from Table 23)

TABLE 25. SUMMARY OF STATISTICAL PROPERTIES OF REPLICATED TESTS BEARING ON SIZE EFFECTS

(Includes all test points in Tables 6, 7, and 9 thru 14)

Material	Specimen Min Width (in)	Stress Level f_{max} (ksi)	No. of Tests n_j	Mean of Log Cycles $\bar{X}_{.j} = \Sigma_i X_{ij}/n_j$	Sum of Sqs of Dev'ns $SS_j = \Sigma_i (X_{ij} - \bar{X}_{.j})^2$	Estimated Std Dev'n $s_j = \sqrt{SS/(n-1)}$	Median of Log Cycles X_m	Scale Factor L_2/L_1	Diff in Means $(\bar{X}_{.2} - \bar{X}_{.1})/s_1$	Increase In Scatter s_2/s_1
-Ti-6Al-4V	0.750	130	6	4.4316	0.0228	0.067	4.4097	1.000	0	1.00
		115	22	4.6613	0.4129	0.140	4.6972		0	1.00
		110	14	4.8767	0.5003	0.196	4.9051		0	1.00
		105	17	5.5713	4.272	0.517	5.5611		0	1.00
		100	5	(6.773)*		(0.15)*				
	0.572	130	3	4.3383	0.0197	0.081	4.3238	.762	-1.38	1.20
		115	8	4.7869	0.1051	0.123	4.7847		1.09	0.86
		110	8	4.9867	0.4185	0.244	4.9036		0.55	1.20
		105	4	5.6881	2.2302	0.863	5.3370		0.23	1.66
		100	2	6.8794						
	0.438	130	3	4.3895	0.0151	0.087	4.4150	.585	-0.61	1.29
		115	8	5.0311	1.2197	0.417	4.8469		2.83	3.00
		110	8	5.4645	3.3805	0.695	5.2166		2.94	3.45
		105	6	(6.350)*		(0.99)*			1.50	1.91
	0.250	130	3	4.4379	0.0067	0.058	4.4683	.333	0.09	0.86
		115	8	5.5091	2.2401	0.566	5.2918		6.24	4.07
		110	8	5.9470	4.4575	0.798	5.9864		5.40	4.05
		105	5	(6.930)*		(0.36)*			2.60	0.69
2024-T3	0.750	55	4	4.4507	0.0139	0.068	4.4799	1.000	0	1.00
		50	8	4.8420	0.1133	0.126	4.8124		0	1.00
		45	8	5.1600	0.2279	0.180	(5.15)		0	1.00
		40	7	(6.777)*		(0.95)*				
	0.438	55	4	4.4062	0.0062	0.037	4.3965	.585	-0.66	0.55
		50	8	4.9017	0.0164	0.048	4.3998		0.48	0.38
		45	8	5.7018	2.0610	0.543	5.4968		3.15	2.99
		40	5	(>6.6990)						
	0.250	55	4	4.4983	0.0070	0.048	4.4989	.333	0.71	0.71
		50	8	5.0006	0.0946	0.116	5.0288		1.26	0.92
		45	8	(6.374)*		(0.86)*			6.73	4.75
		40	4	(>6.6990)						

* Includes run-out points treated by method of maximum likelihood

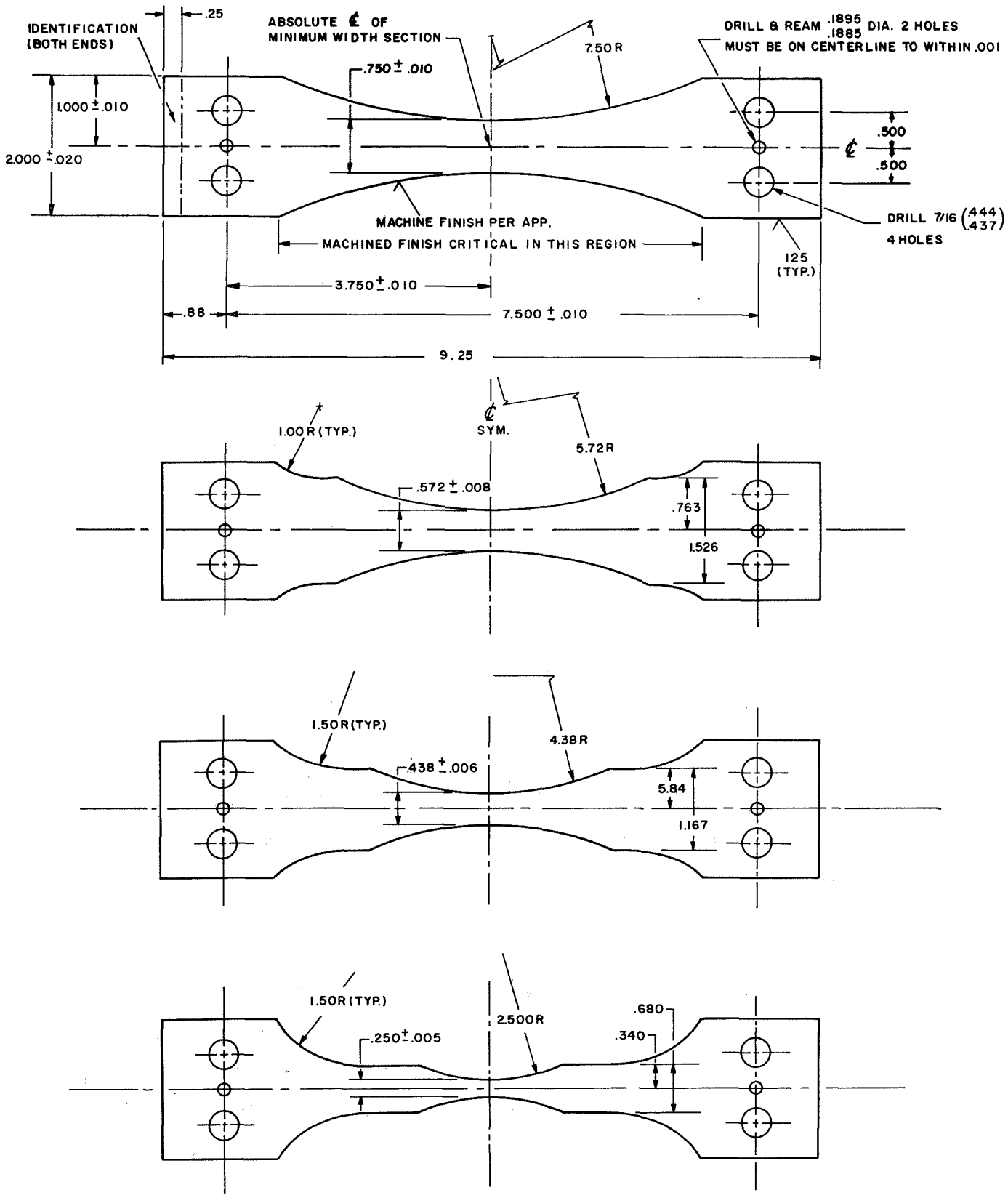

FIGURE 1. Fatigue Test Specimen Details.

LOCKHEED
CALIFORNIA COMPANY

1AT4 1AT3 1AT2 1AT1	1A10	1A15	1A20	1AE	1B5	1B10	1B15	1B20	1BE	1CT4 1CT3 1CT2 1CT1	1C10	1C15	1C20	1CE
1A3	1A9	1A14	1A19	1AE	1B4	1B9	1B14	1B19		1C3	1C9	1C14	1C19	
1A2	1A8	1A13	1A18		1B3	1B8	1B13	1B18		1C2	1C8	1C13	1C18	
1A1	1A7	1A12	1A17		1B2	1B7	1B12	1B17		1C1	1C7	1C12	1C17	
1A6	1A6	1A11	1A16		1B1	1B6	1B11	1B16		1C1	1C6	1C11	1C16	
1DT1	1DT2	1DT3	1DT4	1DE	1E6	1E12	1E18	1E24	1EE	1F6	1F12	1F18	1F24	1FE
1D6	1D12	1D18	1D24		1ET1	1ET2	1ET3	1ET4		1FT1	1FT2	1FT3	1FT4	
1D5	1D11	1D17	1D23		1E5	1E11	1E17	1E23		1F5	1F11	1F17	1F23	
1D4	1D10	1D16	1D22		1E4	1E10	1E16	1E22		1FT6 1FT5	1F10	1F16	1F22	
1D3	1D9	1D15	1D21		1E3	1E9	1E15	1E21		1F3	1F9	1F15	1F21	
1D2	1D8	1D14	1D20		1E2	1E8	1E14	1E20		1F2	1F8	1F14	1F20	
1D1	1D7	1D13	1D19		1E1	1E7	1E13	1E19		1F1	1F7	1F13	1F19	
1G5	1G10	1G15	1G20	1GM	1H5	1H10	1H15	1H20	1HE	1I5	1I10	1I15	1I20	1IE
1G4	1G9	1G14	1G19	1GE	1H4	1H9	1H14	1H19		1I4	1I9	1I14	1I19	1IE
1G3	1G8	1G13	1G18		1H3	1H8	1H13	1H18		1I3	1I8	1I13	1I18	
1G2	1G7	1GT4 1GT3	1G17		1H2	1H7	1H12	1H17		1I2	1I7	1I12	1IT4 1IT3	
1G1	1G6	1GT2 1GT1	1G16		1H1	1H6	1H11	1H16		1I1	1I6	1I11	1IT2 1IT1	

128

CODE

X X X X

SHEET NUMBER

ZONE

SPECIMEN NO.
(T FOR TENSILE TEST)
(M FOR METALLURGICAL)

Ti-6Al-4V SHEET 1
(SHEET 2 IDENTICAL)

2024-T3

A1	A9	A17	A25	B1	B9	B17	B25	B34	C1	C17	C25	C34
A2	A10	A18		B2	B10	B18	B26	B35		C18	C26	C35
A3	A11	A19		B3	B11	B19	B27	B36		C19	C27	C36
A4	A12	A20		B4	B12	B20	B28	B37		C20	C28	C37
A5	A13	A21		B5	B13	B21	B29	B38		C21	C29	C38
A6	A14	A22		B6	B14	B22	B30	B39		C22	C30	C39
A7	A15	A23		B7	B15	B23	B31	B40		C23	C31	C40
A8	A16	A24		B8	B16	B24	B32	B41		C24	C32	C41
D1	D9	D17	D25	E1	E9	E17	E25	E34	F1	F17	F25	F34
D2	D10	D18		E2	E10	E18	E26	E35		F18	F26	F35
D3	D11	D19		E3	E11	E19	E27	E36		F19	F27	F36
D4	D12	D20		E4	E12	E20	E28	E37		F20	F28	F37
D5	D13	D21		E5	E13	E21	E29	E38		F21	F29	F38
D6	D14	D22		E6	E14	E22	E30	E39		F22	F30	F39
D7	D15	D23		E7	E15	E23	E31	E40		F23	F31	F40
D8	D16	D24		E8	E16	E24	E32	E41		F24	F32	F41
G1	G9	G17	G25	H1	H9	H17	H25	H35	I1	I17	I25	I34
G2	G10	G18		H2	H10	H18	H26	H36		I18	I26	I35
G3	G11	G19		H3	H11	H19	H27	H37		I19	I27	I36
G4	G12	G20		H4	H12	H20	H28	H38		I20	I28	I37
G5	G13	G21		H5	H13	H21	H29	H39		I21	I29	I38
G6	G14	G22		H6	H14	H22	H30	H40		I22	I30	I39
G7	G15	G23		H7	H15	H23	H31	H41		I23	I31	I40

144

FIGURE 2 Specimen Locations in Sheet Stock.

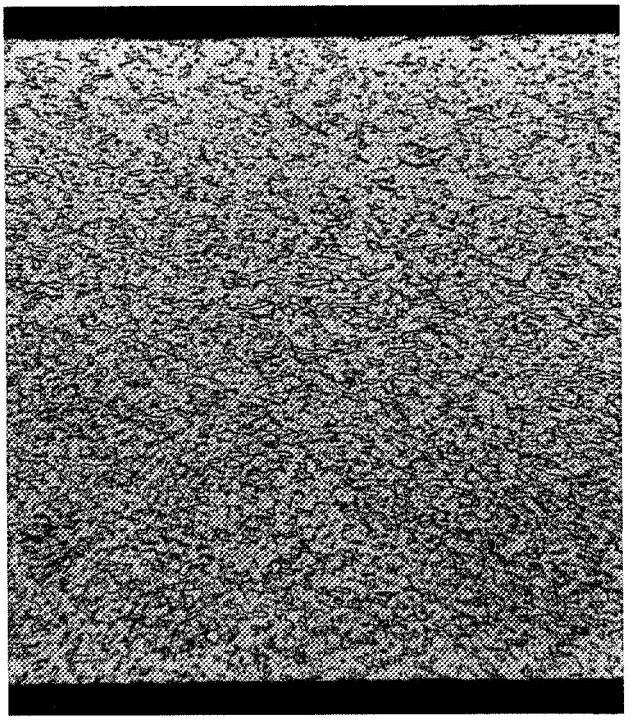

Longitudinal Section of 2IM, 200X

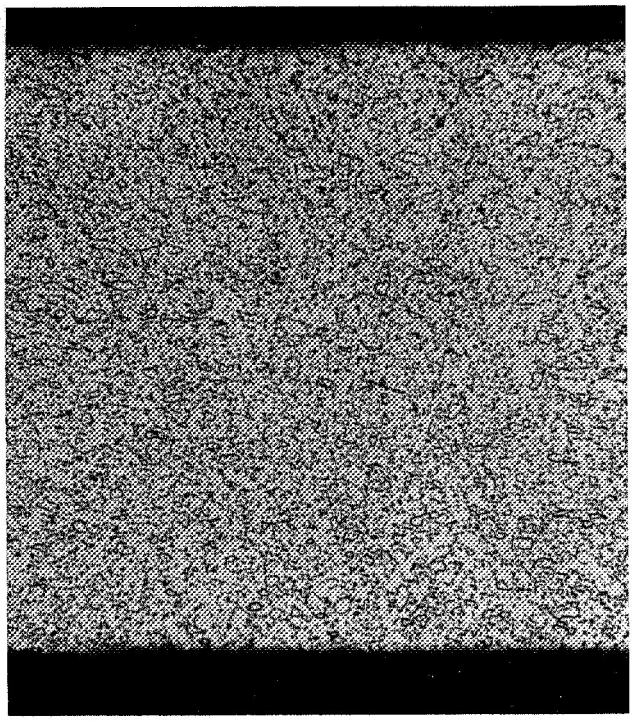

Transverse Section of 1GM, 200X

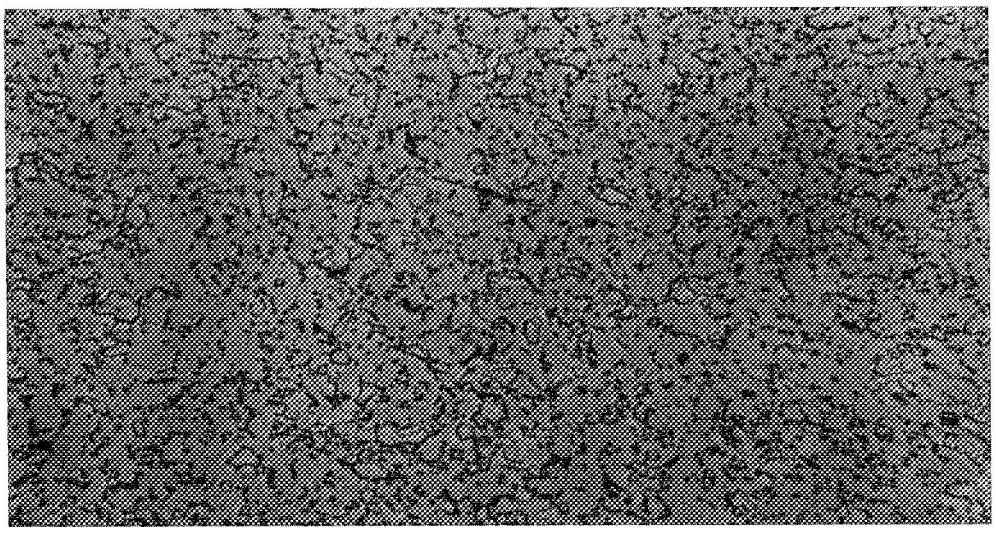

Transverse Section of 1GM at 450X

FIGURE 3. Typical Sectional Micrographs of Ti-6Al-4V Sheet Material.

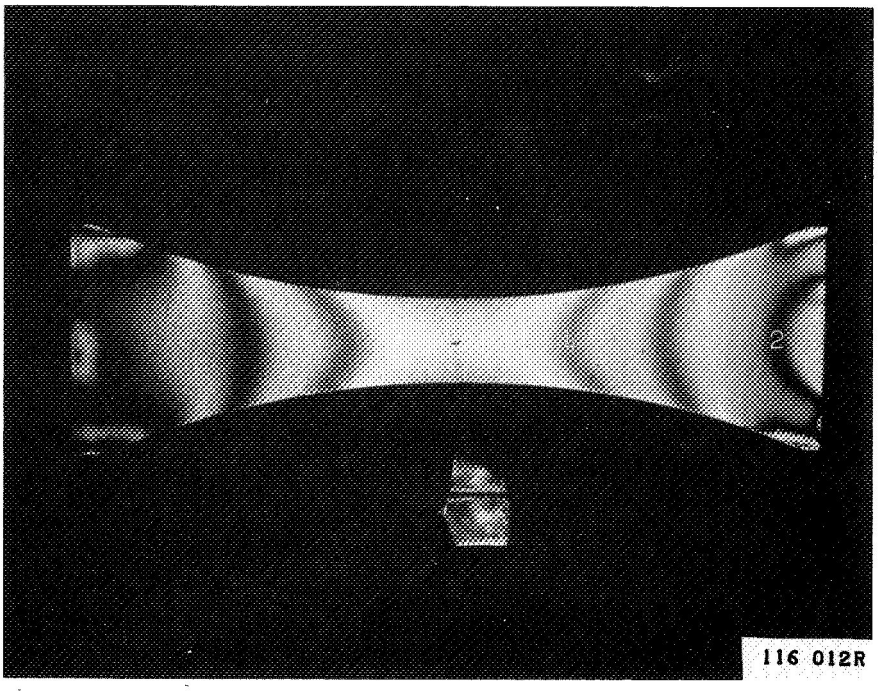

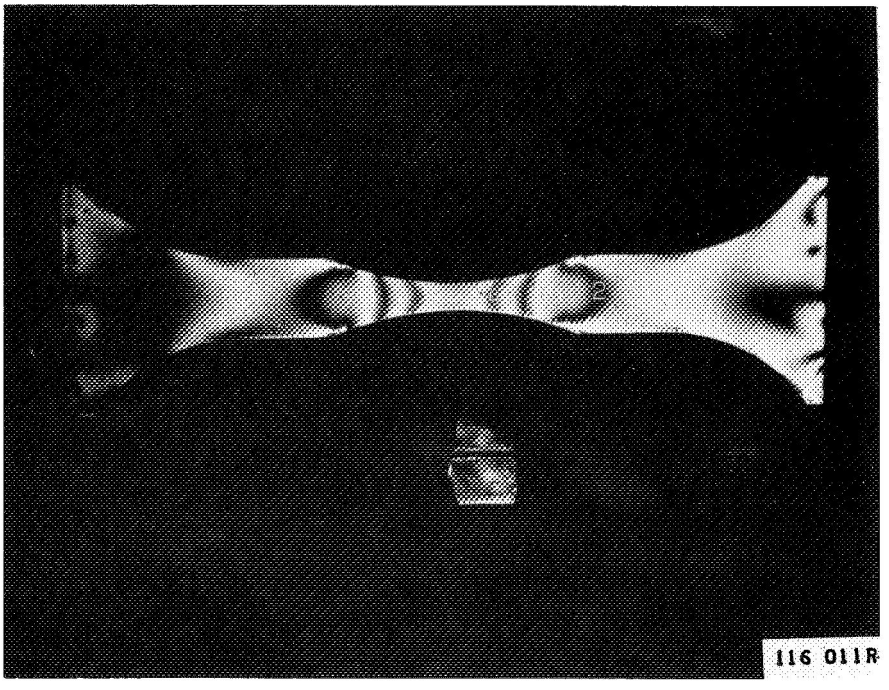

FIGURE 4. Photoelastic Models of 0.750-in and 0.250-in Wide Specimen Geometries Under Static Load in New Low Cap Fatigue Machine. Models were fabricated full-size, of 0.130-in thick plastic, and are shown under 67.0 and 22.3 lb load, respectively.

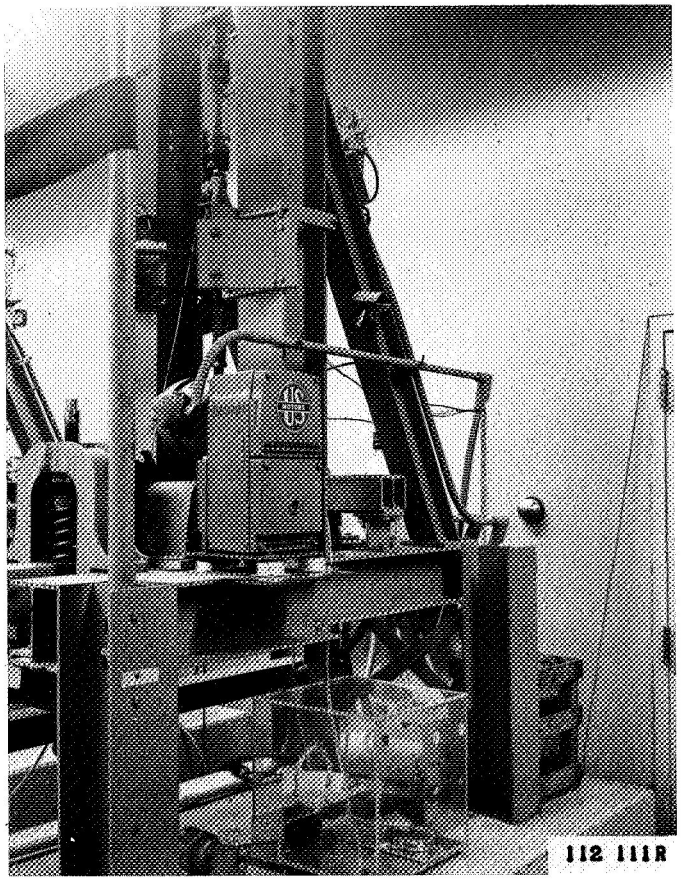

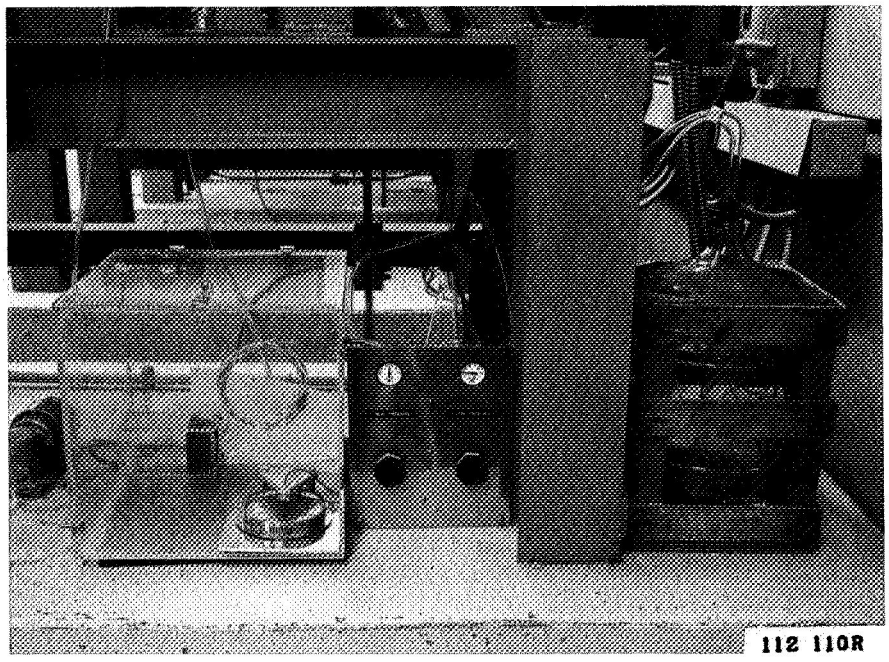

FIGURE 5. Standard 10,000-lb S-N Machine.
Humidity control system shown below.

LOCKHEED
CALIFORNIA COMPANY

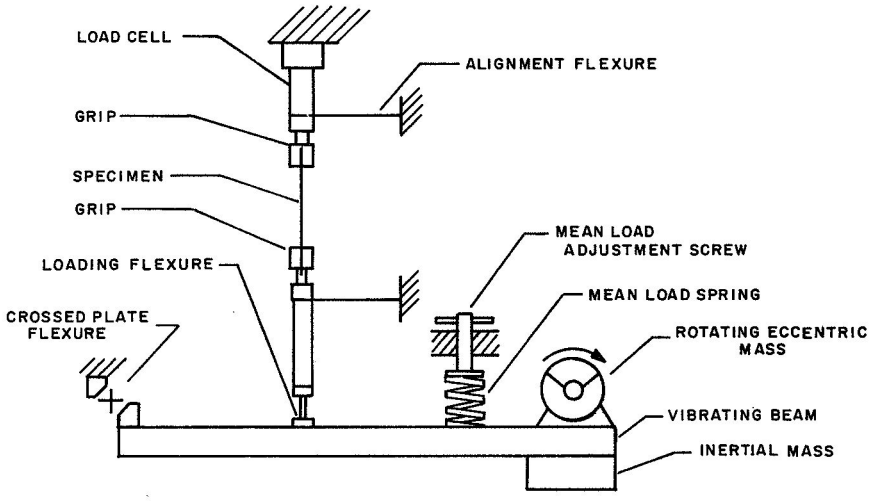

SCHEMATIC, STANDARD 10,000 LB. S-N MACHINE

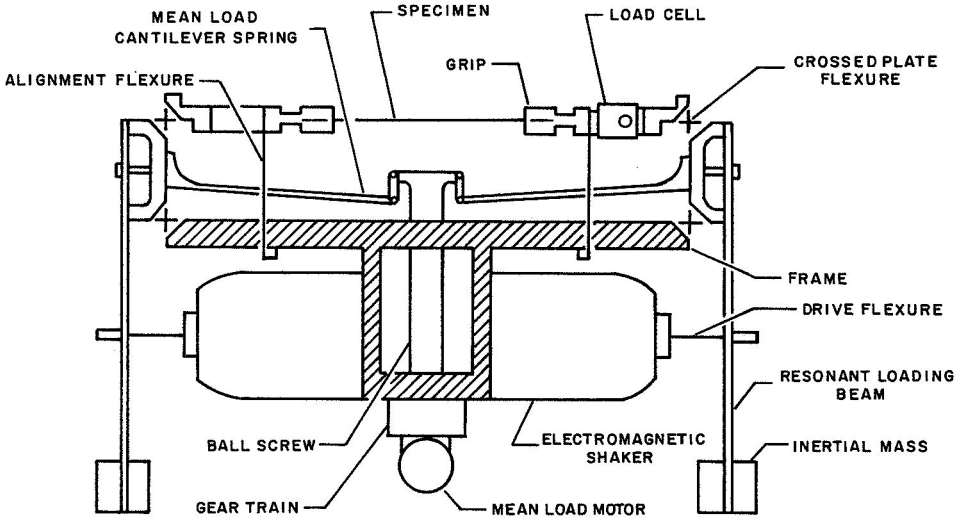

SCHEMATIC, NEW LOW CAPACITY FATIGUE MACHINE

Figure 6. Fatigue Test Machines, Schematic

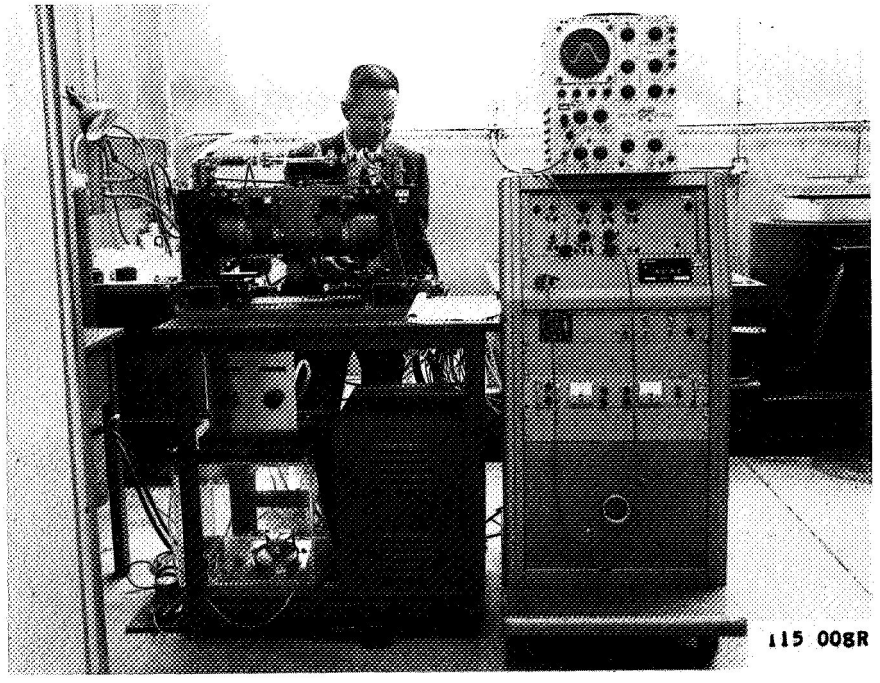

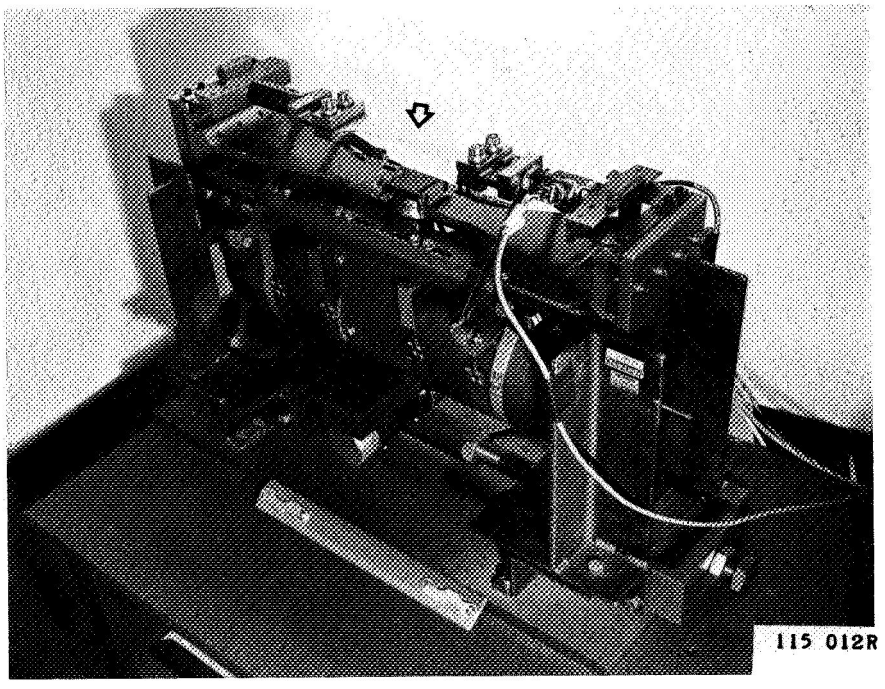

FIGURE 7. New Lockheed Low Capacity Fatigue Machine. Console in upper view houses electronic servo controls. Lower view shows a 0.250-in. wide Ti-6Al-4V specimen installed without humidity control enclosure.

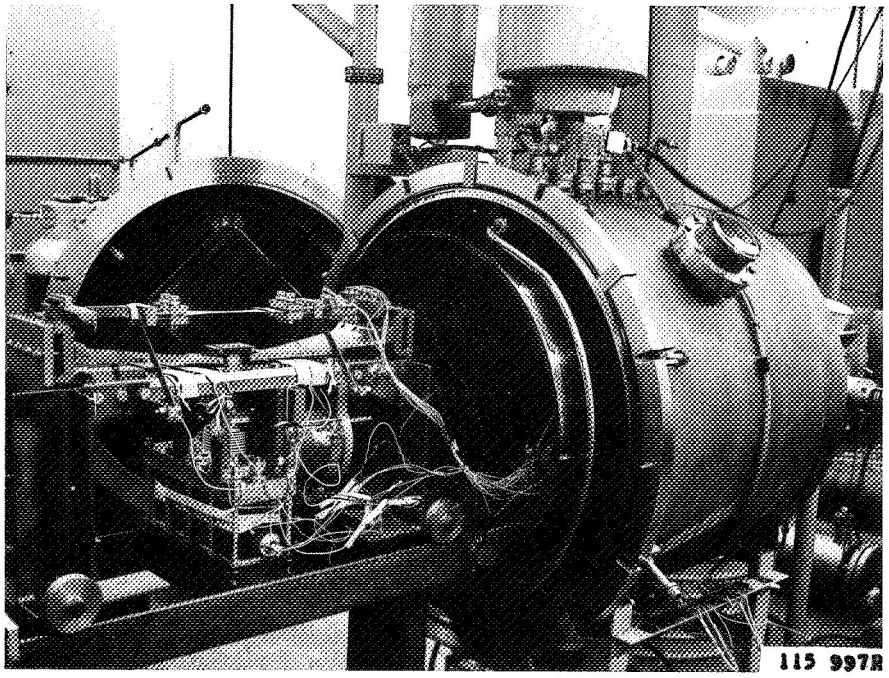

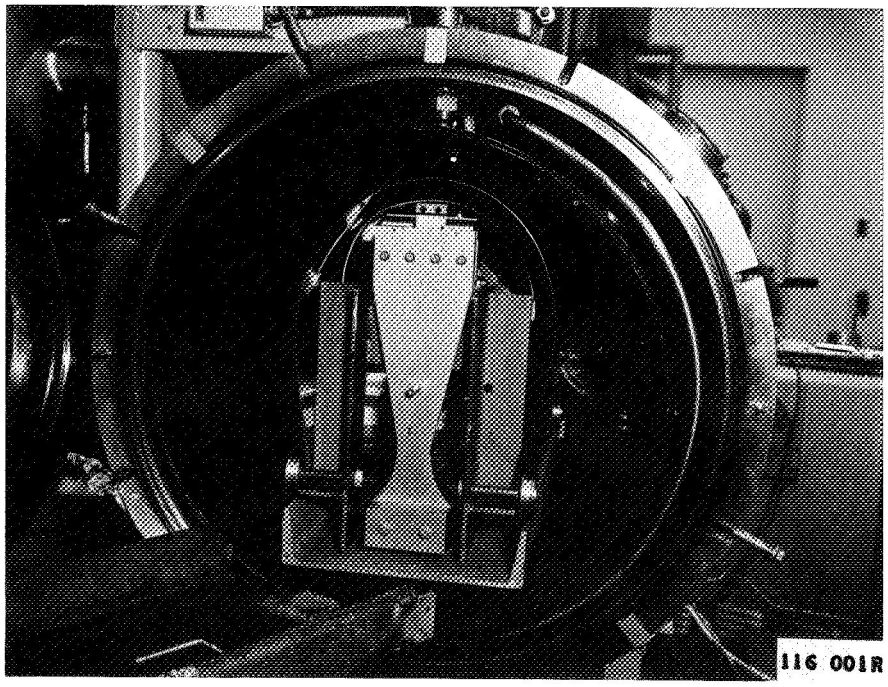

FIGURE 8. Installation of Low Capacity Fatigue Machine in Vacuum Chamber. Upper photograph shows arrangement of machine components, power and control leads, and three of the five heater elements, before mounting the warm wall and the radiation shield. The entire assembly prior to closing the chamber is shown below.

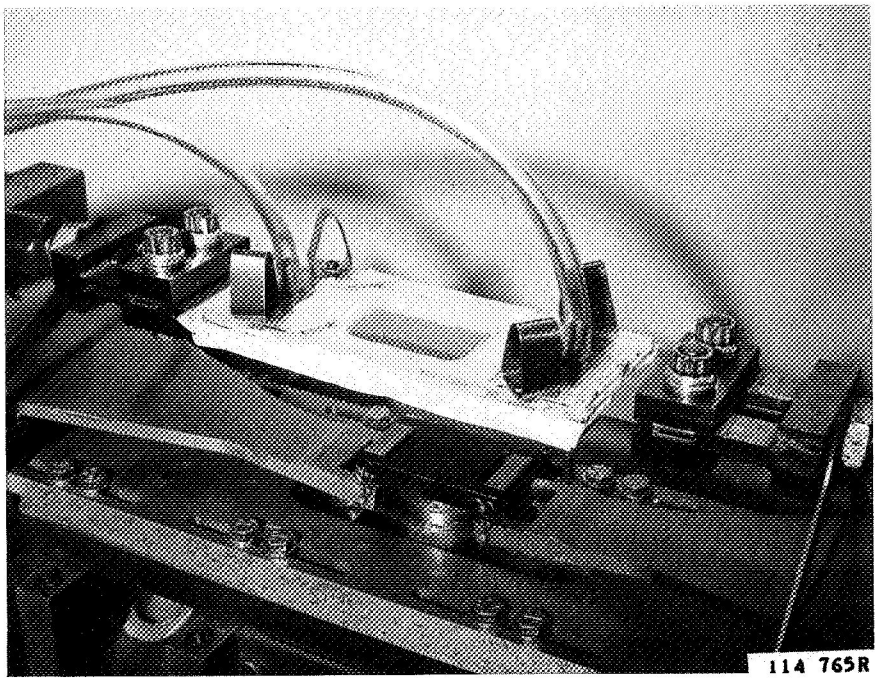

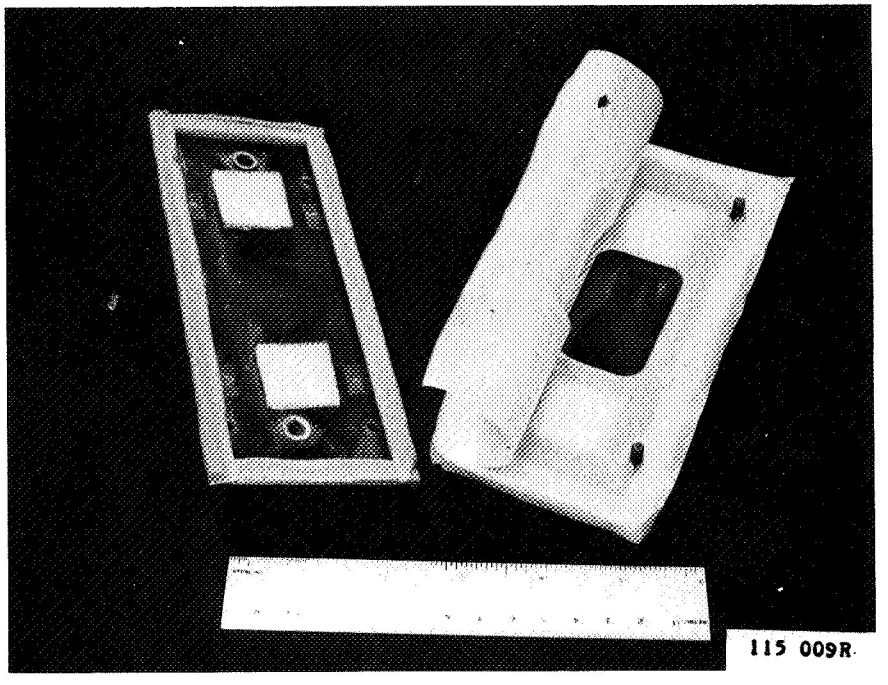

FIGURE 9. Specimen Humidity Control Enclosure.
Installation on a 0.750-in. specimen shown above.
Details of teflon sheet and foam pressure pads shown below.

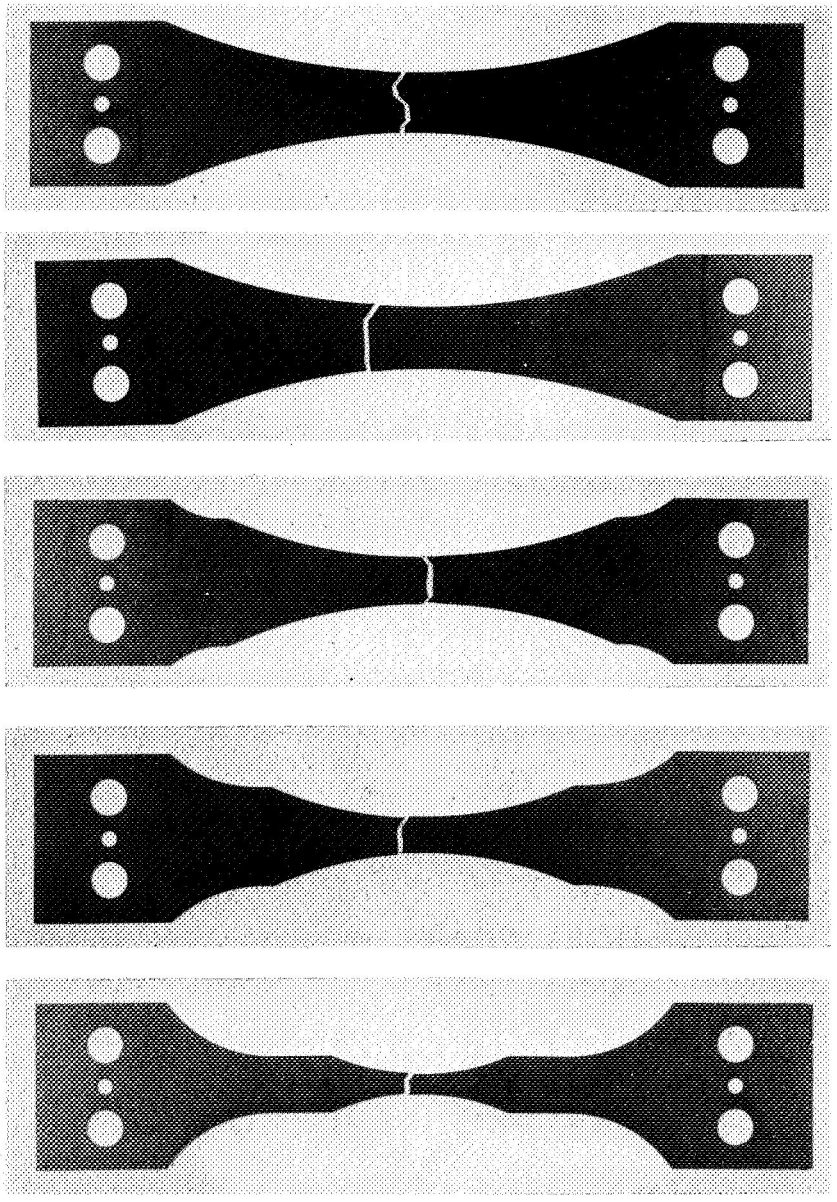

1C15
0.750-inch
130 ksi
24,900 Cycles

2H7
0.750-inch
100 ksi
5,290,000 Cycles

1D11
0.572-inch
115 ksi
70,100 Cycles

1H3
0.483-inch
110 ksi
282,700 Cycles

1G9
0.250-inch
105 ksi
2,920,000 Cycles

FIGURE 10. Typical Ti-6Al-4V Specimens After Fatigue Test.

LOCKHEED
CALIFORNIA COMPANY

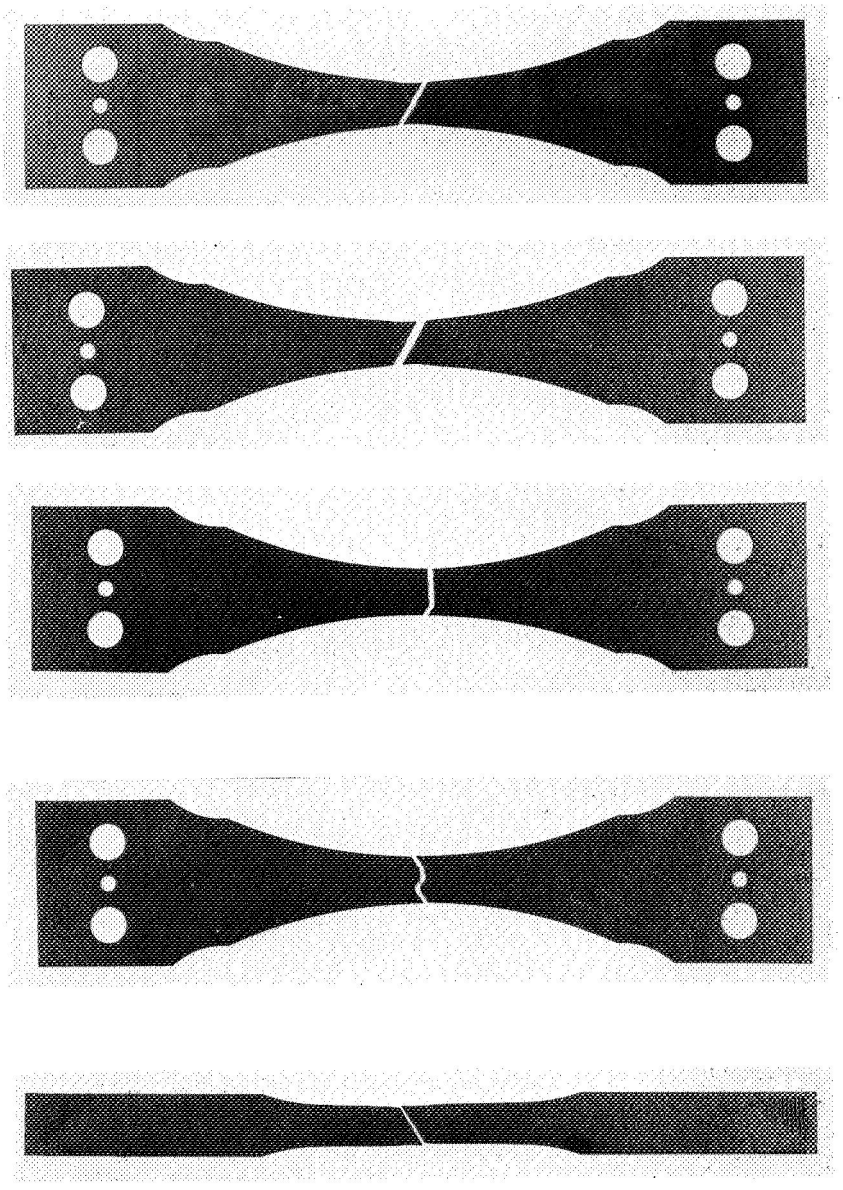

2C18
Norm. Atm. Press.
65-70% RH
137.5 ksi
3500 Cycles

2C17
$< 10^{-6}$ torr
127.5 ksi
49,600 Cycles

2D16
$< 10^{-6}$ torr
125 ksi
2,021,600 Cycles

1F5
Norm. Atm. Press.
65-70% RH
130 ksi
18,900 Cycles

2GT2
Room Conditions
Static Tension
142.0 ksi ult.

FIGURE 11. Typical 0.572-in. Ti-6Al-4V Specimens After Test. Failure modes under fatigue at high vacuum compared with those under fatigue and under static load at normal atmospheric conditions.

LOCKHEED
CALIFORNIA COMPANY

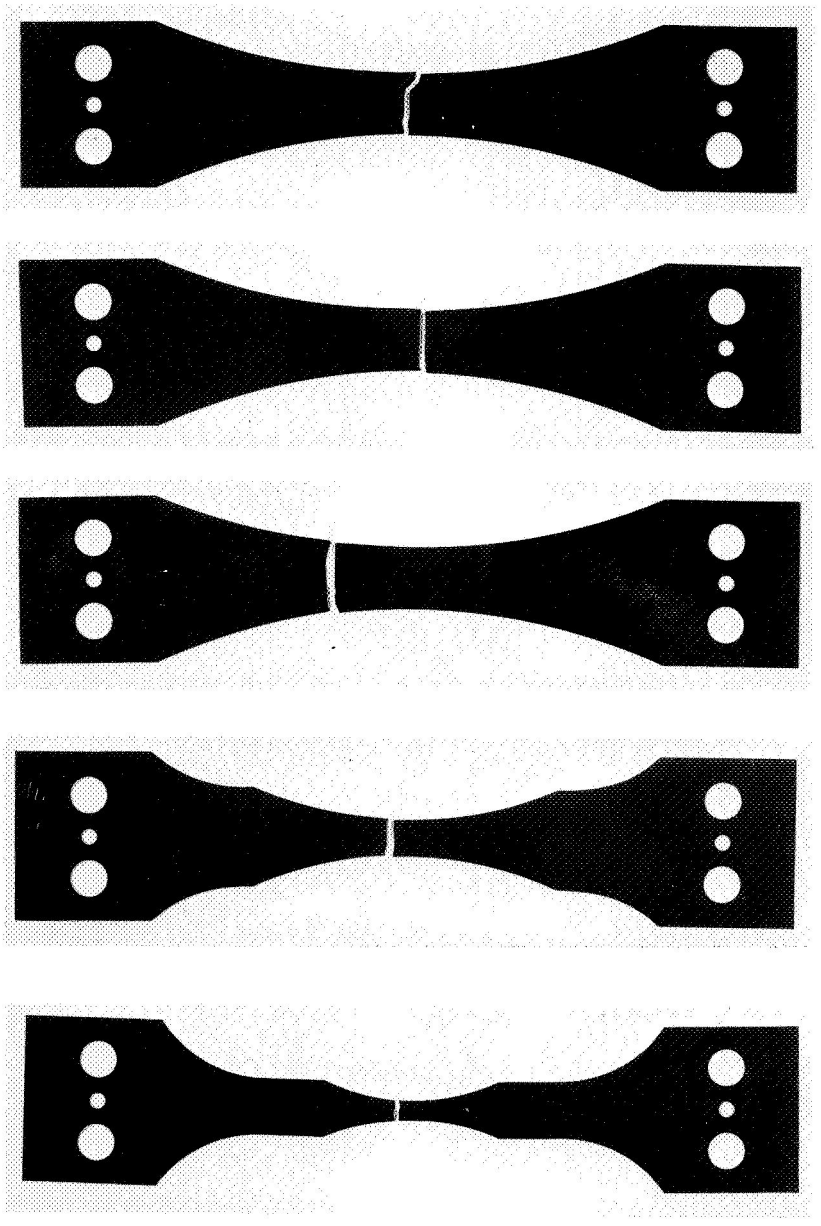

FIGURE 12. Typical 2024-T3 Specimens after Fatigue Test.

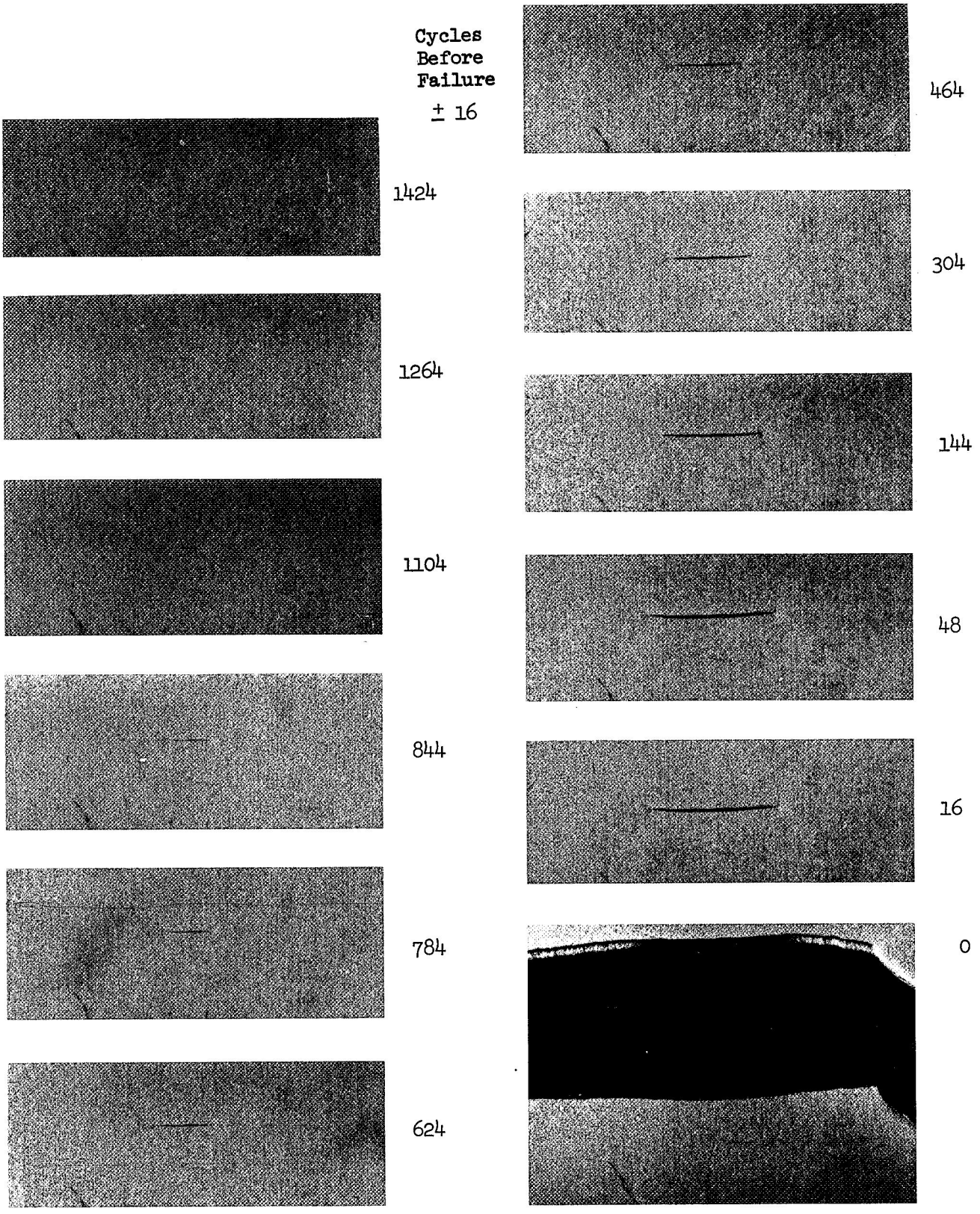

FIGURE 13. Crack Propagation in Ti-6Al-4V Specimen 2B8.
f_{max} = 110 ksi, total cycles 132,000. 5x size.

LOCKHEED
CALIFORNIA COMPANY

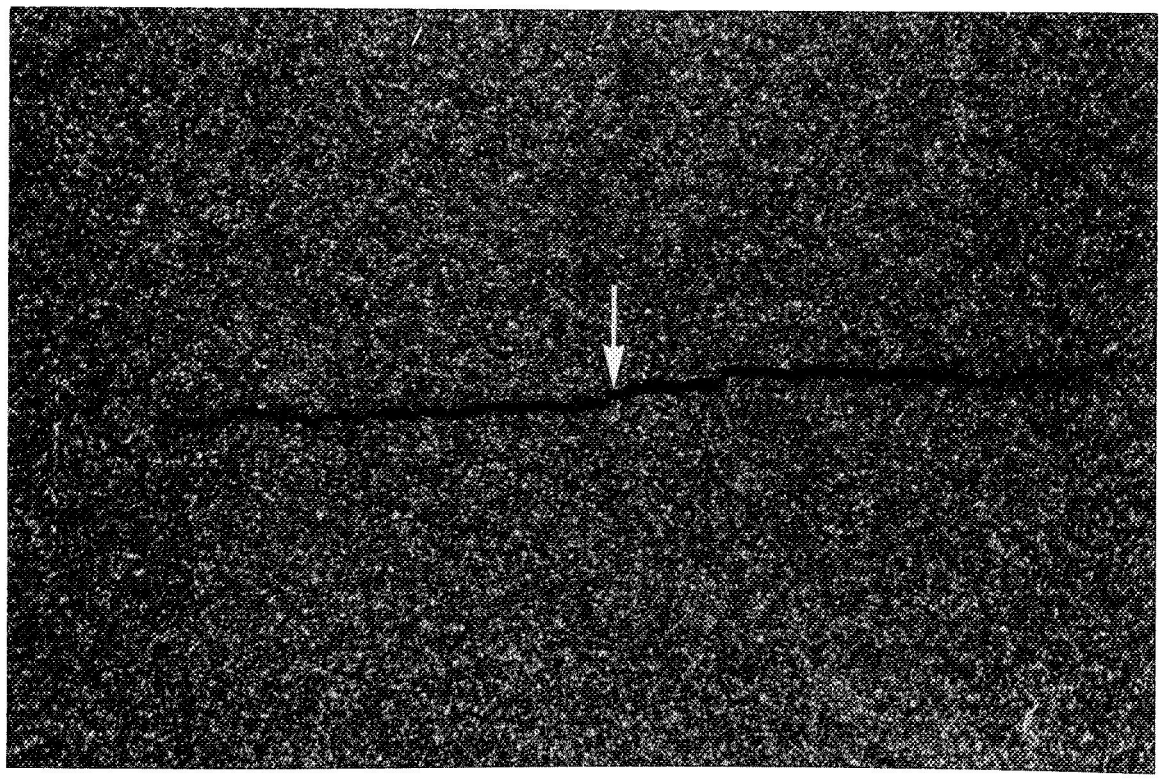

100X

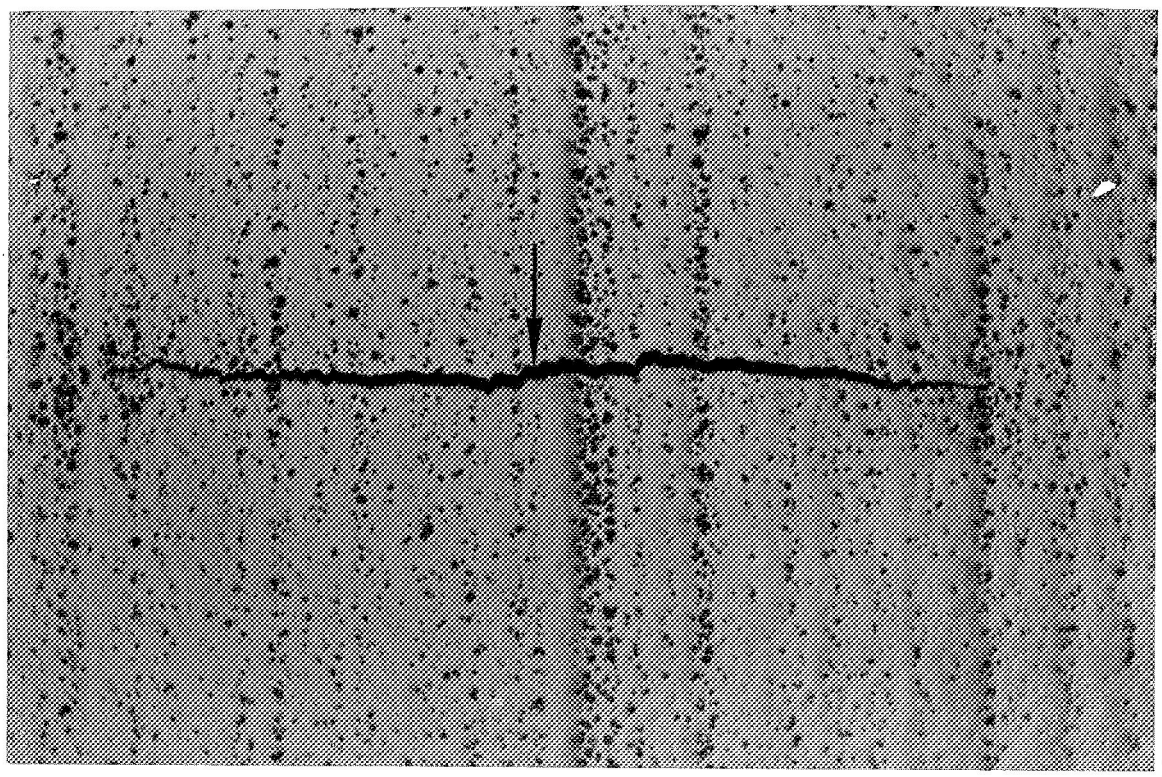

100X

FIGURE 14. Photomicrographs at 100 x of Crack in Ti-6Al-4V Specimen 1D24. After 42,900 cycles, crack 0.045-in. long was noted and test stopped, upper view. Lower view shows same area after removal of 0.0002-in. of surface material by light polishing. No inclusions or irregularities were apparent at crack origin.

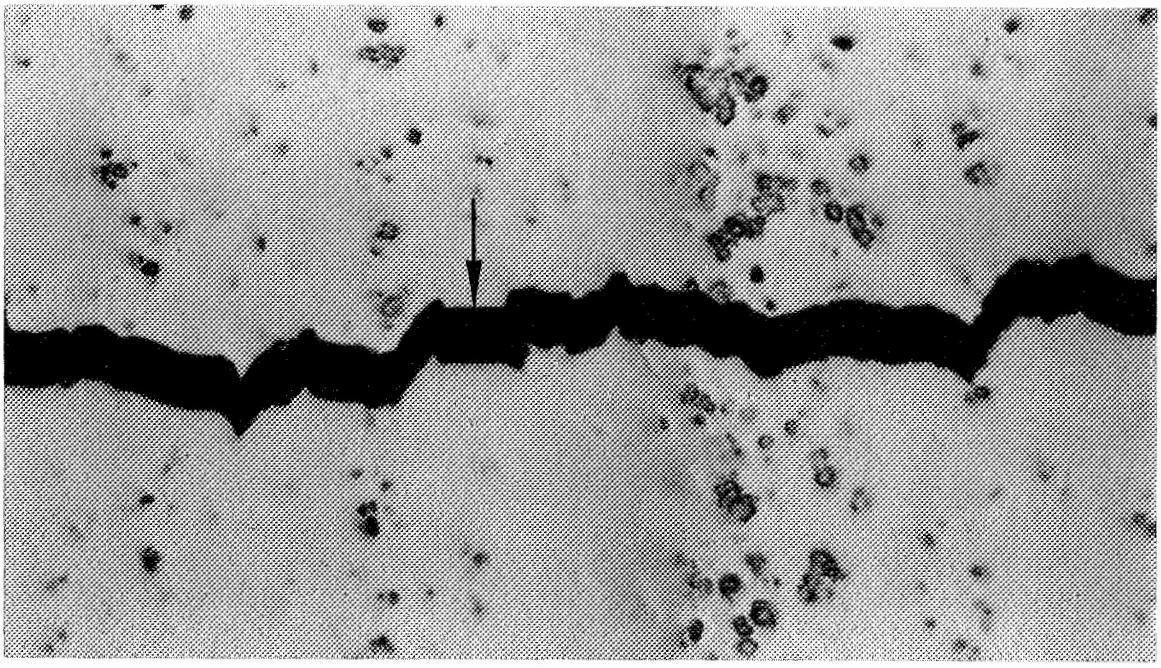

500X

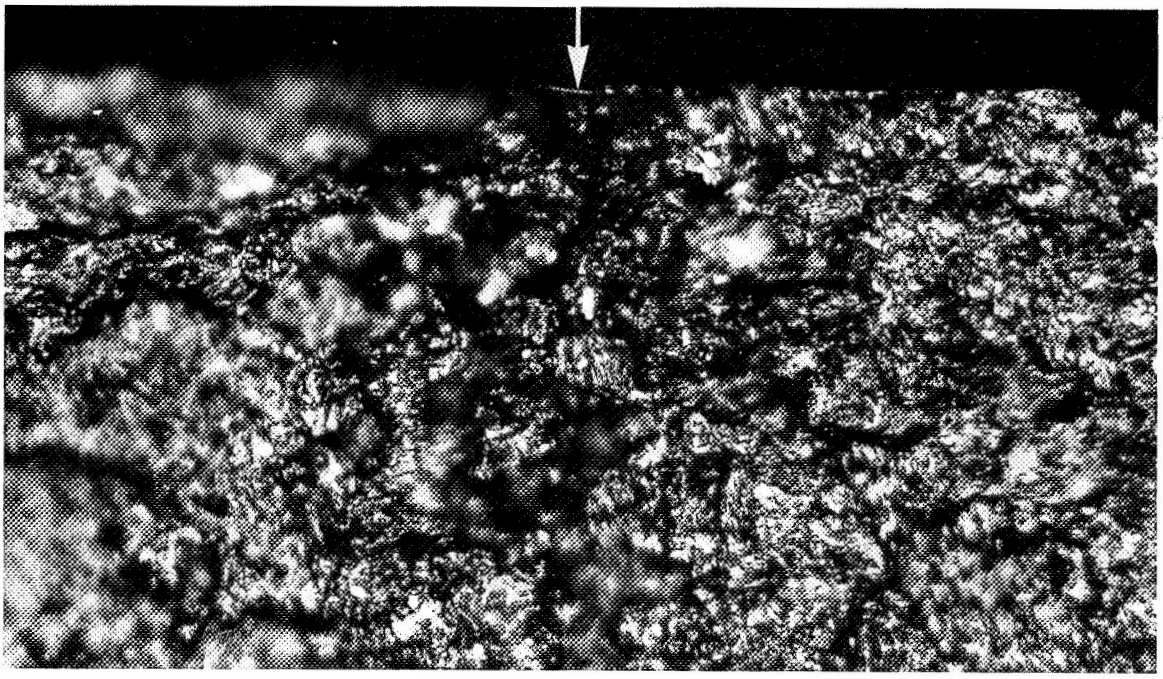

500X

FIGURE 15. Photomicrographs at 500x of Crack in Ti-6Al-4V Specimen 1D24. Upper view same as Figure 14, enlarged. Lower view shows the fracture face, the upper boundary being the sheet surface. Straight section indicated by the arrow is the failure origin. No inclusions are visible.

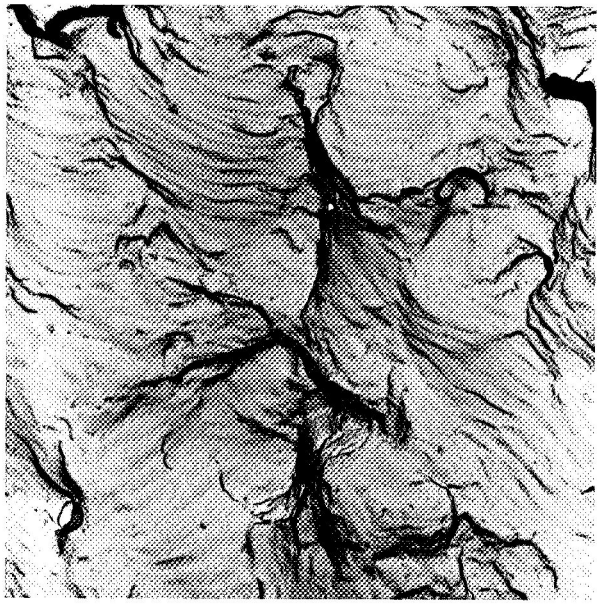

N6334 6500X

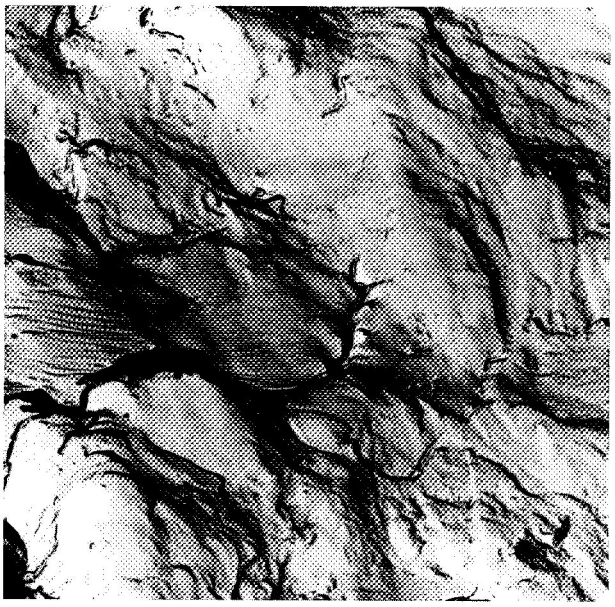

N6336 6500X

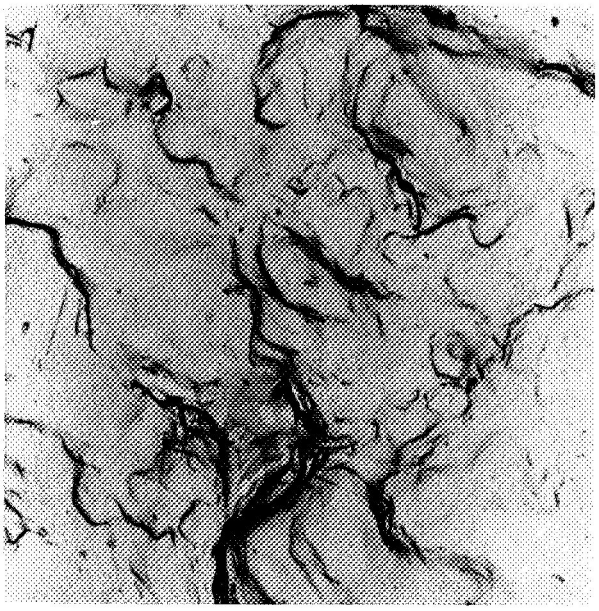

N6342 6500X

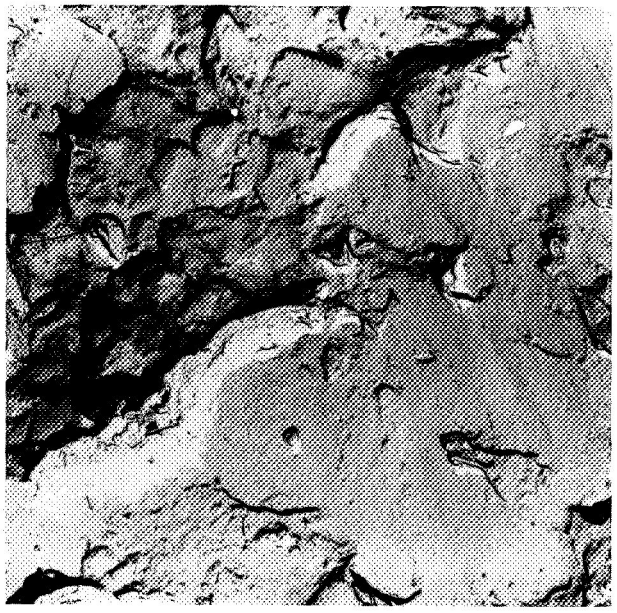

N6341 6500X

FIGURE 16. Electron Microfractographs of Short-Lived Ti-6Al-4V Specimen. Specimen 1H12, 0.750-inch width, f_{max}= 115 ksi, 27,000 cycles.

LOCKHEED
CALIFORNIA COMPANY

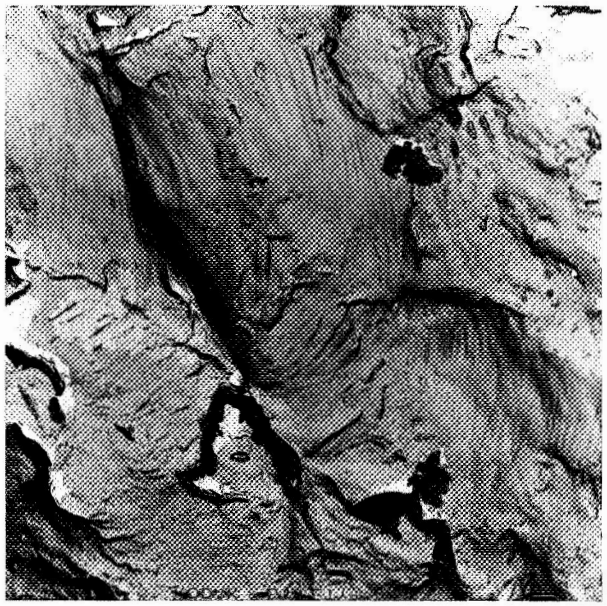

N6381 6500X

N6383 6500X

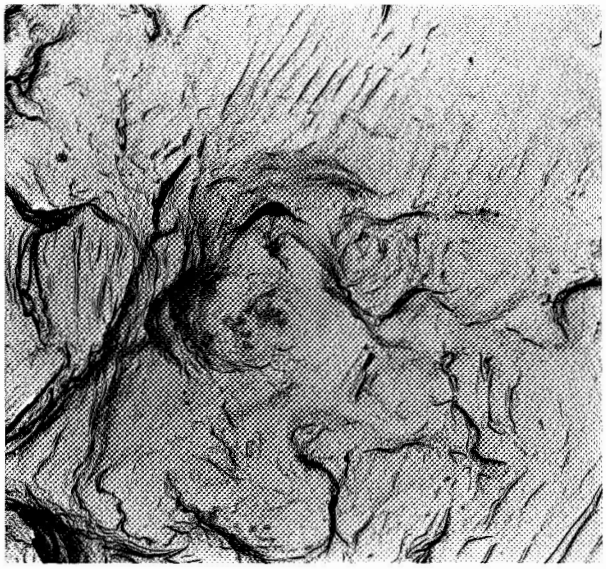

N6400 6500X

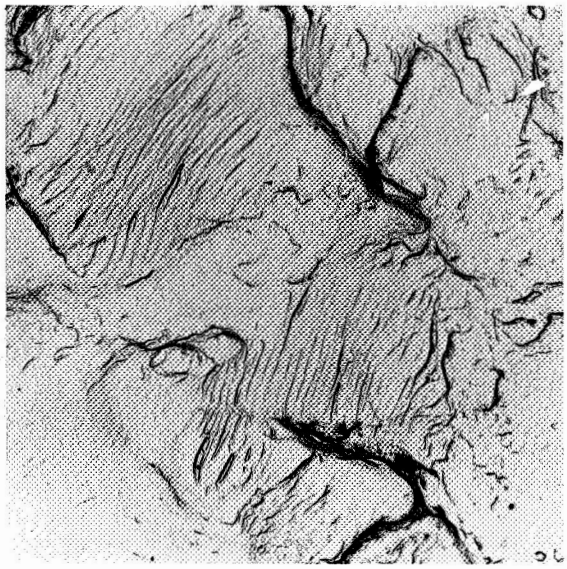

N6403 6500X

FIGURE 17. Electron Microfractographs of Long-Lived Ti-6Al-4V Specimen. Specimen 2H6, 0.250-inch width, f_{max}= 115 ksi, 2,920,000 cycles.

LOCKHEED
CALIFORNIA COMPANY

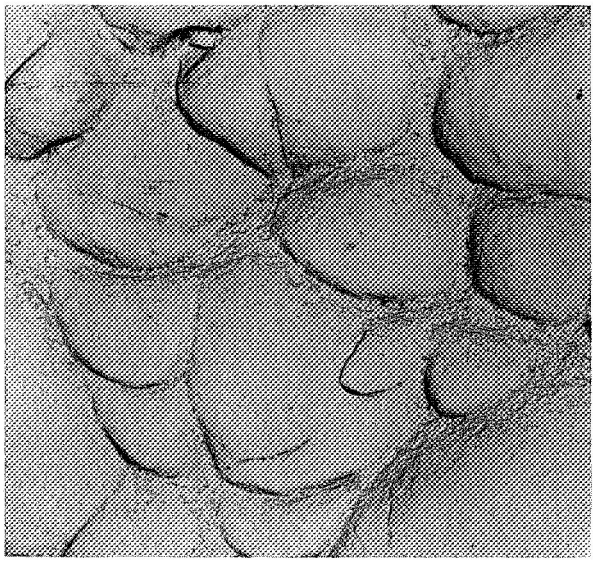

N6482 6500X
At edge of specimen

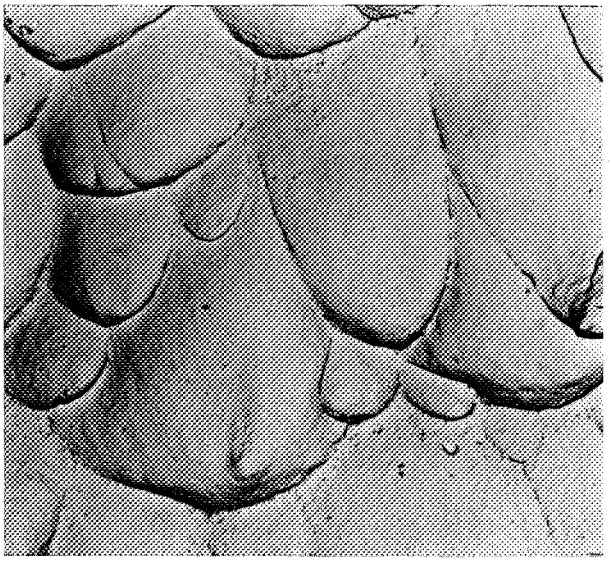

N6463 6500X
Near center of specimen

N6484 6500X
In region of fracture origin

N6469 6500X
In region of fracture origin

FIGURE 18. Electron Microfractographs of Ti-6Al-4V Tested in Fatigue Under Vacuum. Above, left and right, Specimen 2G14; f_{max} = 130 ksi; 19,800 cycles. Below, left and right, Specimen 2D16; f_{max} = 125 ksi; 2,022,000 cycles.

LOCKHEED
CALIFORNIA COMPANY

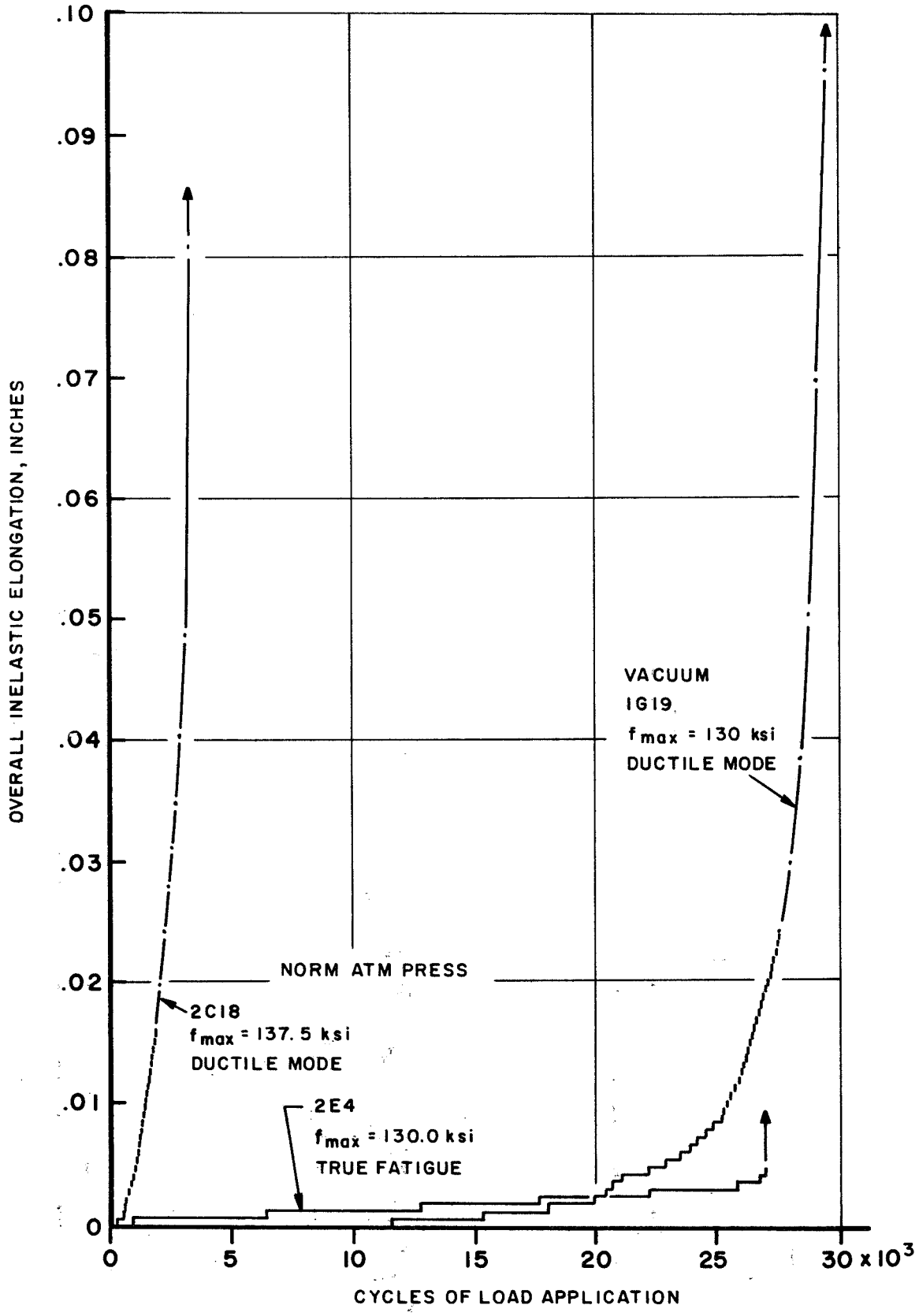

FIGURE 19. Inelastic Deformations in Ti-6Al-4V Fatigue Tests.

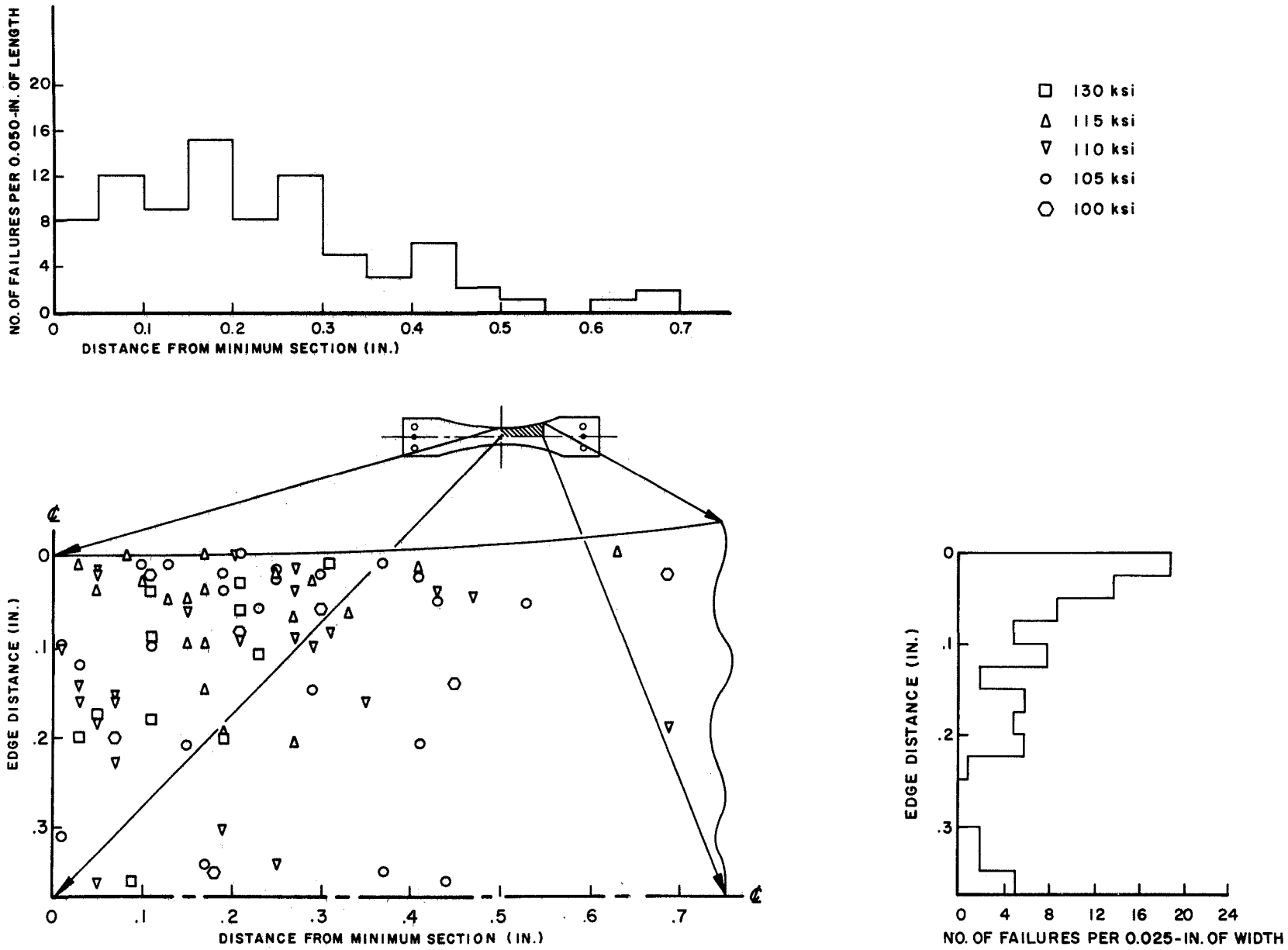

FIGURE 20. Failure Locations, 0.750-inch Wide Ti-6Al-4V Specimens.

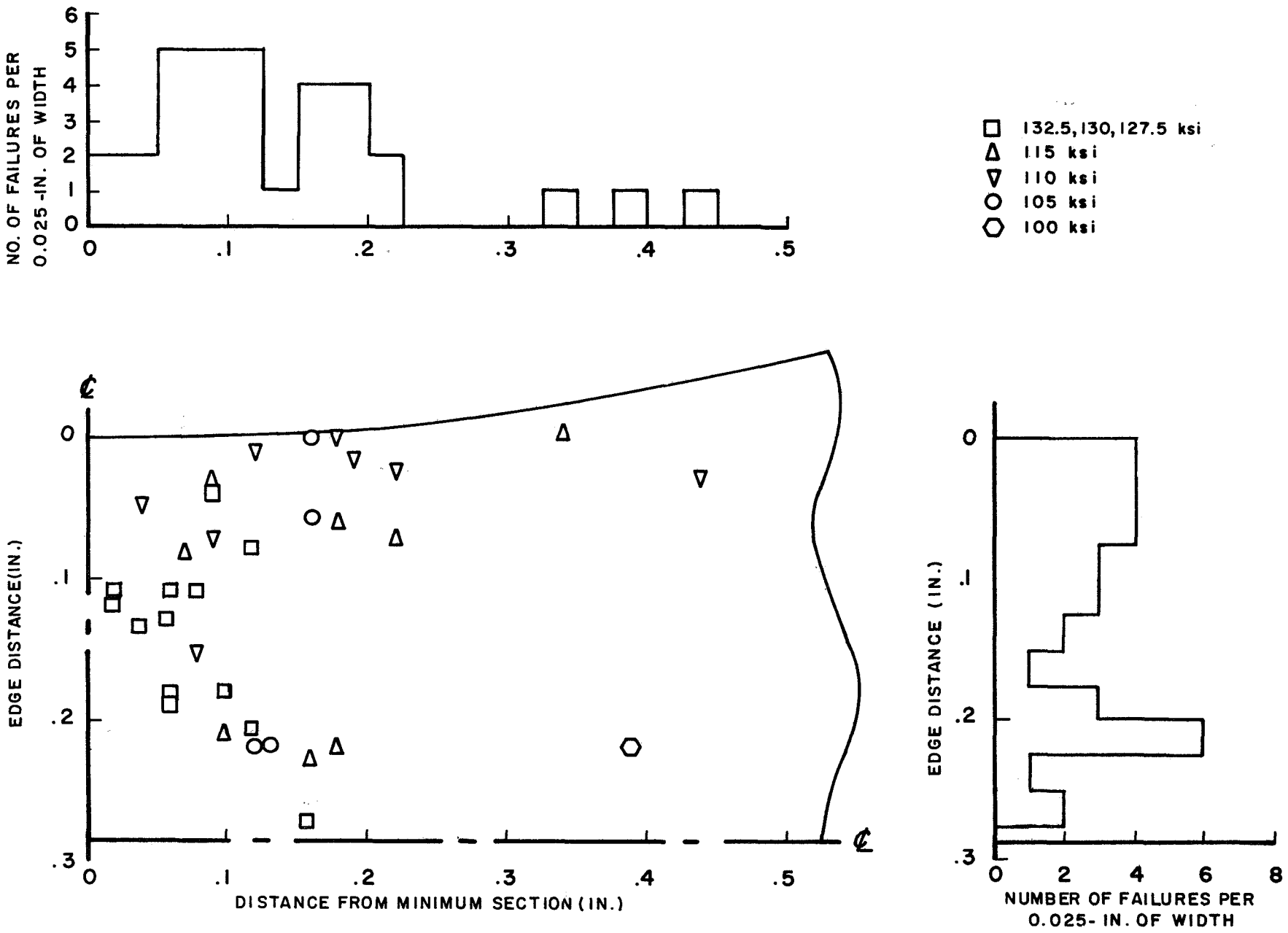

FIGURE 21. Failure Locations, 0.572-inch Wide Ti-6Al-4V Specimens.

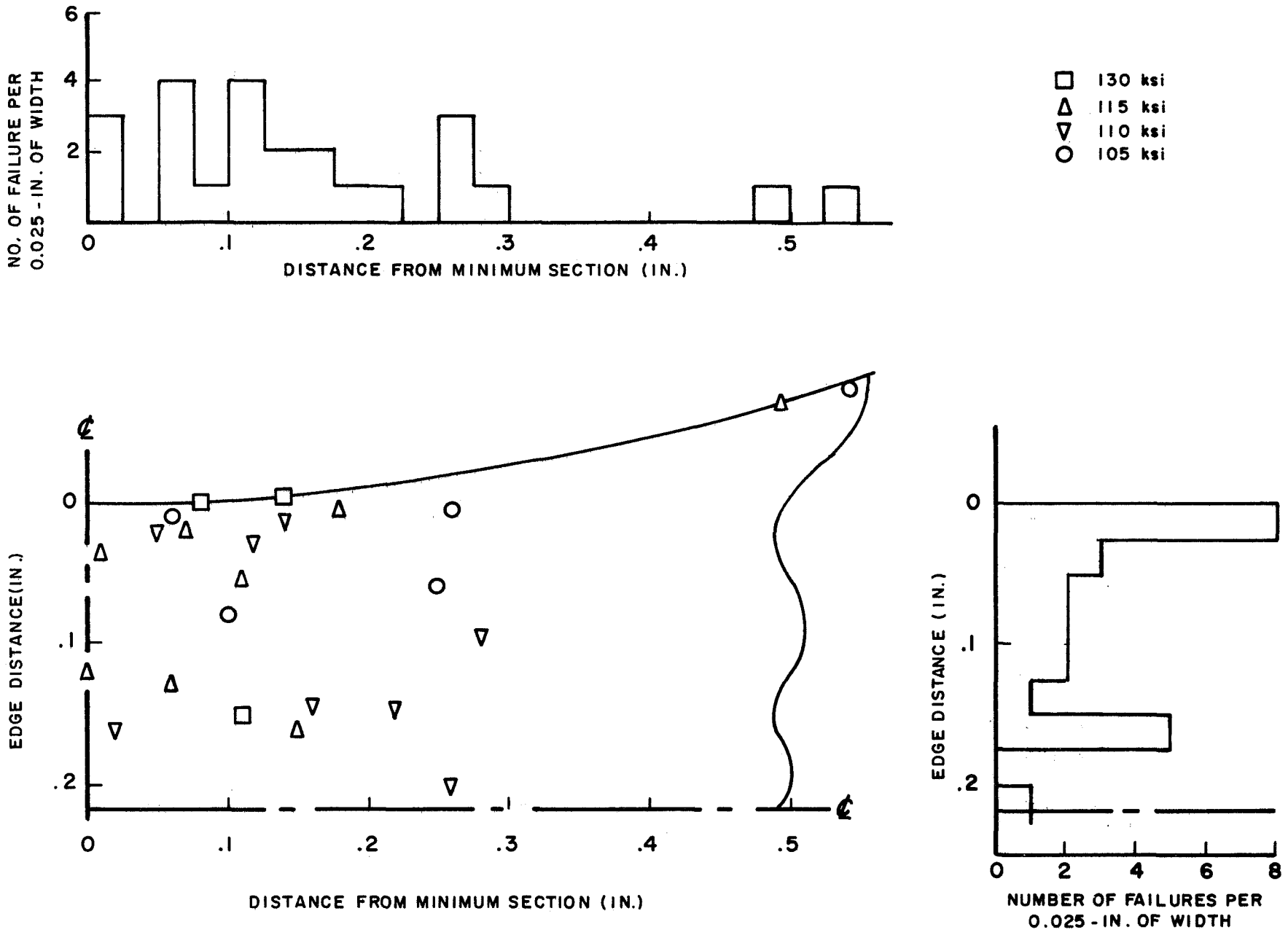

FIGURE 22. Failure Locations, 0.438-inch Wide Ti-6Al-4V Specimens.

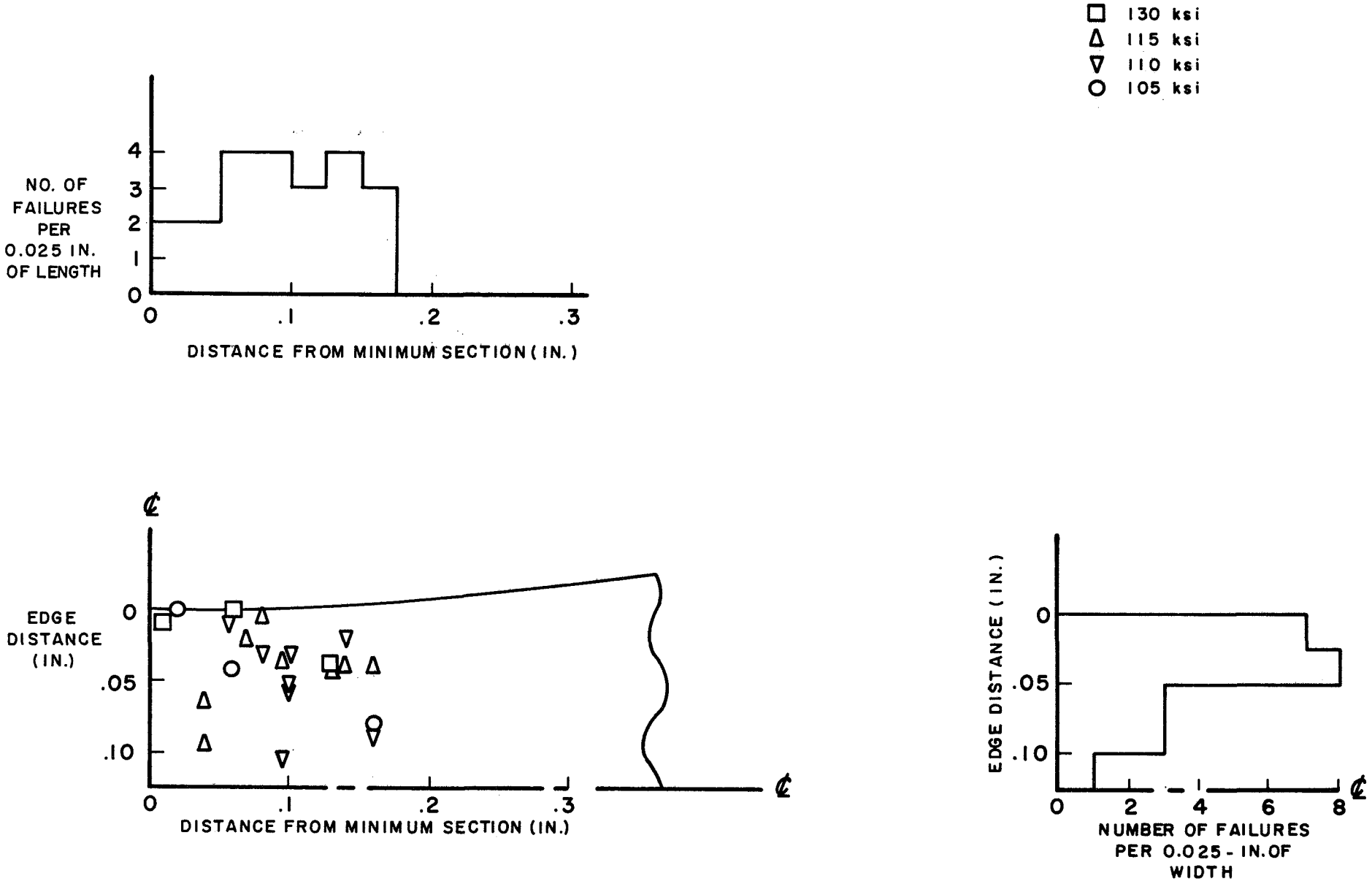

FIGURE 23. Failure Locations, 0.250-inch Wide Ti-6Al-4V Specimens.

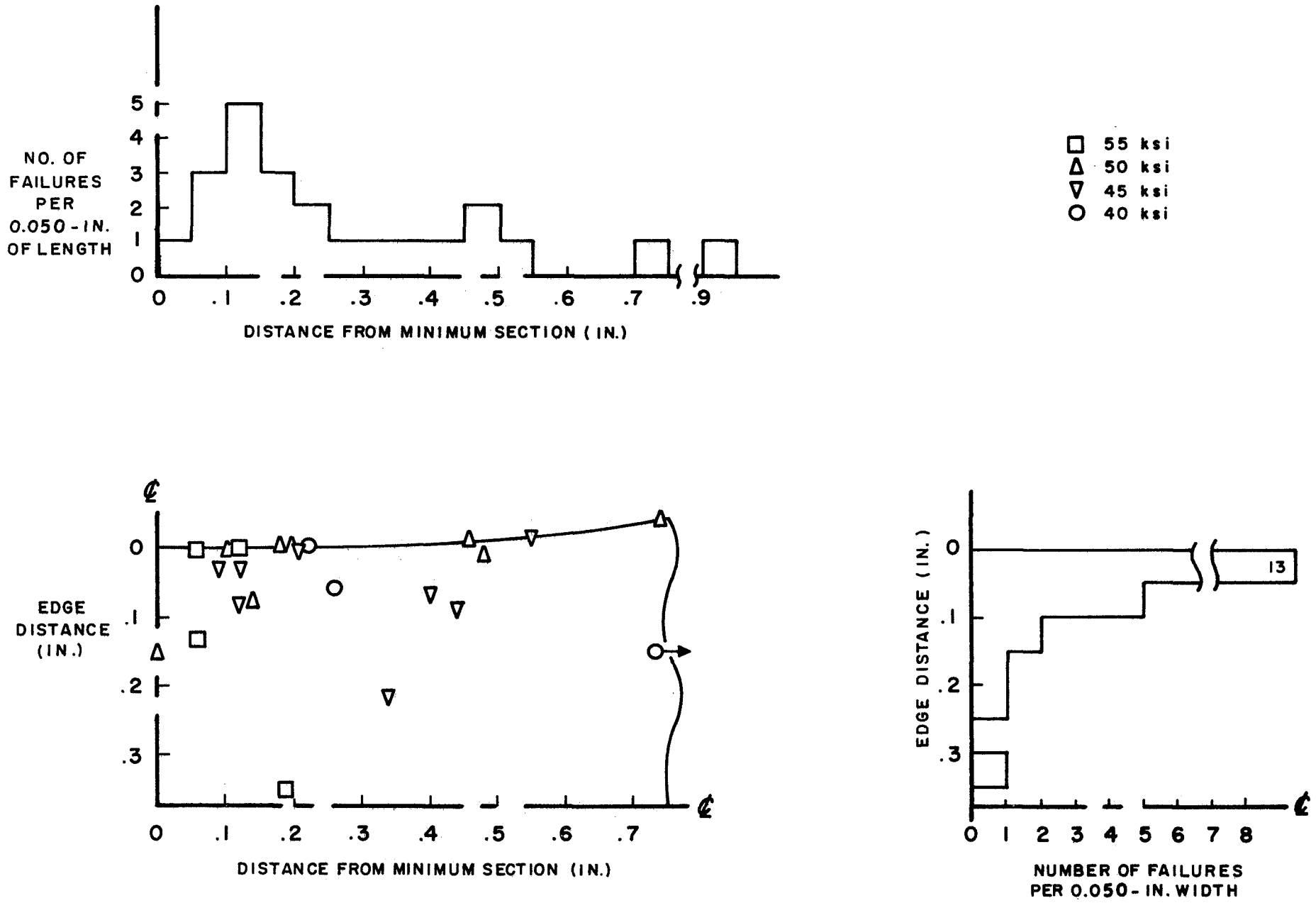

FIGURE 24. Failure Locations, 0.750-inch Wide 2024-T3 Specimens.

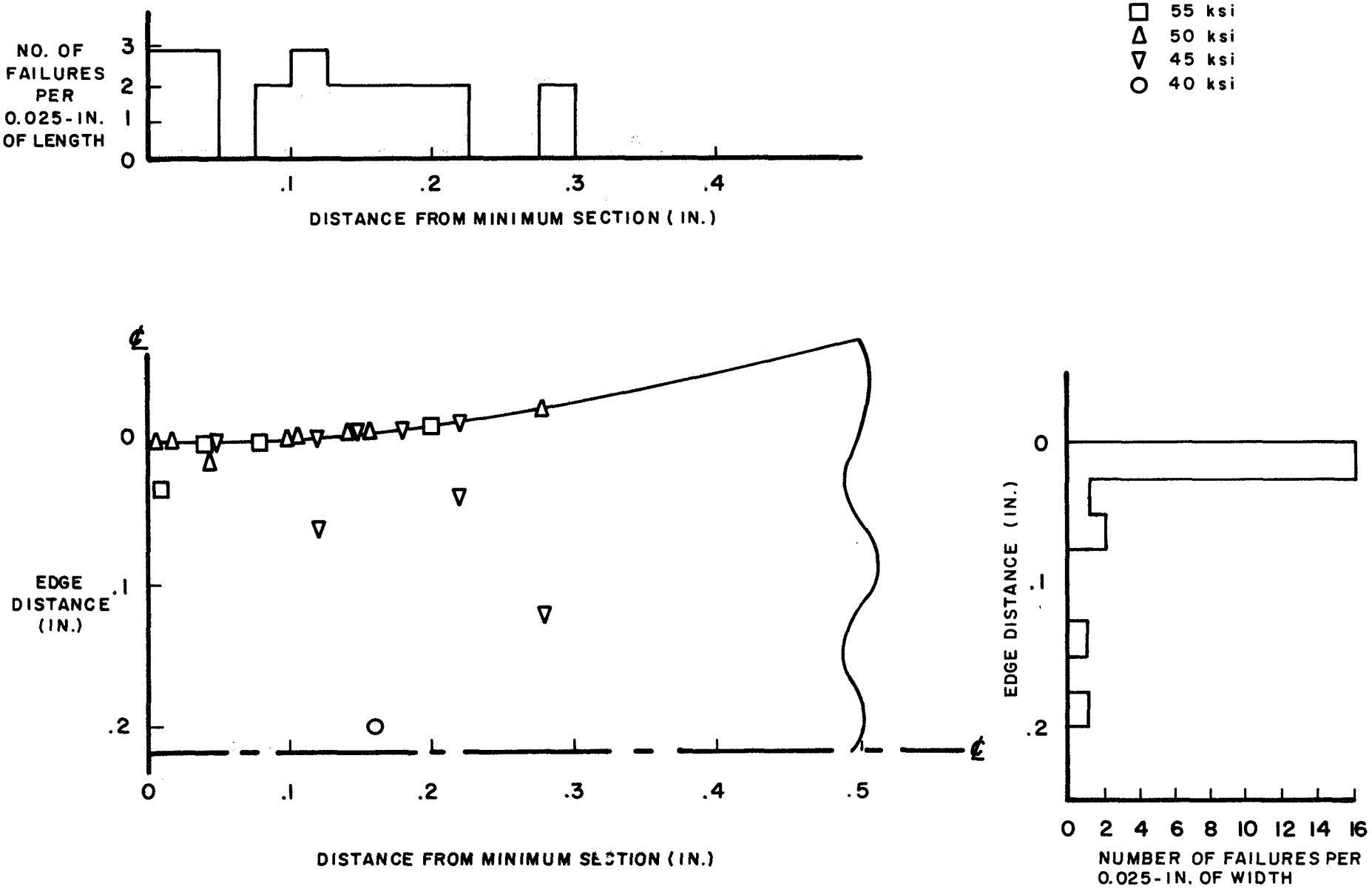

FIGURE 25. Failure Locations, 0.438-inch Wide 2024-T3 Specimens.

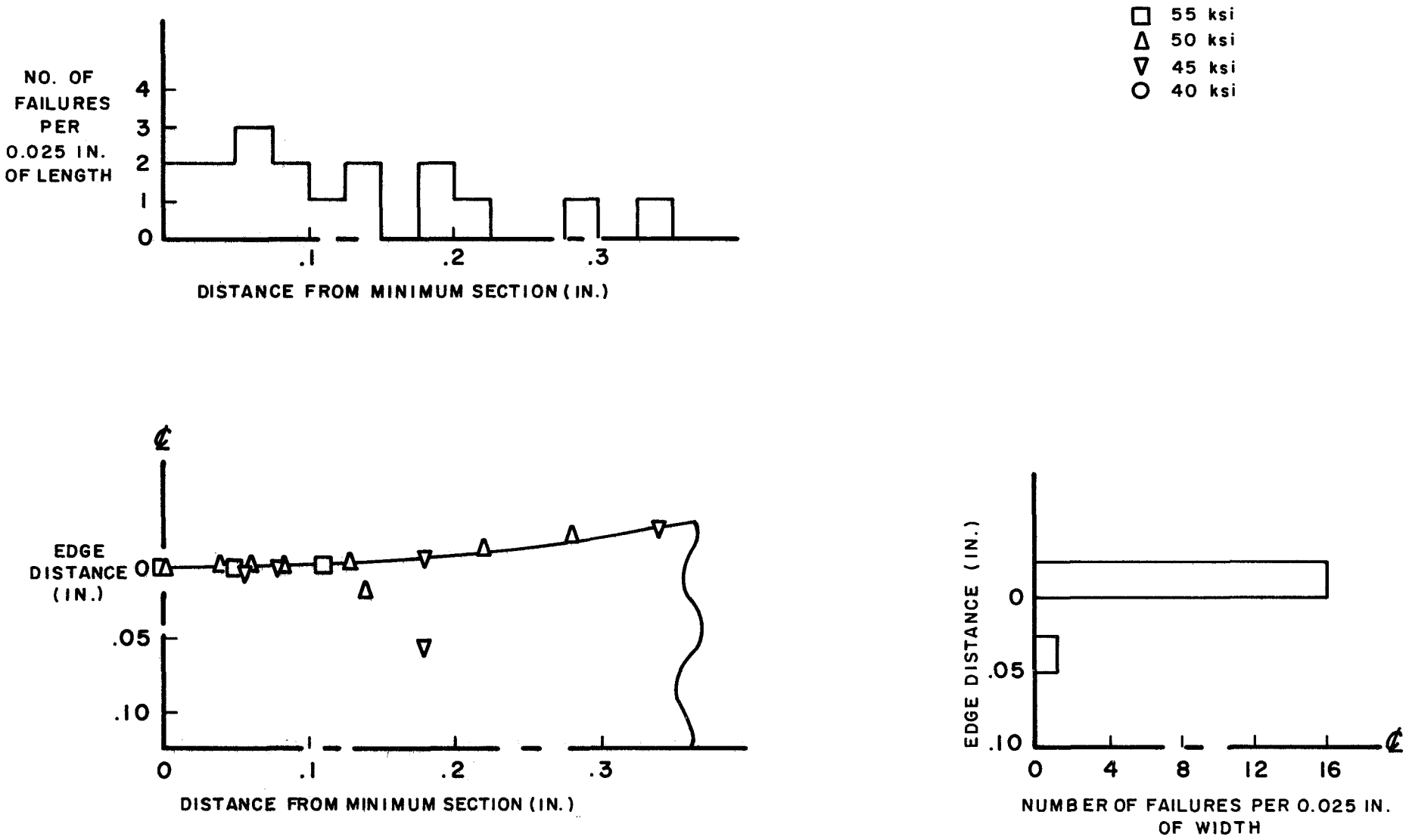

FIGURE 26. Failure Locations, 0.250-inch Wide 2024-T3 Specimens.

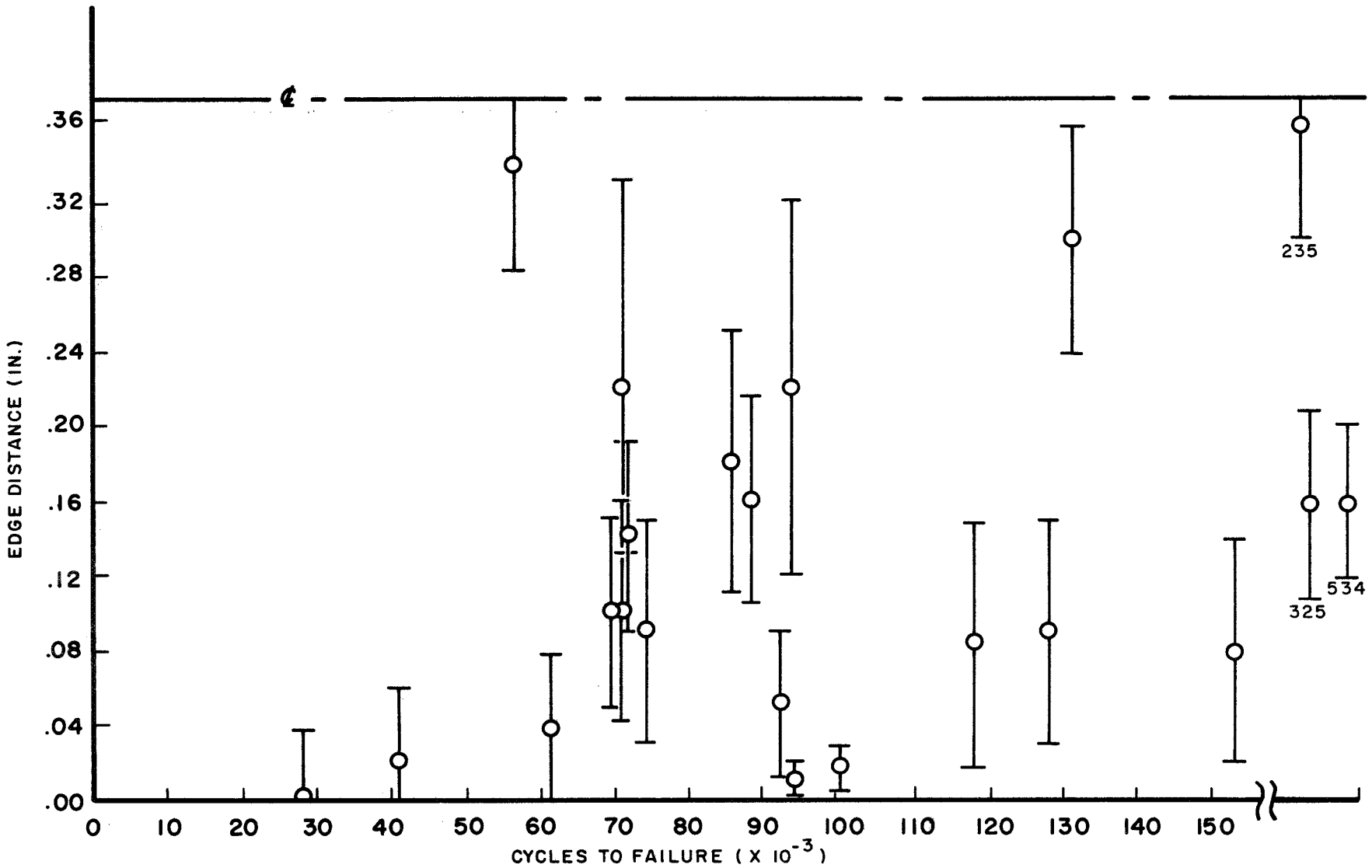

FIGURE 27. Location of Fatigue Crack with Respect to Specimen Edge vs. Fatigue Life. Width of the fatigue portion indicated. All specimens 0.750-inch wide Ti-6Al-4V, tested at f_{max} = 110 ksi (ref. Tables 6, 7, and 8).

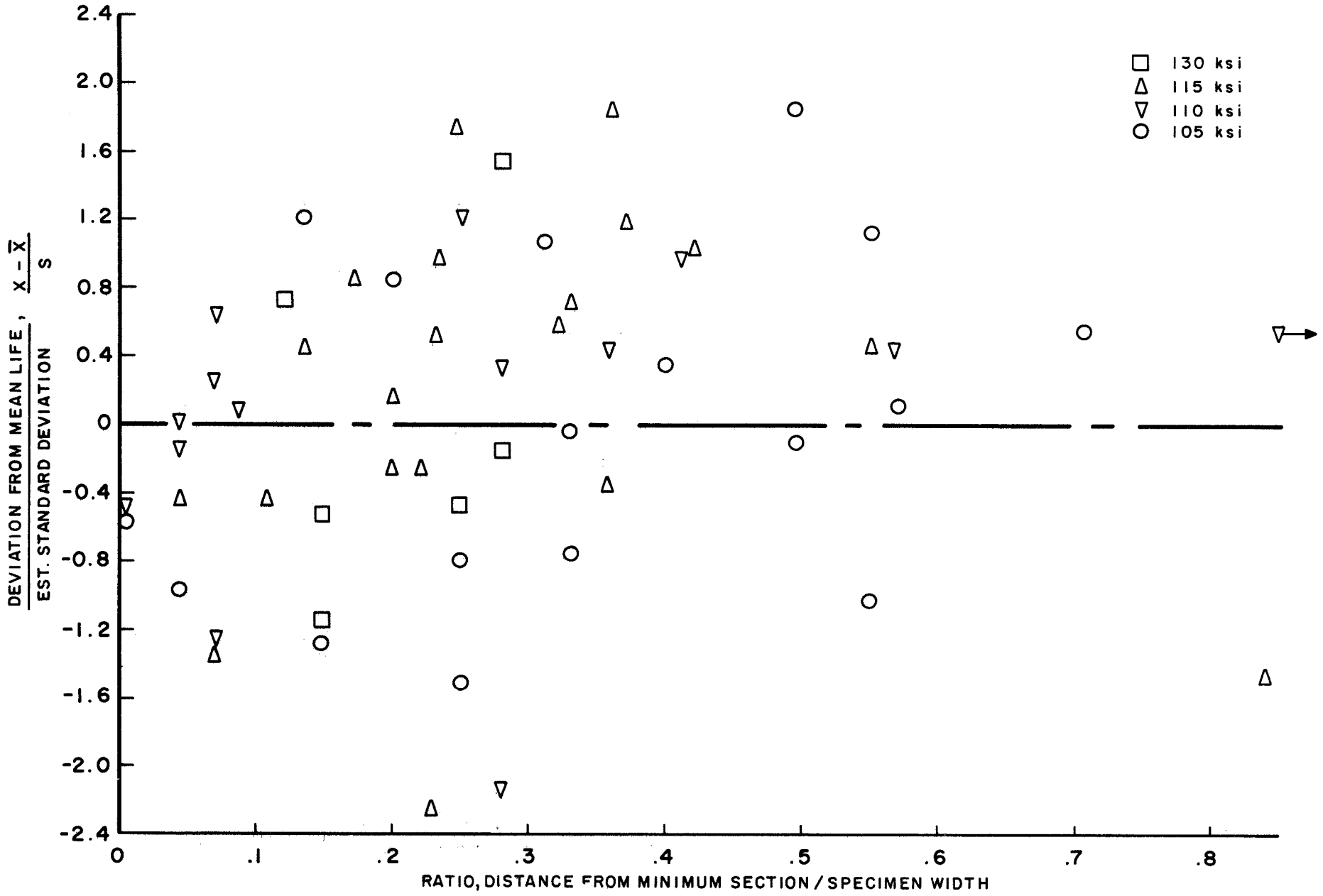

FIGURE 28. Deviation from Mean Life vs. Distance from Minimum Section (Normalized). 0.750-inch wide Ti-6Al-4V specimens (ref. Tables 6 and 7).

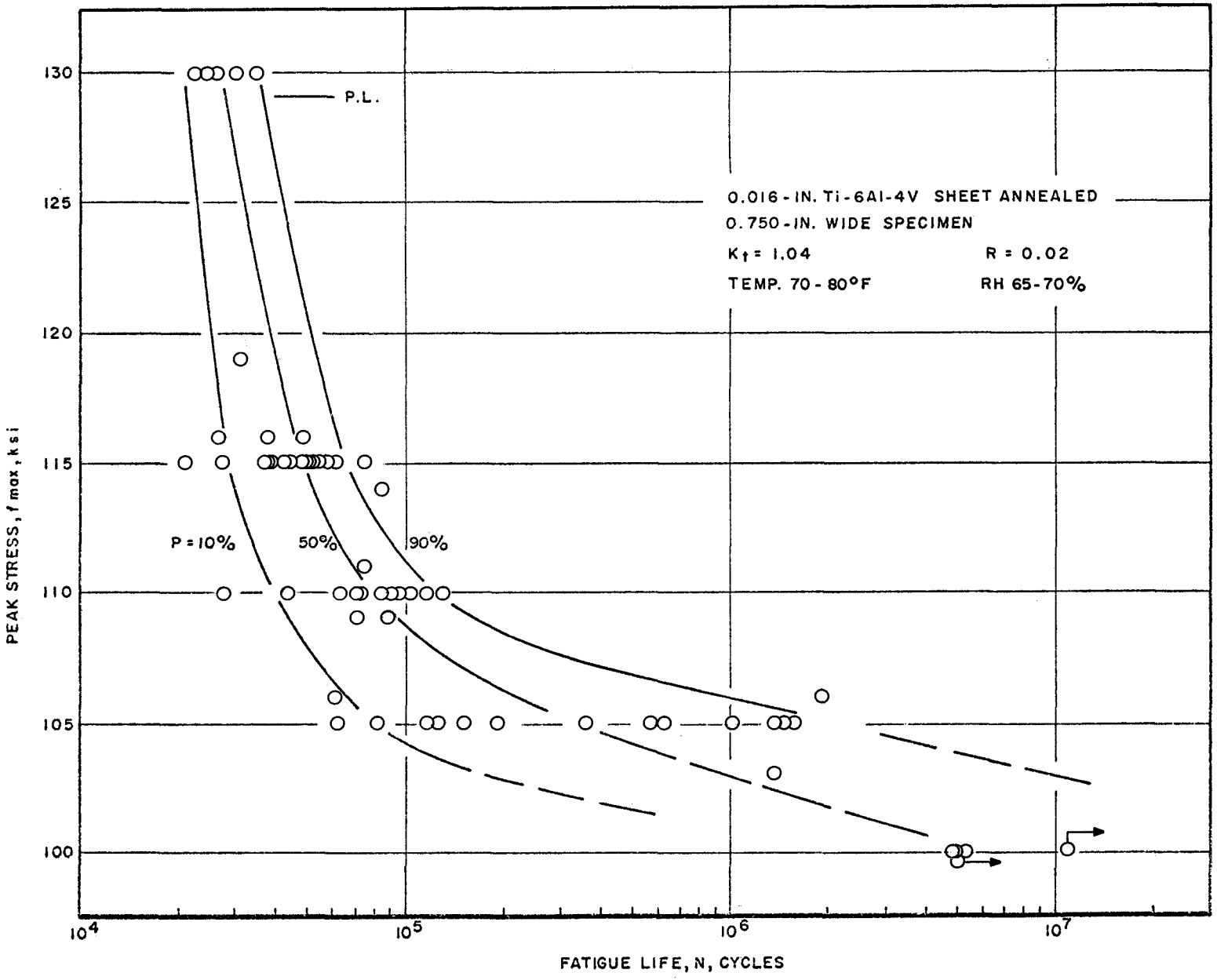

FIGURE 29. Baseline S-N Data: 0.750-inch Wide Ti-6Al-4V Specimens.

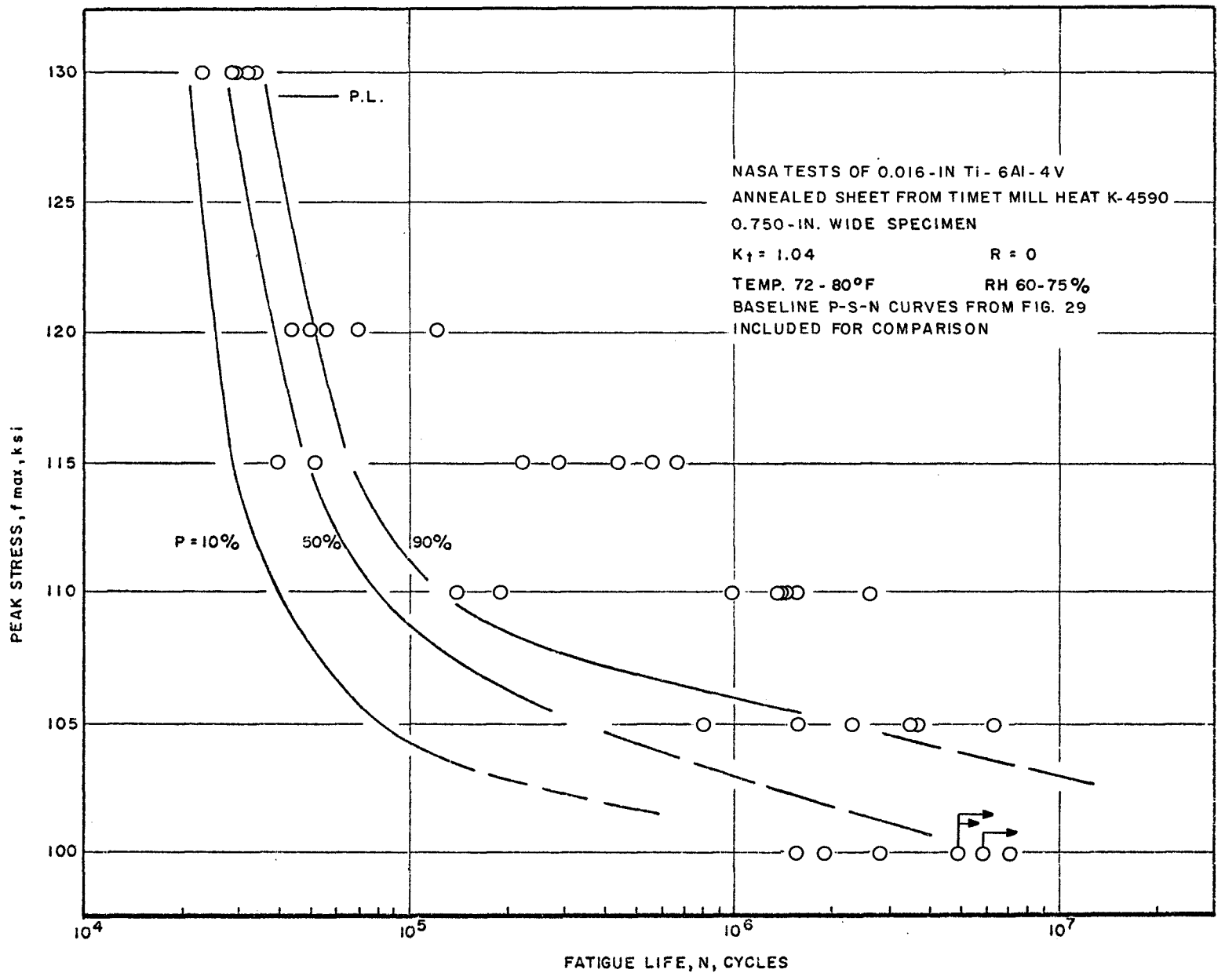

FIGURE 30. NASA Langley Research Center S-N Data.

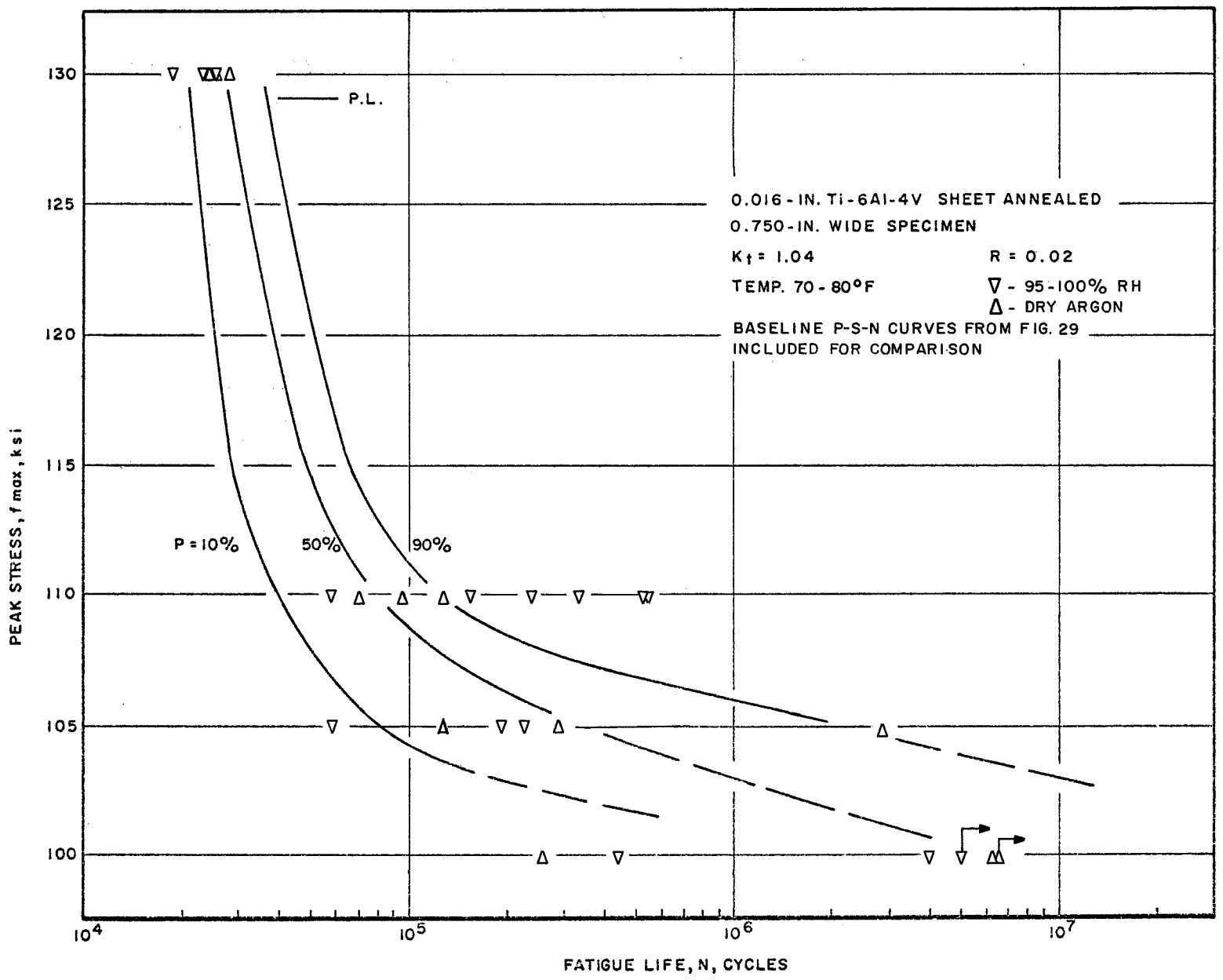

FIGURE 31. S-N Data Obtained at Extremes of Humidity.

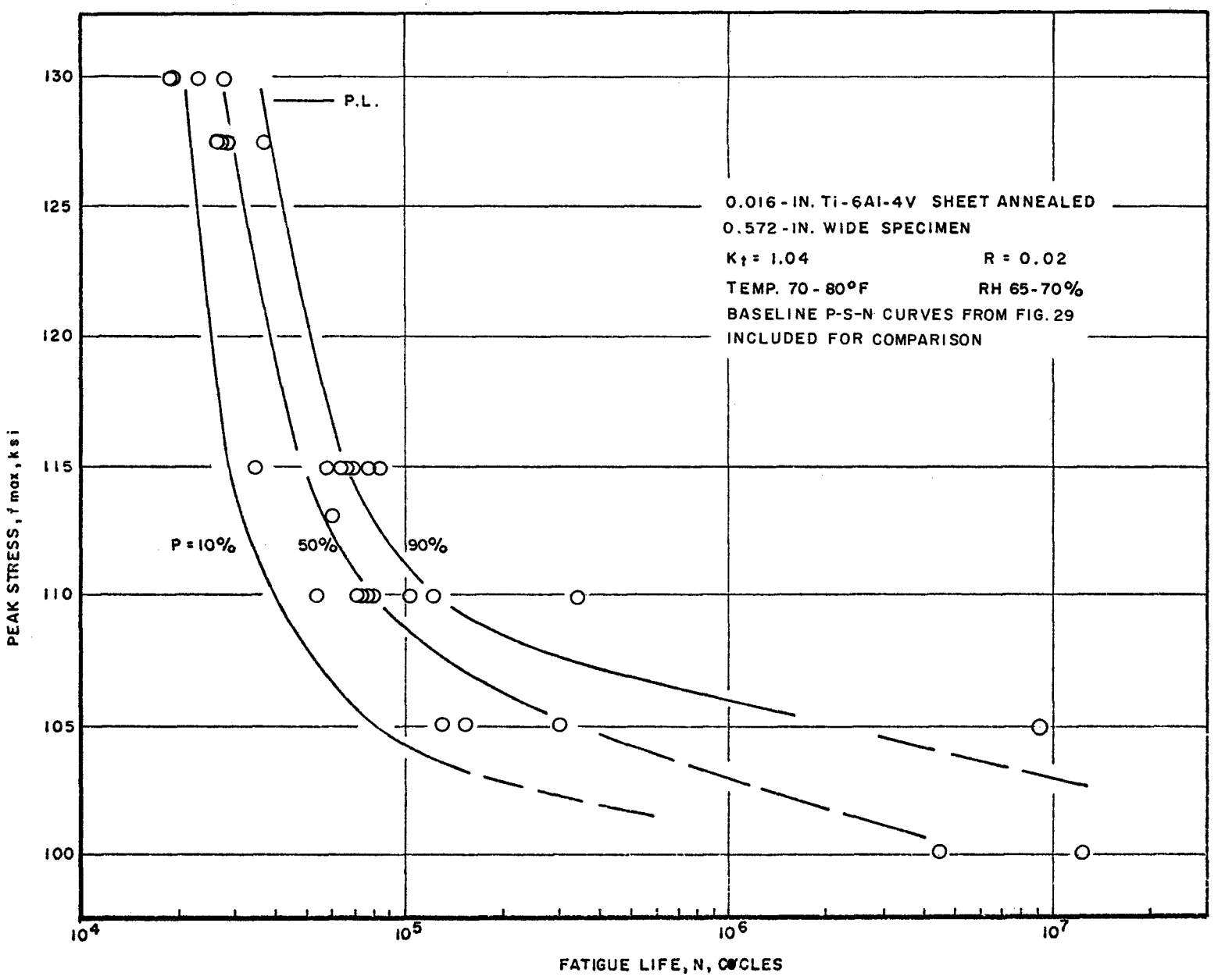

FIGURE 32. S-N Data Obtained on 0.572-inch Wide Ti-6Al-4V Specimens.

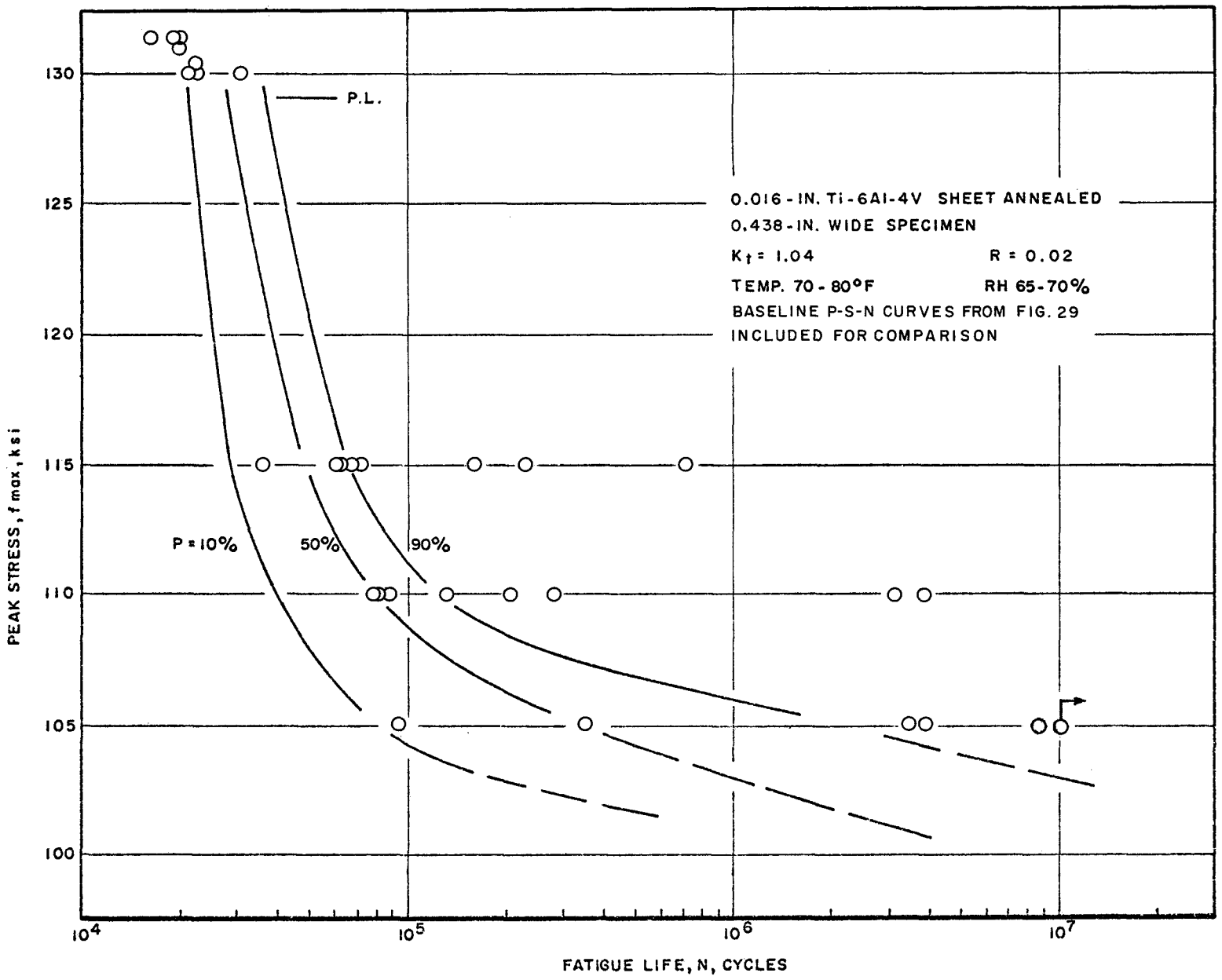

FIGURE 33. S-N Data Obtained on 0.438-inch Wide Ti-6Al-4V Specimens.

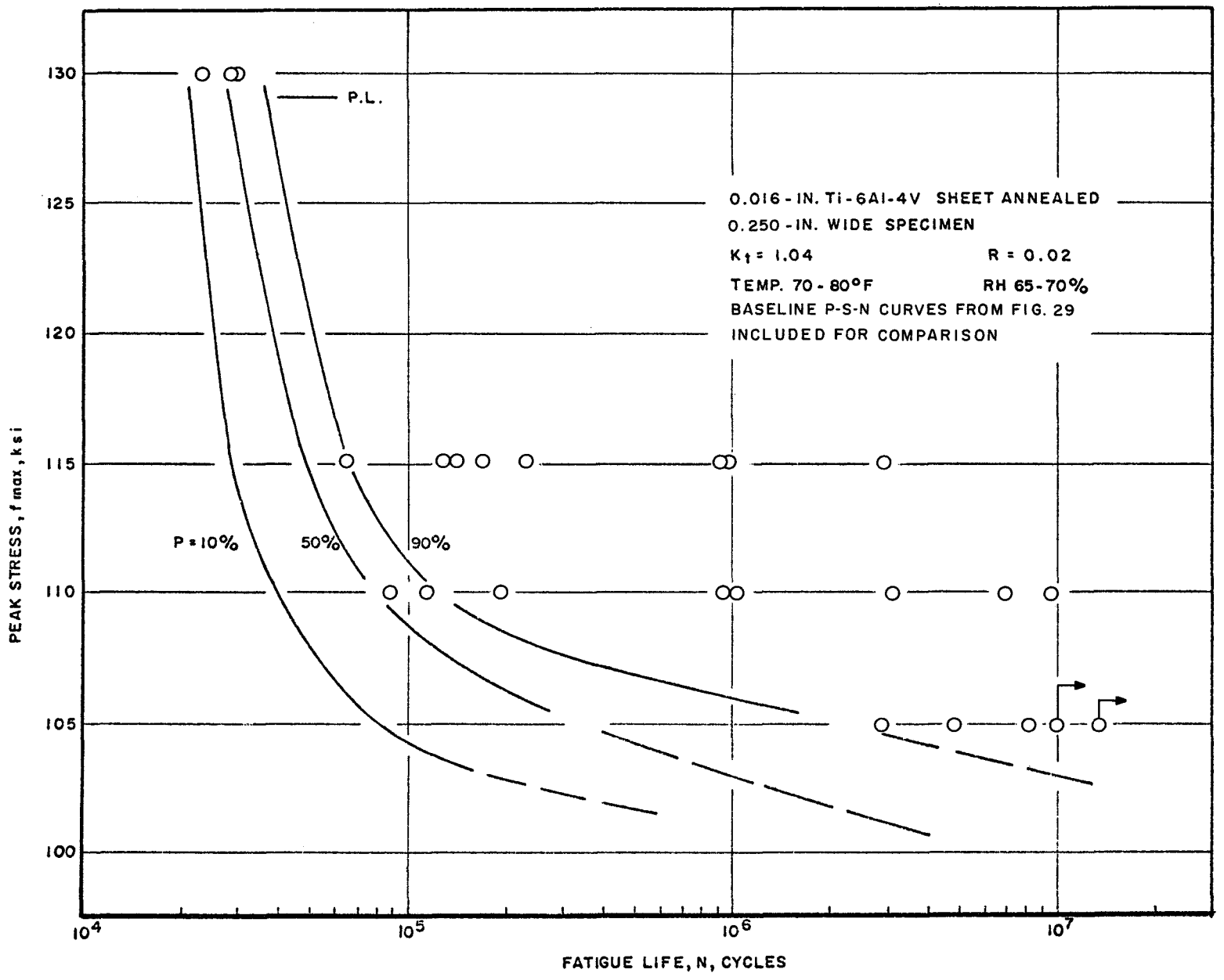

FIGURE 34. S-N Data Obtained on 0.250-inch Wide Ti-6Al-4V Specimens.

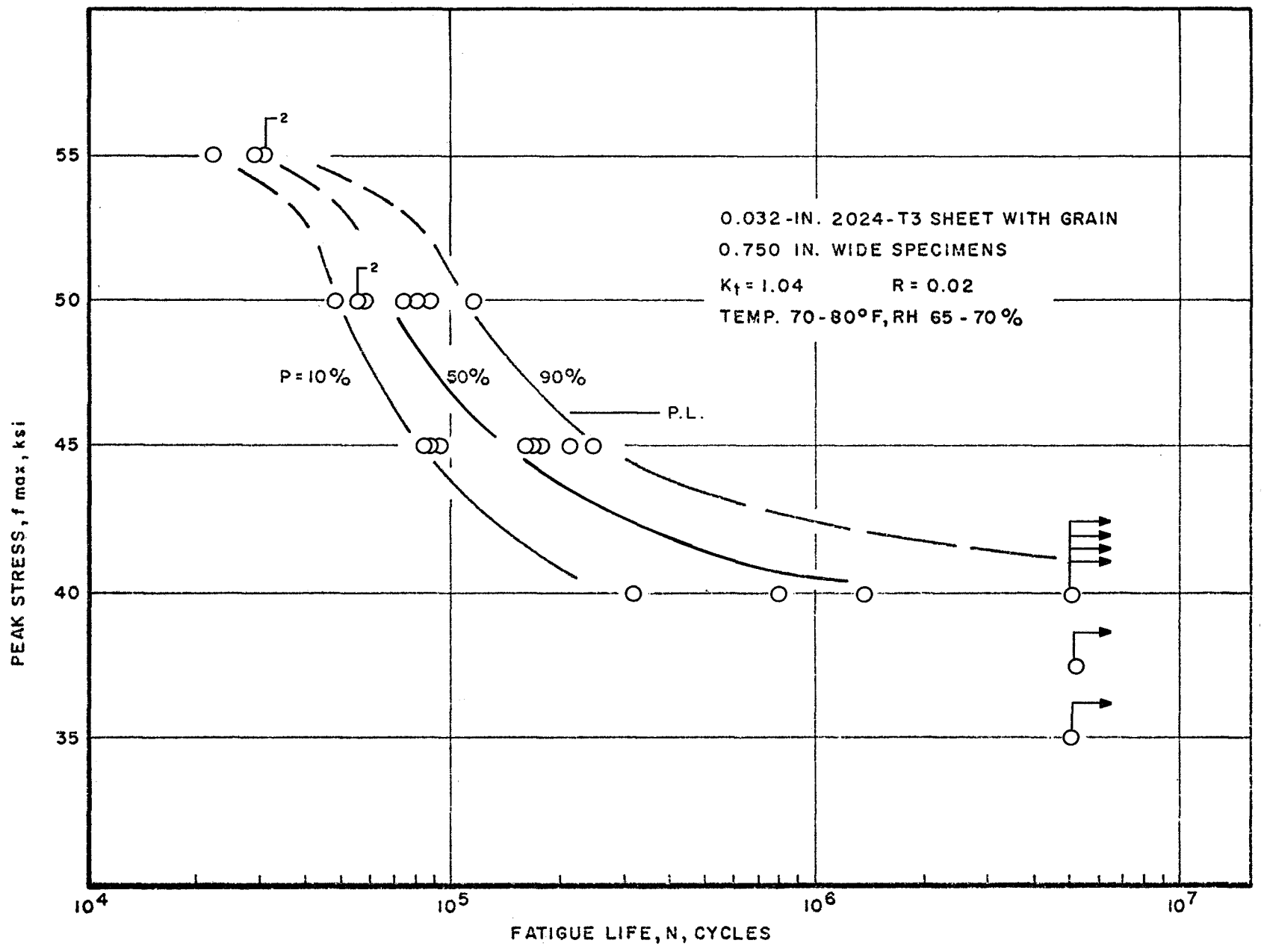

FIGURE 35. S-N Data Obtained on 0.750-inch Wide 2024-T3 Specimens.

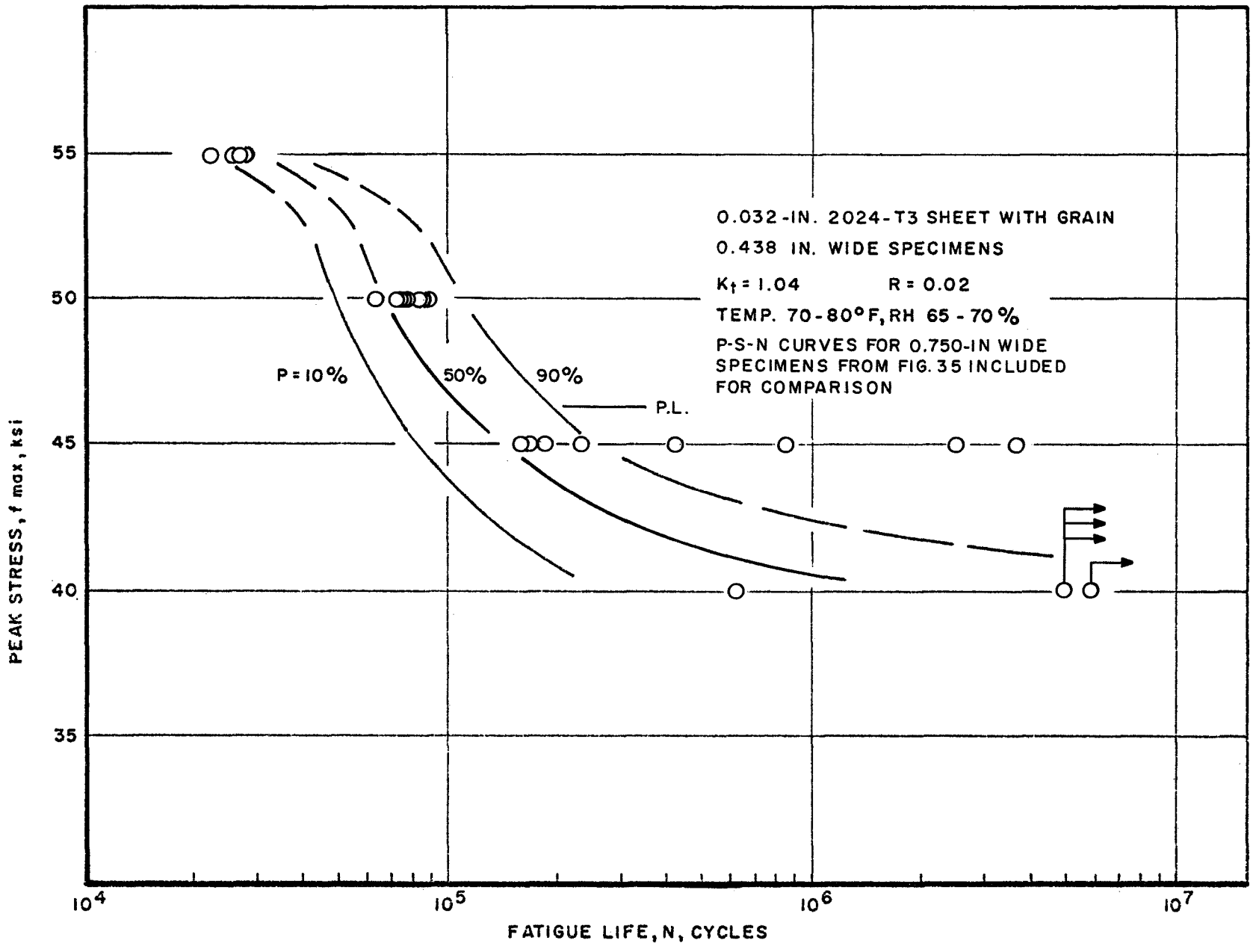

FIGURE 36. S-N Data Obtained on 0.438-inch Wide 2024-T3 Specimens.

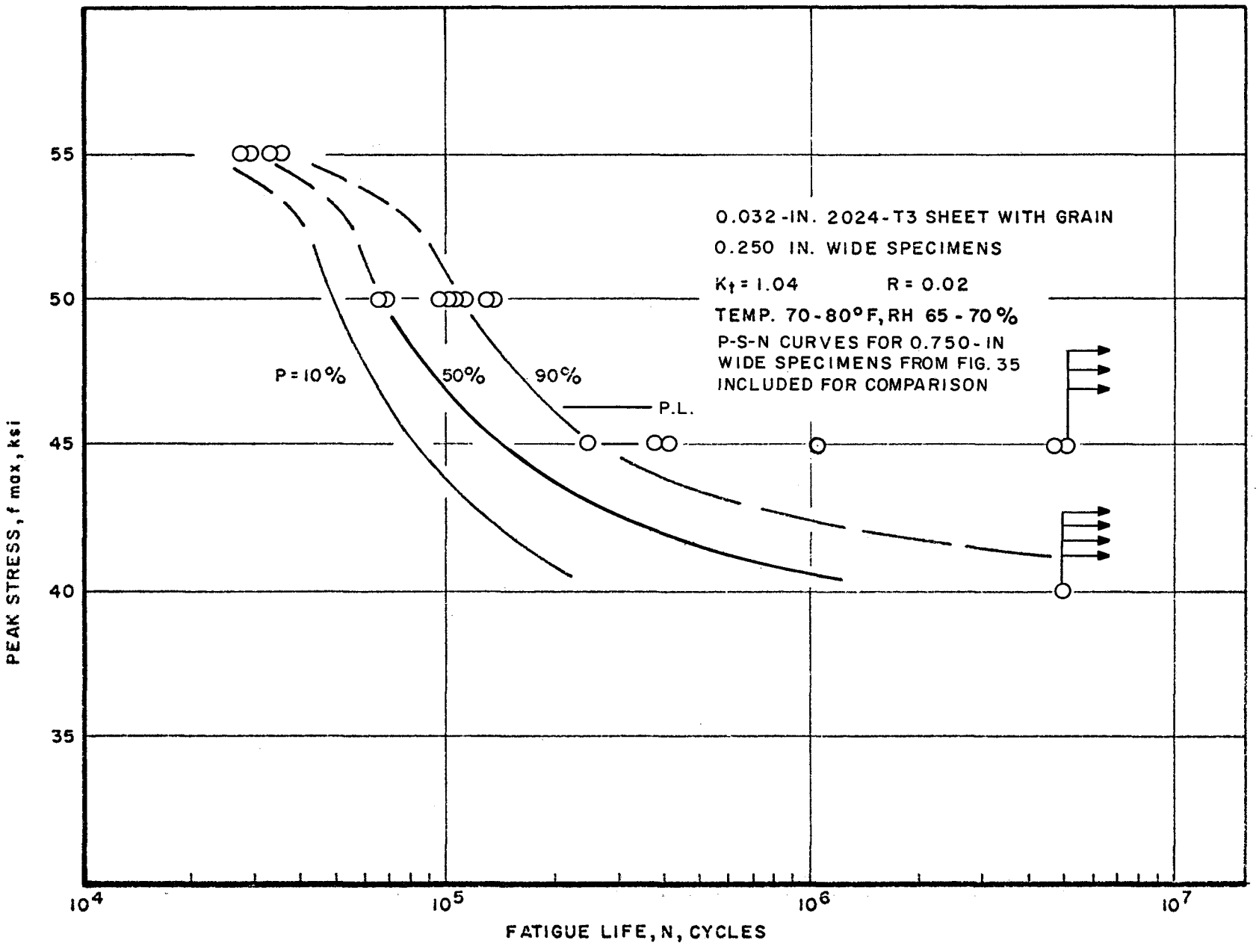

FIGURE 37. S-N Data Obtained on 0.250-inch Wide 2024-T3 Specimens.

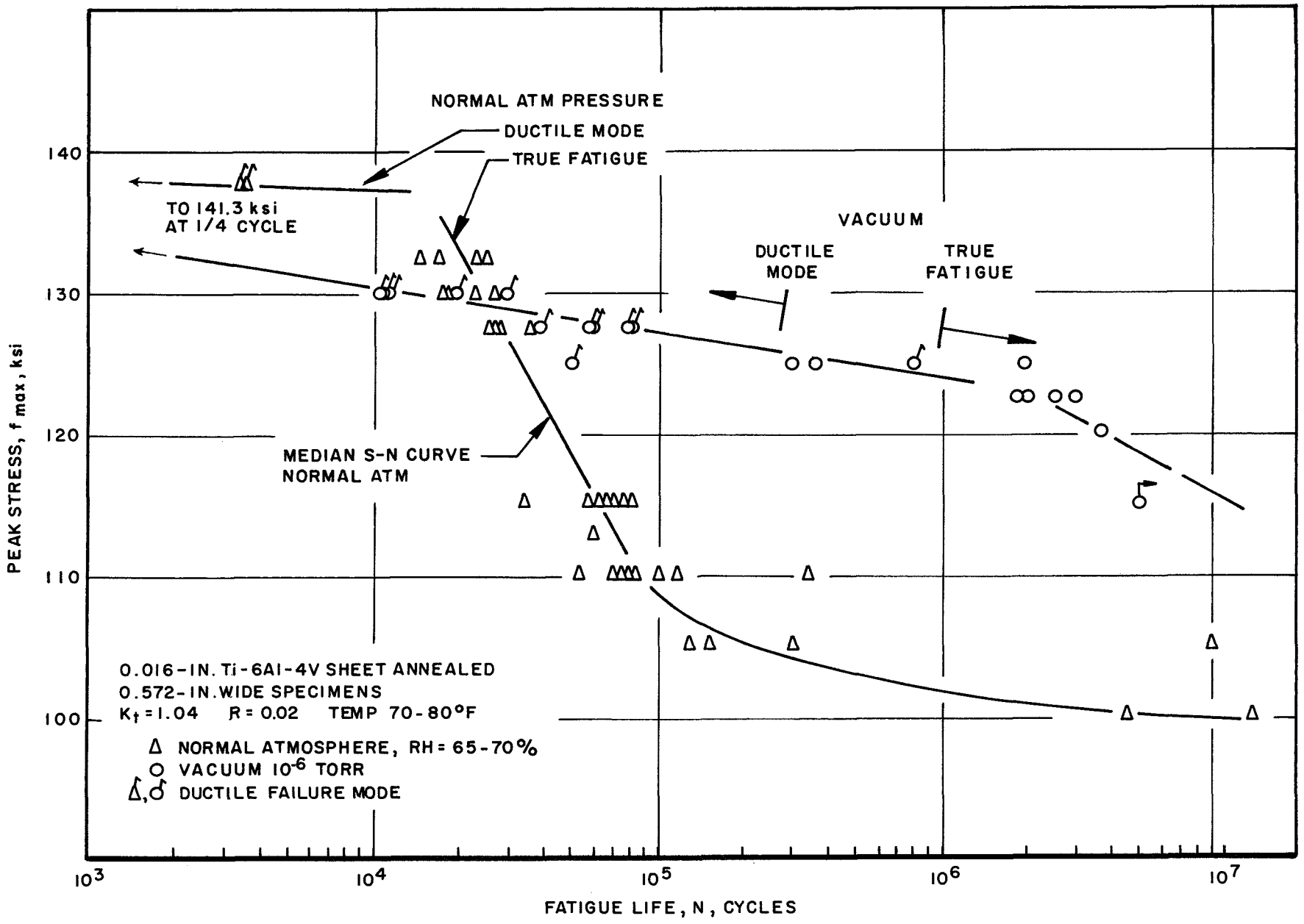

FIGURE 38. S-N Data Obtained on Ti-6Al-4V Specimens Tested in Vacuum Compared with Tests in Air.

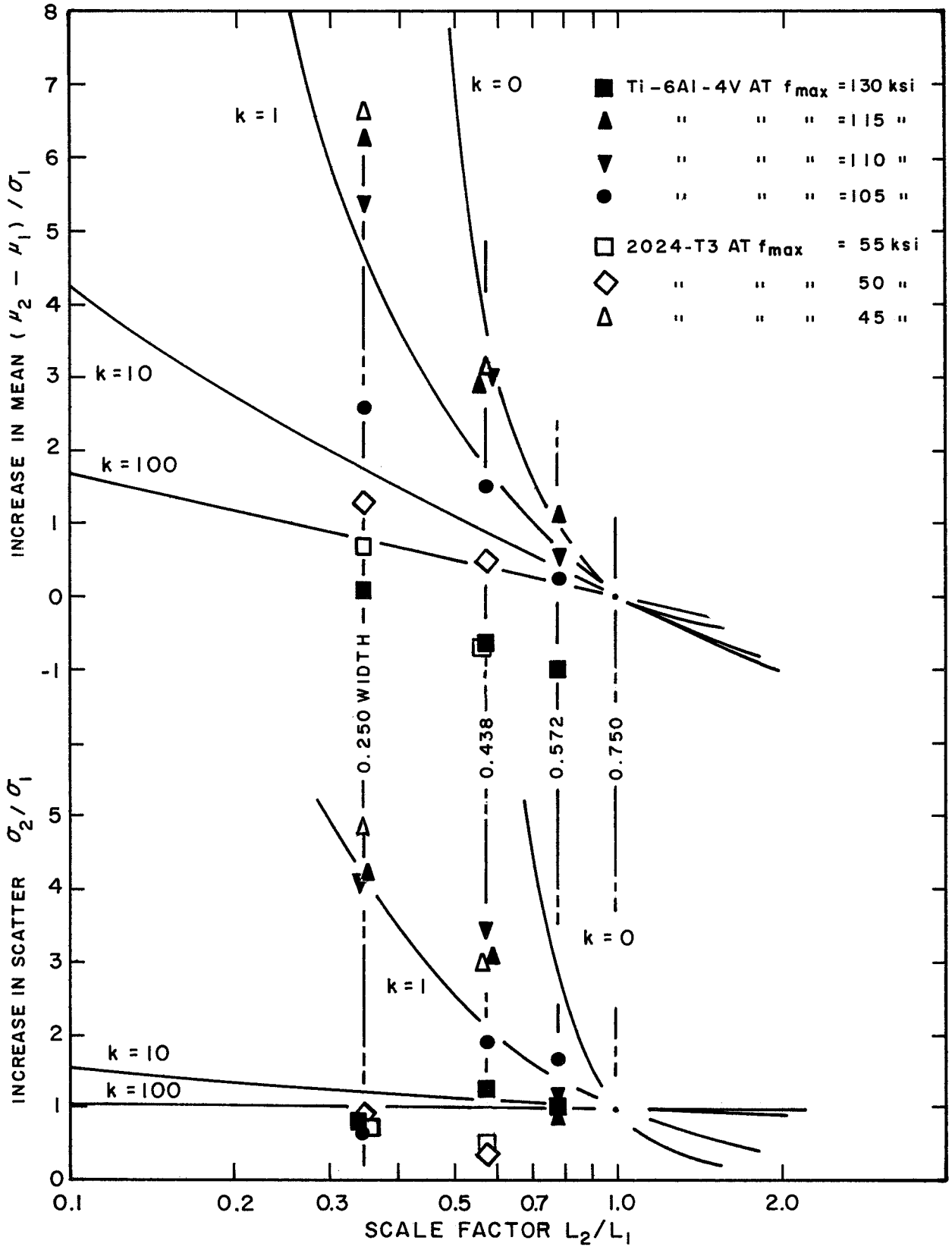

FIGURE 39. Size Effects in S-N Tests.
Theoretical curves based on Ref. 9.

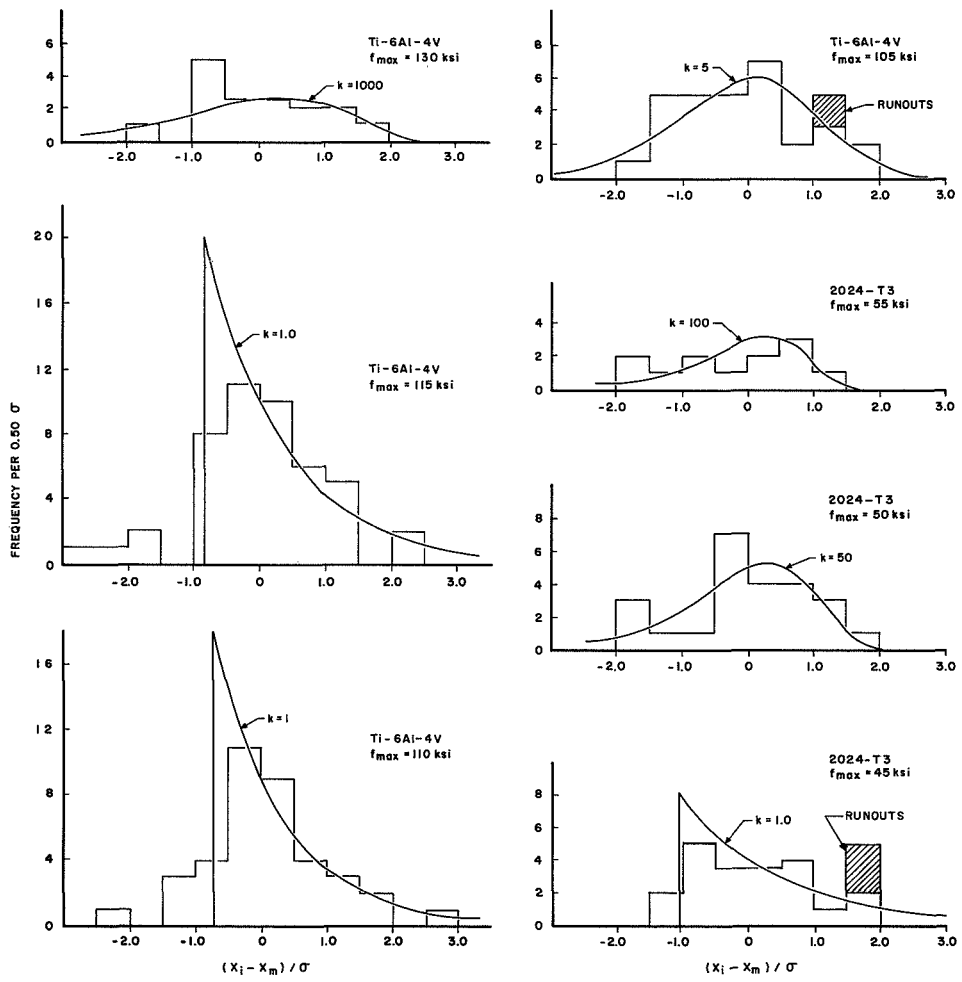

Figure 40. Distributions of Fatigue Life Data

LOCKHEED
CALIFORNIA COMPANY